PLAXIS Version 8
Material Models Manual
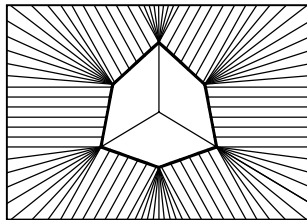
TABLE OF CONTENTS

1   INTRODUCTION

The mechanical behaviour of soils may be modelled at various degrees of accuracy. Hooke's law of linear, isotropic elasticity, for example, may be thought of as the simplest available stress-strain relationship. As it involves only two input parameters, i.e. Young's modulus, E, and Poisson's ratio, v, it is generally too crude to capture essential features of soil and rock behaviour. For modelling massive structural elements and bedrock layers, however, linear elasticity tends to be appropriate.

1.1   ON THE USE OF DIFFERENT MODELS

Mohr-Coulomb model (MC)

The elastic-plastic Mohr-Coulomb model involves five input parameters, i.e. E and v for soil elasticity; φ and c for soil plasticity and ψ as an angle of dilatancy. This Mohr-Coulomb model represents a 'first-order' approximation of soil or rock behaviour. It is recommended to use this model for a first analysis of the problem considered. For each layer one estimates a constant average stiffness. Due to this constant stiffness, computations tend to be relatively fast and one obtains a first impression of deformations. Besides the five model parameters mentioned above, initial soil conditions play an essential role in most soil deformation problems. Initial horizontal soil stresses have to be generated by selecting proper K_0-values.

Jointed Rock model (JR)

The Jointed Rock model is an anisotropic elastic-plastic model, especially meant to simulate the behaviour of rock layers involving a stratification and particular fault directions. Plasticity can only occur in a maximum of three shear directions (shear planes). Each plane has its own strength parameters φ and c. The intact rock is considered to behave fully elastic with constant stiffness properties E and v. Reduced elastic properties may be defined for the stratification direction.

Hardening-Soil model (HS)

The Hardening-Soil model is an advanced model for the simulation of soil behaviour. As for the Mohr-Coulomb model, limiting states of stress are described by means of the friction angle, φ, the cohesion, c, and the dilatancy angle, ψ. However, soil stiffness is described much more accurately by using three different input stiffnesses: the triaxial loading stiffness, E_{50}, the triaxial unloading stiffness, E_{ur}, and the oedometer loading stiffness, E_{oed}. As average values for various soil types, we have $E_{ur} \approx 3\ E_{50}$ and $E_{oed} \approx E_{50}$, but both very soft and very stiff soils tend to give other ratios of E_{oed} / E_{50}.

In contrast to the Mohr-Coulomb model, the Hardening-Soil model also accounts for stress-dependency of stiffness moduli. This means that all stiffnesses increase with

pressure. Hence, all three input stiffnesses relate to a reference stress, being usually taken as 100 kPa (1 bar).

Soft-Soil-Creep model (SSC)

The above Hardening-Soil model is suitable for all soils, but it does not account for viscous effects, i.e. creep and stress relaxation. In fact, all soils exhibit some creep and primary compression is thus followed by a certain amount of secondary compression.

The latter is most dominant in soft soils, i.e. normally consolidated clays, silts and peat, and we thus implemented a model under the name Soft-Soil-Creep model. Please note that the Soft-Soil-Creep model is a relatively new model that has been developed for application to settlement problems of foundations, embankments, etc. For unloading problems, as normally encountered in tunnelling and other excavation problems, the Soft-Soil-Creep model hardly supersedes the simple Mohr-Coulomb model. As for the Mohr-Coulomb model, proper initial soil conditions are also essential when using the Soft-Soil-Creep model. For the Hardening-Soil model and the Soft-Soil-Creep model this also includes data on the preconsolidation stress, as these models account for the effect of overconsolidation.

Soft Soil model (SS)

The Soft Soil model is a Cam-Clay type model especially meant for primary compression of near normally-consolidated clay-type soils. Although the modelling capabilities of this model are superceded by the Hardening Soil model, the Soft Soil model is still retained in the current version, because existing PLAXIS users might be comfortable with this model and still like to use it in their applications.

Analyses with different models

It is advised to use the Mohr-Coulomb model for a relatively quick and simple first analysis of the problem considered. When good soil data is lacking, there is no use in further more advanced analyses.

In many cases, one has good data on dominant soil layers, and it is appropriate to use the Hardening-Soil model in an additional analysis. No doubt, one seldom has test results from both triaxial and oedometer tests, but good quality data from one type of test can be supplemented by data from correlations and/or in situ testing.

Finally, a Soft-Soil-Creep analysis can be performed to estimate creep, i.e. secondary compression in very soft soils. The above idea of analyzing geotechnical problems with different soil models may seem costly, but it tends to pay off. First of all due to the fact that the Mohr-Coulomb analysis is relatively quick and simple and secondly as the procedure tends to reduce errors.

1.2   LIMITATIONS

The PLAXIS code and its soil models have been developed to perform calculations of realistic geotechnical problems. In this respect PLAXIS can be considered as a geotechnical simulation tool. The soil models can be regarded as a qualitative representation of soil behaviour whereas the model parameters are used to quantify the soil behaviour. Although much care has been taken for the development of the PLAXIS code and its soil models, the simulation of reality remains an approximation, which implicitly involves some inevitable numerical and modelling errors. Moreover, the accuracy at which reality is approximated depends highly on the expertise of the user regarding the modelling of the problem, the understanding of the soil models and their limitations, the selection of model parameters, and the ability to judge the reliability of the computational results.

Both the soil models and the PLAXIS code are constantly being improved such that each new version is an update of the previous ones. Some of the present limitations are listed below:

HS-model

It is a hardening model that does not account for softening due to soil dilatancy and de-bonding effects. In fact, it is an isotropic hardening model so that it models neither hysteretic and cyclic loading nor cyclic mobility. In order to model cyclic loading with good accuracy one would need a more complex model. As a final remark, the use of the Hardening Soil model generally results in longer calculation times, since the material stiffness matrix is formed and decomposed in each calculation step.

SSC-model

All above limitations also hold true for the Soft-Soil-Creep model. In addition this model tends to over predict the range of elastic soil behaviour. This is especially the case for excavation problems, including tunnelling.

SS-model

The same limitations (including these in the SSC-model) hold in the SS-model. In fact the SS-model is superceded by the HS-model, but is kept for users who are familiar with this model. The utilization of the SS-model should be limited to the situations that are dominated primarily by compression. It is certainly not recommended for use in excavation problems.

Interfaces

Interface elements are generally modelled by means of the bilinear Mohr-Coulomb model. When a more advanced model is used for the corresponding cluster material data set, the interface element will only pick up the relevant data (c, φ, ψ, E, ν) for the Mohr-Coulomb model, as described in Section 3.5.2 of the Reference Manual. In such cases

the interface stiffness is taken to be the elastic soil stiffness. Hence, $E = E_{ur}$ where E_{ur} is stress level dependent, following a power law with E_{ur} proportional to σ_m. For the Soft-Soil-Creep model, the power m is equal to 1 and E_{ur} is largely determined by the swelling constant κ^*.

2 PRELIMINARIES ON MATERIAL MODELLING

A material model is a set of mathematical equations that describes the relationship between stress and strain. Material models are often expressed in a form in which infinitesimal increments of stress (or 'stress rates') are related to infinitesimal increments of strain (or 'strain rates'). All material models implemented in the PLAXIS are based on a relationship between the effective stress rates, $\dot{\sigma}'$, and the strain rates, $\dot{\varepsilon}$. In the following section it is described how stresses and strains are defined in PLAXIS. In subsequent sections the basic stress-strain relationship is formulated and the influence of pore pressures in undrained materials is described. Later sections focus on initial conditions for advanced material models.

> Element and material model formulations in PLAXIS are fully three dimensional. However, in Version 8 only plane strain and axisymmetric conditions are considered.

2.1 GENERAL DEFINITIONS OF STRESS

Stress is a tensor which can be represented by a matrix in Cartesian coordinates:

$$\underline{\underline{\sigma}} = \begin{bmatrix} \sigma_{xx} & \sigma_{xy} & \sigma_{xz} \\ \sigma_{yx} & \sigma_{yy} & \sigma_{yz} \\ \sigma_{zx} & \sigma_{zy} & \sigma_{zz} \end{bmatrix} \tag{2.1}$$

In the standard deformation theory, the stress tensor is symmetric such that $\sigma_{xy} = \sigma_{yx}$, $\sigma_{yz} = \sigma_{zy}$ and $\sigma_{zx} = \sigma_{xz}$. In this situation, stresses are often written in vector notation, which involve only six different components:

$$\underline{\sigma} = \begin{pmatrix} \sigma_{xx} & \sigma_{yy} & \sigma_{zz} & \sigma_{xy} & \sigma_{yz} & \sigma_{zx} \end{pmatrix}^{T} \tag{2.2}$$

In plane strain condition, however,

$$\sigma_{yz} = \sigma_{zx} = 0$$

According to Terzaghi's principle, stresses in the soil are divided into effective stresses, $\underline{\sigma}'$, and pore pressures, $\underline{\sigma}_w$:

$$\underline{\sigma} = \underline{\sigma}' + \underline{\sigma}_w \tag{2.3}$$

Water is considered not to sustain any shear stresses. As a result, effective shear stresses are equal to total shear stresses. Positive normal stress components are considered to

represent tension, whereas negative normal stress components indicate pressure (or compression).

Material models for soil and rock are generally expressed as a relationship between infinitesimal increments of effective stress and infinitesimal increments of strain. In such a relationship, infinitesimal increments of effective stress are represented by stress rates (with a dot above the stress symbol):

$$\underline{\dot{\sigma}}' = \left(\dot{\sigma}'_{xx} \quad \dot{\sigma}'_{yy} \quad \dot{\sigma}'_{zz} \quad \dot{\sigma}_{xy} \quad \dot{\sigma}_{yz} \quad \dot{\sigma}_{zx} \right)^T \tag{2.4}$$
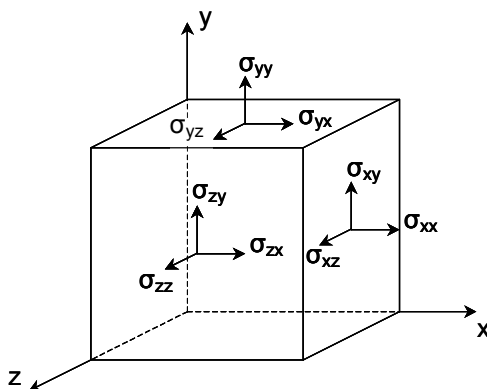
Figure 2.1 General three-dimensional coordinate system and sign convention for stresses

It is often useful to use principal stresses rather than Cartesian stress components when formulating material models. Principal stresses are the stresses in such a coordinate system direction that all shear stress components are zero. Principal stresses are, in fact, the eigenvalues of the stress tensor. Principal effective stresses can be determined in the following way:

$$\det\left(\underline{\underline{\sigma}}' - \sigma'\underline{\underline{I}} \right) = 0 \tag{2.5}$$

where $\underline{I}$ is the identity matrix. This equation gives three solutions for σ', i.e. the principal effective stresses (σ'_1, σ'_2, σ'_3). In PLAXIS the principal effective stresses are arranged in algebraic order:

$$\sigma'_1 \leq \sigma'_2 \leq \sigma'_3 \tag{2.6}$$

Hence, σ'_1 is the largest compressive principal stress and σ'_3 is the smallest compressive principal stress. In this manual, models are often presented with reference to the principal stress space, as indicated in Figure 2.2.
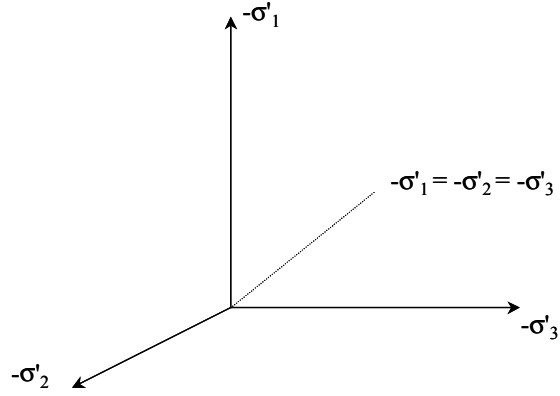
Figure 2.2 Principal stress space

In addition to principal stresses it is also useful to define invariants of stress, which are stress measures that are independent of the orientation of the coordinate system. Two useful stress invariants are:

$$p' = -\tfrac{1}{3}\left(\sigma'_{xx} + \sigma'_{yy} + \sigma'_{zz}\right) = -\tfrac{1}{3}\left(\sigma'_1 + \sigma'_2 + \sigma'_3\right) \tag{2.7a}$$

$$q = \sqrt{\tfrac{1}{2}\left(\left(\sigma'_{xx} - \sigma'_{yy}\right)^2 + \left(\sigma'_{yy} - \sigma'_{zz}\right)^2 + \left(\sigma'_{zz} - \sigma'_{xx}\right)^2 + 6\left(\sigma_{xy}^2 + \sigma_{yz}^2 + \sigma_{zx}^2\right)\right)} \tag{2.7b}$$

where p' is the isotropic effective stress, or mean effective stress, and q is the equivalent shear stress. Note that the convention adopted for p' is positive for compression in contrast to other stress measures. The equivalent shear stress, q, has the important property that it reduces to $q = |\sigma_1' - \sigma_3'|$ for triaxial stress states with $\sigma_2' = \sigma_3'$.

Principal effective stresses can be written in terms of the invariants:

$$-\sigma'_1 = p' + \tfrac{2}{3}q\sin\left(\theta - \tfrac{2}{3}\pi\right) \tag{2.8a}$$

$$-\sigma'_2 = p' + \tfrac{2}{3}q\sin(\theta) \tag{2.8b}$$

$$-\sigma'_3 = p' + \tfrac{2}{3}q\sin\left(\theta + \tfrac{2}{3}\pi\right) \tag{2.8c}$$

in which θ is referred to as Lode's angle (a third invariant), which is defined as:

$$\theta = \tfrac{1}{3}\arcsin\left(\frac{27}{3}\frac{J_3}{q^3}\right) \tag{2.9}$$

with

$$J_3 = (\sigma'_{xx}\text{-}p')(\sigma'_{yy}\text{-}p')(\sigma'_{zz}\text{-}p') + (\sigma'_{xx}\text{-}p')\sigma^2_{yz} + (\sigma'_{yy}\text{-}p')\sigma^2_{zx} + (\sigma'_{zz}\text{-}p')\sigma^2_{xy} + 2\sigma_{xy}\sigma_{yz}\sigma_{zx}$$

(2.10)

2.2 GENERAL DEFINITIONS OF STRAIN

Strain is a tensor which can be represented by a matrix with Cartesian coordinates as:

$$\underline{\underline{\varepsilon}} = \begin{bmatrix} \varepsilon_{xx} & \varepsilon_{xy} & \varepsilon_{xz} \\ \varepsilon_{yx} & \varepsilon_{yy} & \varepsilon_{yz} \\ \varepsilon_{zx} & \varepsilon_{zy} & \varepsilon_{zz} \end{bmatrix}$$

(2.11)

According to the small deformation theory, only the sum of complementing Cartesian shear strain components ε_{ij} and ε_{ji} result in shear stress. This sum is denoted as the shear strain γ. Hence, instead of ε_{xy}, ε_{yx}, ε_{yz}, ε_{zy}, ε_{zx} and ε_{xz} the shear strain components γ_{xy}, γ_{yz} and γ_{zx} are used respectively. Under the above conditions, strains are often written in vector notation, which involve only six different components:

$$\underline{\varepsilon} = \begin{pmatrix} \varepsilon_{xx} & \varepsilon_{yy} & \varepsilon_{zz} & \gamma_{xy} & \gamma_{yz} & \gamma_{zx} \end{pmatrix}^T$$

(2.12)

$$\varepsilon_{xx} = \frac{\partial u_x}{\partial x}$$

(2.13a)

$$\varepsilon_{yy} = \frac{\partial u_y}{\partial y}$$

(2.13b)

$$\varepsilon_{zz} = \frac{\partial u_z}{\partial z}$$

(2.13c)

$$\gamma_{xy} = \varepsilon_{xy} + \varepsilon_{yx} = \frac{\partial u_x}{\partial y} + \frac{\partial u_y}{\partial x}$$

(2.13d)

$$\gamma_{yz} = \varepsilon_{yz} + \varepsilon_{zy} = \frac{\partial u_y}{\partial z} + \frac{\partial u_z}{\partial y}$$

(2.13e)

$$\gamma_{zx} = \varepsilon_{zx} + \varepsilon_{xz} = \frac{\partial u_z}{\partial x} + \frac{\partial u_x}{\partial z}$$ (2.13f)

Similarly as for stresses, positive normal strain components refer to extension, whereas negative normal strain components indicate compression.

In the formulation of material models, where infinitesimal increments of strain are considered, these increments are represented by strain rates (with a dot above the strain symbol).

$$\dot{\underline{\varepsilon}} = \begin{pmatrix} \dot{\varepsilon}_{xx} & \dot{\varepsilon}_{yy} & \dot{\varepsilon}_{zz} & \dot{\gamma}_{xy} & \dot{\gamma}_{yz} & \dot{\gamma}_{zx} \end{pmatrix}^T$$ (2.14)

for plane strain conditions, as considered in PLAXIS version 8,

$$\varepsilon_{zz} = \gamma_{xz} = \gamma_{yz} = 0$$

whereas for axisymmetric conditions,

$$\varepsilon_{zz} = \frac{1}{r} u_x \text{ and } \gamma_{xz} = \gamma_{yz} = 0 \text{ (r = radius)}$$

In analogy to the invariants of stress, it is also useful to define invariants of strain. A strain invariant that is often used is the volumetric strain, ε_v, which is defined as the sum of all normal strain components:

$$\varepsilon_v = \varepsilon_{xx} + \varepsilon_{yy} + \varepsilon_{zz} = \varepsilon_1 + \varepsilon_2 + \varepsilon_3$$ (2.15)

The volumetric strain is defined as negative for compaction and as positive for dilatancy.

For elastoplastic models, as used in PLAXIS program, strains are decomposed into elastic and plastic components:

$$\underline{\varepsilon} = \underline{\varepsilon}^e + \underline{\varepsilon}^p$$ (2.16)

Throughout this manual, the superscript e will be used to denote elastic strains and the superscript p will be used to denote plastic strains.

2.3   ELASTIC STRAINS

Material models for soil and rock are generally expressed as a relationship between infinitesimal increments of effective stress ('effective stress rates') and infinitesimal increments of strain ('strain rates'). This relationship may be expressed in the form:

$$\dot{\underline{\sigma}}' = \underline{\underline{M}}\ \dot{\underline{\varepsilon}} \tag{2.17}$$

$\underline{M}$ is a material stiffness matrix. Note that in this type of approach, pore-pressures are explicitly excluded from the stress-strain relationship.

The simplest material model in PLAXIS is based on Hooke's law for isotropic linear elastic behaviour. This model is available under the name Linear Elastic model, but it is also the basis of other models. Hooke's law can be given by the equation:

$$\begin{bmatrix} \dot{\sigma}'_{xx} \\ \dot{\sigma}'_{yy} \\ \dot{\sigma}'_{zz} \\ \dot{\sigma}'_{xy} \\ \dot{\sigma}'_{yz} \\ \dot{\sigma}'_{zx} \end{bmatrix} = \frac{E'}{(1-2v')(1+v')} \begin{bmatrix} 1-v' & v' & v' & 0 & 0 & 0 \\ v' & 1-v' & v' & 0 & 0 & 0 \\ v' & v' & 1-v' & 0 & 0 & 0 \\ 0 & 0 & 0 & \frac{1}{2}-v' & 0 & 0 \\ 0 & 0 & 0 & 0 & \frac{1}{2}-v' & 0 \\ 0 & 0 & 0 & 0 & 0 & \frac{1}{2}-v' \end{bmatrix} \begin{bmatrix} \dot{\varepsilon}_{xx} \\ \dot{\varepsilon}_{yy} \\ \dot{\varepsilon}_{zz} \\ \dot{\gamma}_{xy} \\ \dot{\gamma}_{yz} \\ \dot{\gamma}_{zx} \end{bmatrix} \tag{2.18}$$

The elastic material stiffness matrix is often denoted as $\underline{D}^e$. Two parameters are used in this model, the effective Young's modulus, E', and the effective Poisson's ratio, v'. In the remaining part of this manual effective parameters are denoted without dash ('), unless a different meaning is explicitly stated. The symbols E and v are sometimes used in this manual in combination with the subscript ur to emphasize that the parameter is explicitly meant for unloading and reloading. A stiffness modulus may also be indicated with the subscript ref to emphasize that it refers to a particular reference level (y_{ref}) (see further).

The relationship between Young's modulus E and other stiffness moduli, such as the shear modulus G, the bulk modulus K, and the oedometer modulus E_{oed}, is given by:

$$G = \frac{E}{2(1+v)} \tag{2.19a}$$

$$K = \frac{E}{3(1-2v)} \tag{2.19b}$$

$$E_{oed} = \frac{(1-v)E}{(1-2v)(1+v)} \tag{2.19c}$$

During the input of material parameters for the Linear Elastic model or the Mohr-Coulomb model the values of G and E_{oed} are presented as auxiliary parameters (alternatives), calculated from Eq. (2.19). Note that the alternatives are influenced by the input values of E and v. Entering a particular value for one of the alternatives G or E_{oed} results in a change of the E modulus.

Figure 2.3 Parameters tab for the Linear Elastic model
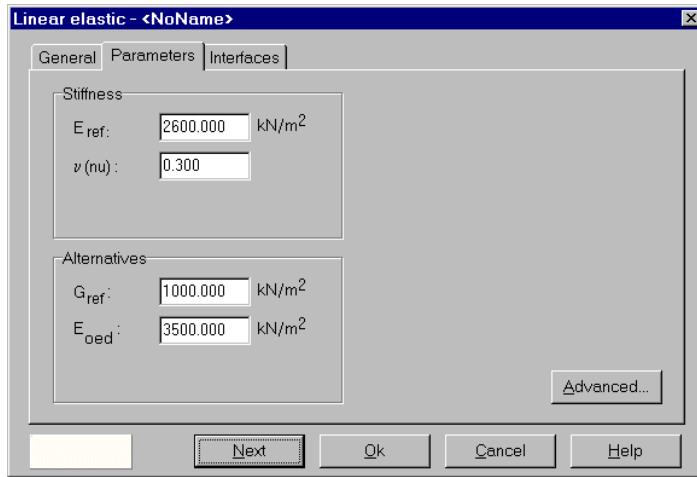
It is possible for the Linear Elastic model to specify a stiffness that varies linearly with depth. This can be done by entering the advanced parameters window using the *Advanced* button, as shown in Figure 2.3. Here one may enter a value for $E_{increment}$ which is the increment of stiffness per unit of depth, as indicated in Figure 2.4.
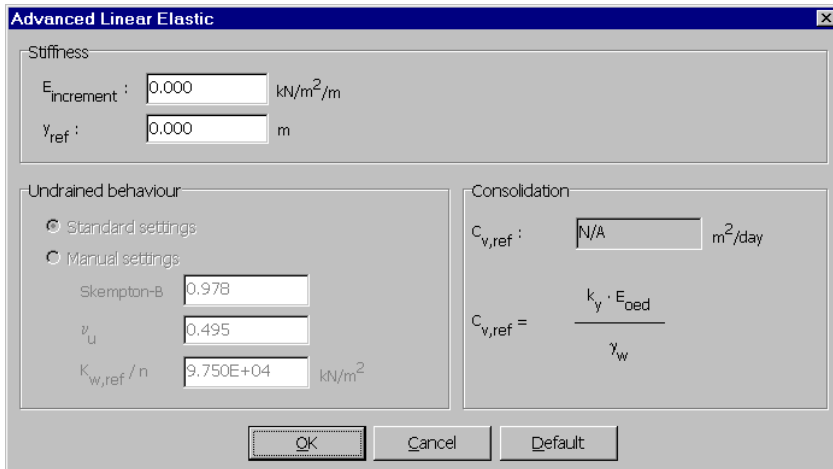
Figure 2.4 Advanced parameter window

Together with the input of $E_{increment}$ the input of y_{ref} becomes relevant. Above y_{ref} the stiffness is equal to E_{ref}. Below the stiffness is given by:

$$E_{actual} = E_{ref} + (y_{ref} - y)E_{increment} \qquad\qquad y < y_{ref} \qquad\qquad (2.20)$$

The Linear Elastic model is usually inappropriate to model the highly non-linear behaviour of soil, but it is of interest to simulate structural behaviour, such as thick concrete walls or plates, for which strength properties are usually very high compared with those of soil. For these applications, the Linear Elastic model will often be selected together with *Non-porous* type of material behaviour in order to exclude pore pressures from these structural elements.

2.4 UNDRAINED ANALYSIS WITH EFFECTIVE PARAMETERS

In the PLAXIS it is possible to specify undrained behaviour in an effective stress analysis using effective model parameters. This is achieved by identifying the Type of material behaviour (*Material type*) of a soil layer as *Undrained*. In this Section, it is explained how PLAXIS deals with this special option.

The presence of pore pressures in a soil body, usually caused by water, contributes to the total stress level. According to Terzaghi's principle, total stresses σ can be divided into effective stresses σ' and pore pressures σ_w (see also Eq. 2.3). However, water is supposed not to sustain any shear stress, and therefore the effective shear stresses are equal to the total shear stresses:

$$\sigma_{xx} = \sigma'_{xx} + \sigma_w \qquad\qquad (2.21a)$$

$$\sigma_{yy} = \sigma'_{yy} + \sigma_w \qquad\qquad (2.21b)$$

$$\sigma_{zz} = \sigma'_{zz} + \sigma_w \qquad\qquad (2.21c)$$

$$\sigma_{xy} = \sigma'_{xy} \qquad\qquad (2.21d)$$

$$\sigma_{yz} = \sigma'_{yz} \qquad\qquad (2.21e)$$

$$\sigma_{zx} = \sigma'_{zx} \qquad\qquad (2.21f)$$

Note that, similar to the total and the effective stress components, σ_w is considered negative for pressure.

A further distinction is made between steady state pore stress, p_{steady}, and excess pore stress, p_{excess}:

$$\sigma_w = p_{steady} + p_{excess} \tag{2.22}$$

Steady state pore pressures are considered to be input data, i.e. generated on the basis of phreatic levels or groundwater flow. This generation of steady state pore pressures is discussed in Section 3.8 of the Reference Manual. Excess pore pressures are generated during plastic calculations for the case of undrained material behaviour. Undrained material behaviour and the corresponding calculation of excess pore pressures is described below.

Since the time derivative of the steady state component equals zero, it follows:

$$\dot{\sigma}_w = \dot{p}_{excess} \tag{2.23}$$

Hooke's law can be inverted to obtain:

$$
\begin{bmatrix} \dot{\varepsilon}^e_{xx} \\ \dot{\varepsilon}^e_{yy} \\ \dot{\varepsilon}^e_{zz} \\ \dot{\gamma}^e_{xy} \\ \dot{\gamma}^e_{yz} \\ \dot{\gamma}^e_{zx} \end{bmatrix}
= \frac{1}{E'}
\begin{bmatrix}
1 & -v' & -v' & 0 & 0 & 0 \\
-v' & 1 & -v' & 0 & 0 & 0 \\
-v' & -v' & 1 & 0 & 0 & 0 \\
0 & 0 & 0 & 2+2v' & 0 & 0 \\
0 & 0 & 0 & 0 & 2+2v' & 0 \\
0 & 0 & 0 & 0 & 0 & 2+2v'
\end{bmatrix}
\begin{bmatrix} \dot{\sigma}'_{xx} \\ \dot{\sigma}'_{yy} \\ \dot{\sigma}'_{zz} \\ \dot{\sigma}_{xy} \\ \dot{\sigma}_{yz} \\ \dot{\sigma}_{zx} \end{bmatrix}
\tag{2.24}
$$

Substituting Eq. (2.21) gives:

$$
\begin{bmatrix} \dot{\varepsilon}^e_{xx} \\ \dot{\varepsilon}^e_{yy} \\ \dot{\varepsilon}^e_{zz} \\ \dot{\gamma}^e_{xy} \\ \dot{\gamma}^e_{yz} \\ \dot{\gamma}^e_{zx} \end{bmatrix}
= \frac{1}{E'}
\begin{bmatrix}
1 & -v' & -v' & 0 & 0 & 0 \\
-v' & 1 & -v' & 0 & 0 & 0 \\
-v' & -v' & 1 & 0 & 0 & 0 \\
0 & 0 & 0 & 2+2v' & 0 & 0 \\
0 & 0 & 0 & 0 & 2+2v' & 0 \\
0 & 0 & 0 & 0 & 0 & 2+2v'
\end{bmatrix}
\begin{bmatrix} \dot{\sigma}_{xx} - \dot{\sigma}_w \\ \dot{\sigma}_{yy} - \dot{\sigma}_w \\ \dot{\sigma}_{zz} - \dot{\sigma}_w \\ \dot{\sigma}_{xy} \\ \dot{\sigma}_{yz} \\ \dot{\sigma}_{zx} \end{bmatrix}
\tag{2.25}
$$

Considering slightly compressible water, the rate of pore pressure is written as:

$$\dot{\sigma}_w = \frac{K_w}{n}\left(\dot{\varepsilon}^e_{xx} + \dot{\varepsilon}^e_{yy} + \dot{\varepsilon}^e_{zz}\right) \tag{2.26}$$

in which K_w is the bulk modulus of the water and n is the soil porosity.

The inverted form of Hooke's law may be written in terms of the total stress rates and the undrained parameters E_u and ν_u:

$$
\begin{bmatrix} \dot{\varepsilon}^e_{xx} \\ \dot{\varepsilon}^e_{yy} \\ \dot{\varepsilon}^e_{zz} \\ \dot{\gamma}^e_{xy} \\ \dot{\gamma}^e_{yz} \\ \dot{\gamma}^e_{zx} \end{bmatrix} = \frac{1}{E_u} \begin{bmatrix} 1 & -\nu_u & -\nu_u & 0 & 0 & 0 \\ -\nu_u & 1 & -\nu_u & 0 & 0 & 0 \\ -\nu_u & -\nu_u & 1 & 0 & 0 & 0 \\ 0 & 0 & 0 & 2+2\nu_u & 0 & 0 \\ 0 & 0 & 0 & 0 & 2+2\nu_u & 0 \\ 0 & 0 & 0 & 0 & 0 & 2+2\nu_u \end{bmatrix} \begin{bmatrix} \dot{\sigma}'_{xx} \\ \dot{\sigma}'_{yy} \\ \dot{\sigma}'_{zz} \\ \dot{\sigma}_{xy} \\ \dot{\sigma}_{yz} \\ \dot{\sigma}_{zx} \end{bmatrix}
\tag{2.27}
$$

where:

$$
E_u = 2\,G\left(1 + \nu_u\right) \qquad\qquad \nu_u = \frac{\nu' + \mu\left(1 + \nu'\right)}{1 + 2\mu\left(1 + \nu'\right)}
\tag{2.28}
$$

$$
\mu = \frac{1}{3}\frac{K_w}{n}\,\frac{1}{K'} \qquad\qquad K' = \frac{E'}{3\left(1 - 2\nu'\right)}
\tag{2.29}
$$

Hence, the special option for undrained behaviour in PLAXIS is such that the effective parameters G and ν are transferred into undrained parameters E_u and ν_u according to Eq. (2.21) and (2.22). Note that the index u is used to indicate auxiliary parameters for undrained soil. Hence, E_u and ν_u should not be confused with E_{ur} and ν_{ur} as used to denote unloading / reloading.

Fully incompressible behaviour is obtained for $\nu_u = 0.5$. However, taking $\nu_u = 0.5$ leads to singularity of the stiffness matrix. In fact, water is not fully incompressible, but a realistic bulk modulus for water is very large. In order to avoid numerical problems caused by an extremely low compressibility, ν_u is by default taken as 0.495, which makes the undrained soil body slightly compressible. In order to ensure realistic computational results, the bulk modulus of the water must be high compared with the bulk modulus of the soil skeleton, i.e. $K_w >> n\,K'$. This condition is sufficiently ensured by requiring $\nu' \le 0.35$. Users will get a warning as soon as larger Poisson's ratios are used in combination with undrained material behaviour.

Consequently, for undrained material behaviour a bulk modulus for water is automatically added to the stiffness matrix. The value of the bulk modulus is given by:

$$
\frac{K_w}{n} = \frac{3\left(\nu_u - \nu'\right)}{\left(1 - 2\nu_u\right)\left(1 + \nu'\right)}K' = 300\,\frac{0.495 - \nu'}{1 + \nu'}K' > 30K'
\tag{2.30}
$$

at least for $v' \leq 0.35$. In retrospect it is worth mentioning here a review about the Skempton B-parameter.

Skempton B-parameter:

When the *Material type* (type of material behaviour) is set to *Undrained*, PLAXIS automatically assumes an implicit undrained bulk modulus, K_u, for the soil as a whole (soil skeleton + water) and distinguishes between total stresses, effective stresses and excess pore pressures (see Undrained behaviour):

Total stress: $\quad\quad\quad\quad \Delta p = K_u \Delta \varepsilon_v$

Effective stress: $\quad\quad\quad \Delta p' = (1 - B)\Delta p = K' \Delta \varepsilon_v$

Excess pore pressure: $\quad \Delta p_w = B\Delta p = \dfrac{K_w}{n}\Delta \varepsilon_v$

Note that effective model parameters should be entered in the material data set, i.e. E', v', c', φ' and not E_u, v_u, c_u (s_u), φ_u. The undrained bulk modulus is automatically calculated by PLAXIS using Hooke's law of elasticity:

$$K_u = \frac{2G(1+v_u)}{3(1-2v_u)} \quad\quad \text{where} \quad\quad G = \frac{E'}{2(1+v')}$$

and $\quad\quad v_u = 0.495 \quad\quad\quad\quad$ (when using the Standard setting)

or $\quad\quad v_u = \dfrac{3v' + B(1-2v')}{3 - B(1-2v')} \quad\quad$ (when using the Manual setting)

A particular value of the undrained Poisson's ratio, v_u, implies a corresponding reference bulk stiffness of the pore fluid, $K_{w,ref}/n$:

$$\frac{K_{w,ref}}{n} = K_u - K' \quad\quad \text{where} \quad\quad K' = \frac{E'}{3(1-2v')}$$

This value of $K_{w,ref}/n$ is generally much smaller than the real bulk stiffness of pure water, K_w^0 $(= 2 \cdot 10^6 \text{ kN/m}^2)$.

If the value of Skempton's B-parameter is unknown, but the degree of saturation, S, and the porosity, n, are known instead, the bulk stiffness of the pore fluid can be estimated from:

$$\frac{K_w}{n} = \frac{K_w^0 K_{air}}{SK_{air} + (1-S)K_w^0} \frac{1}{n} \qquad \text{where} \qquad K' = \frac{E'}{3(1-2v')}$$

and K_{air} = 200 kN/m^2 for air under atmospheric pressure. The value of Skempton's B-parameter can now be calculated from the ratio of the bulk stiffnesses of the soil skeleton and the pore fluid:

$$B = \frac{1}{1 + \dfrac{nK'}{K_w}}$$

The rate of excess pore pressure is calculated from the (small) volumetric strain rate, according to:

$$\dot{\sigma}_w = \frac{K_w}{n}\dot{\varepsilon}_v \tag{2.31}$$

The type of elements used in the PLAXIS are sufficiently adequate to avoid mesh locking effects for nearly incompressible materials.

This special option to model undrained material behaviour on the basis of effective model parameters is available for all material models in the PLAXIS program. This enables undrained calculations to be executed with effective input parameters, with explicit distinction between effective stresses and (excess) pore pressures.

Such an analysis requires effective soil parameters and is therefore highly convenient when such parameters are available. For soft soil projects, accurate data on effective parameters may not always be available. Instead, in situ tests and laboratory tests may have been performed to obtain undrained soil parameters. In such situations measured undrained Young's moduli can be easily converted into effective Young's moduli by:

$$E' = \frac{2(1+v')}{3}E_u \tag{2.32}$$

Undrained shear strengths, however, cannot easily be used to determine the effective strength parameters φ and c. For such projects PLAXIS offers the possibility of an undrained analysis with direct input of the undrained shear strength (c_u or s_u) and $\varphi = \varphi_u = 0°$. This option is only available for the Mohr-Coulomb model and the Hardening-Soil model, but not for the Soft Soil (Creep) model. Note that whenever the *Material type* parameter is set to *Undrained*, effective values must be entered for the elastic parameters E and v !

2.5   UNDRAINED ANALYSIS WITH UNDRAINED PARAMETERS

If, for any reason, it is desired not to use the *Undrained* option in PLAXIS to perform an undrained analysis, one may simulate undrained behaviour by selecting the *Non-porous* option and directly entering undrained elastic properties $E = E_u$ and $v = v_u = 0.495$ in combination with the undrained strength properties $c = c_u$ and $\varphi = \varphi_u = 0°$. In this case a total stress analysis is performed without distinction between effective stresses and pore pressures. Hence, all tabulated output referring to effective stresses should now be interpreted as total stresses and all pore pressures are equal to zero. In graphical output of stresses the stresses in *Non-porous* clusters are not plotted. If one does want graphical output of stresses one should select *Drained* instead of *Non-porous* for the type of material behaviour and make sure that no pore pressures are generated in these clusters.

Note that this type of approach is not possible when using the Soft Soil Creep model. In general, an effective stress analysis using the *Undrained* option in PLAXIS to simulate undrained behaviour is preferable over a total stress analysis.

2.6   THE INITIAL PRECONSOLIDATION STRESS IN ADVANCED MODELS

When using advanced models in PLAXIS an initial preconsolidation stress has to be determined. In the engineering practice it is common to use a vertical preconsolidation stress, σ_p, but PLAXIS needs an equivalent isotropic preconsolidation stress, p_p^{eq} to determine the initial position of a cap-type yield surface. If a material is overconsolidated, information is required about the Over-Consolidation Ratio (*OCR*), i.e. the ratio of the greatest vertical stress previously reached, σ_p (see Figure 2.5), and the in-situ effective vertical stress, $\sigma_{yy}'^0$.

$$OCR = \frac{\sigma_p}{\sigma'^0_{yy}} \qquad (2.33)$$

It is also possible to specify the initial stress state using the Pre-Overburden Pressure (*POP*) as an alternative to prescribing the overconsolidation ratio. The Pre-Overburden Pressure is defined by:

$$POP = |\sigma_p - \sigma'^0_{yy}| \qquad (2.34)$$

These two ways of specifying the vertical preconsolidation stress are illustrated in Figure 2.5.
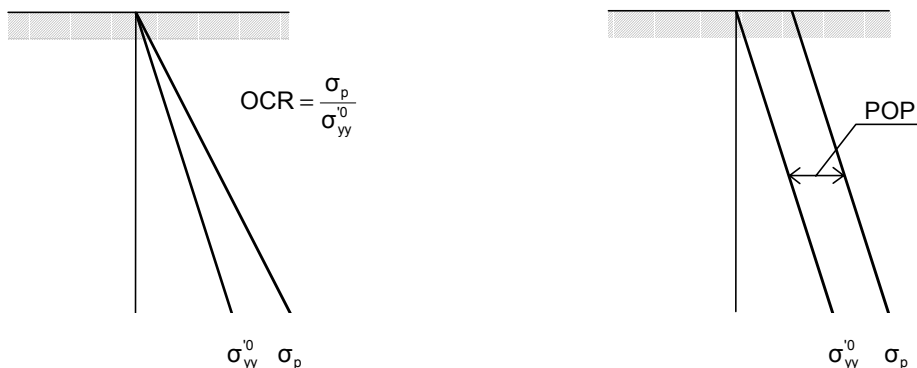
Figure 2.5   Illustration of vertical preconsolidation stress in relation to the in-situ vertical stress. 2.5a. Using *OCR*; 2.5b. Using *POP*

The pre-consolidation stress σ_p is used to compute $p_p{}^{eq}$ which determines the initial position of a cap-type yield surface in the advanced soil models. The calculation of $p_p{}^{eq}$ is based on the stress state:

$$\sigma'_1 = \sigma_p \qquad \text{and:} \qquad \sigma'_2 = \sigma'_3 = K_0^{NC} \sigma_p \qquad (2.35)$$

Where K_0^{NC} is the K_0-value associated with normally consolidated states of stress. For the Hardening-Soil model the default parameter settings is such that we have the Jaky formula $K_0^{NC} \approx 1 - \sin\varphi$. For the Soft-Soil-Creep model, the default setting is slightly different, but differences with the Jaky correlation are modest.

2.7   ON THE INITIAL STRESSES

In overconsolidated soils the coefficient of lateral earth pressure is larger than for normally consolidated soils. This effect is automatically taken into account for advanced soil models when generating the initial stresses using the K_0-procedure. The procedure that is followed here is described below.

Consider a one-dimensional compression test, preloaded to $\sigma_{yy}'=\sigma_p$ and subsequently unloaded to $\sigma_{yy}' = \sigma_{yy}'^0$. During unloading the sample behaves elastically and the incremental stress ratio is, according to Hooke's law, given by (see Figure 2.6):

$$\frac{\Delta\sigma'_{xx}}{\Delta\sigma'_{yy}} = \frac{K_0^{NC}\sigma_p - \sigma'^0_{xx}}{\sigma_p - \sigma'^0_{yy}} = \frac{K_0^{NC}OCR\sigma'^0_{yy} - \sigma'^0_{xx}}{(OCR-1)\sigma'^0_{yy}} = \frac{\nu_{ur}}{1-\nu_{ur}} \qquad (2.36)$$

where K_0^{nc} is the stress ratio in the normally consolidated state. Hence, the stress ratio of the overconsolidated soil sample is given by:

$$\frac{\sigma'^0_{xx}}{\sigma'^0_{yy}} = K_0^{NC} \; OCR \; - \; \frac{\nu_{ur}}{1 - \nu_{ur}} \; (OCR - 1) \qquad (2.37)$$

The use of a small Poisson's ratio, as discussed previously, will lead to a relatively large ratio of lateral stress and vertical stress, as generally observed in overconsolidated soils. Note that Eq. (2.37) is only valid in the elastic domain, because the formula was derived from Hooke's law of elasticity. If a soil sample is unloaded by a large amount, resulting in a high degree of overconsolidation, the stress ratio will be limited by the Mohr-Coulomb failure condition.
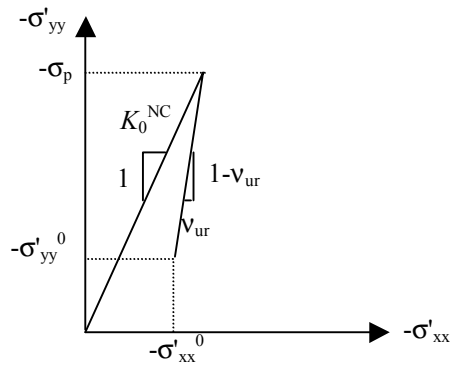
Figure 2.6   Overconsolidated stress state obtained from primary loading and subsequent unloading

3   THE MOHR-COULOMB MODEL (PERFECT-PLASTICITY)

Plasticity is associated with the development of irreversible strains. In order to evaluate whether or not plasticity occurs in a calculation, a yield function, f, is introduced as a function of stress and strain. A yield function can often be presented as a surface in principal stress space. A perfectly-plastic model is a constitutive model with a fixed yield surface, i.e. a yield surface that is fully defined by model parameters and not affected by (plastic) straining. For stress states represented by points within the yield surface, the behaviour is purely elastic and all strains are reversible.

3.1   ELASTIC PERFECTLY-PLASTIC BEHAVIOUR

The basic principle of elastoplasticity is that strains and strain rates are decomposed into an elastic part and a plastic part:

$$\underline{\varepsilon} = \underline{\varepsilon}^e + \underline{\varepsilon}^p \qquad\qquad \underline{\dot{\varepsilon}} = \underline{\dot{\varepsilon}}^e + \underline{\dot{\varepsilon}}^p \qquad\qquad (3.1)$$

Hooke's law is used to relate the stress rates to the elastic strain rates. Substitution of Eq. (3.1) into Hooke's law (2.18) leads to:

$$\underline{\dot{\sigma}}' = \underline{\underline{D}}^e \, \underline{\dot{\varepsilon}}^e = \underline{\underline{D}}^e \left(\underline{\dot{\varepsilon}} - \underline{\dot{\varepsilon}}^p \right) \qquad\qquad (3.2)$$

According to the classical theory of plasticity (Hill, 1950), plastic strain rates are proportional to the derivative of the yield function with respect to the stresses. This means that the plastic strain rates can be represented as vectors perpendicular to the yield surface. This classical form of the theory is referred to as associated plasticity. However, for Mohr-Coulomb type yield functions, the theory of associated plasticity leads to an overprediction of dilatancy. Therefore, in addition to the yield function, a plastic potential function g is introduced. The case $g \neq f$ is denoted as non-associated plasticity. In general, the plastic strain rates are written as:

$$\underline{\dot{\varepsilon}}^p = \lambda \frac{\partial g}{\partial \underline{\sigma}'} \qquad\qquad (3.3)$$

in which λ is the plastic multiplier. For purely elastic behaviour λ is zero, whereas in the case of plastic behaviour λ is positive:

$$\lambda = 0 \quad \text{for:} \quad f < 0 \quad \text{or:} \quad \frac{\partial f}{\partial \underline{\sigma}'}^T \underline{\underline{D}}^e \, \underline{\dot{\varepsilon}} \leq 0 \qquad \text{(Elasticity)} \quad (3.4a)$$

$$\lambda > 0 \quad \text{for:} \quad f = 0 \quad \text{and:} \quad \frac{\partial f}{\partial \underline{\sigma}'}^T \underline{\underline{D}}^e \, \underline{\dot{\varepsilon}} > 0 \qquad \text{(Plasticity)} \quad (3.4b)$$
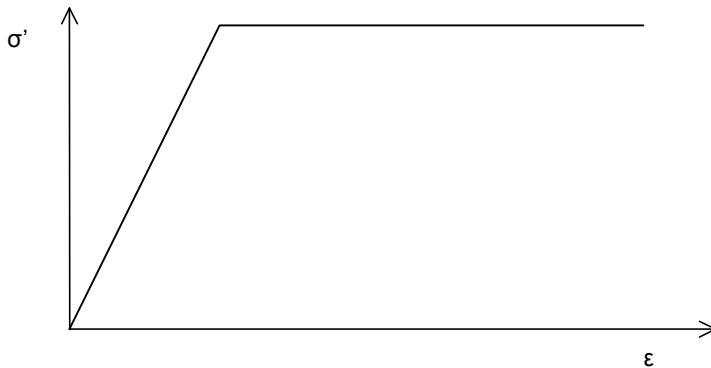
Figure 3.1 Basic idea of an elastic perfectly plastic model

These equations may be used to obtain the following relationship between the effective stress rates and strain rates for elastoplasticity (Smith & Griffith, 1982; Vermeer & de Borst, 1984):

$$\underline{\dot{\sigma}}' = \left(\underline{\underline{D}}^e - \frac{\alpha}{d} \underline{\underline{D}}^e \frac{\partial g}{\partial \underline{\sigma}'} \frac{\partial f}{\partial \underline{\sigma}'}^{T} \underline{\underline{D}}^e \right) \underline{\dot{\varepsilon}} \tag{3.5a}$$

where:

$$d = \frac{\partial f}{\partial \underline{\sigma}'}^{T} \underline{\underline{D}}^e \frac{\partial g}{\partial \underline{\sigma}'} \tag{3.5b}$$

The parameter α is used as a switch. If the material behaviour is elastic, as defined by Eq. (3.4a), the value of α is equal to zero, whilst for plasticity, as defined by Eq. (3.4b), the value of α is equal to unity.

The above theory of plasticity is restricted to smooth yield surfaces and does not cover a multi surface yield contour as present in the Mohr-Coulomb model. For such a yield surface the theory of plasticity has been extended by Koiter (1960) and others to account for flow vertices involving two or more plastic potential functions:

$$\underline{\dot{\varepsilon}}^p = \lambda_1 \frac{\partial g_1}{\partial \underline{\sigma}'} + \lambda_2 \frac{\partial g_2}{\partial \underline{\sigma}'} + ... \tag{3.6}$$

Similarly, several quasi independent yield functions ($f_1, f_2, ...$) are used to determine the magnitude of the multipliers ($\lambda_1, \lambda_2, ...$).

3.2   FORMULATION OF THE MOHR-COULOMB MODEL

The Mohr-Coulomb yield condition is an extension of Coulomb's friction law to general states of stress. In fact, this condition ensures that Coulomb's friction law is obeyed in any plane within a material element.

The full Mohr-Coulomb yield condition consists of six yield functions when formulated in terms of principal stresses (see for instance Smith & Griffith, 1982):

$$f_{1a} = \tfrac{1}{2}\left(\sigma'_2 - \sigma'_3\right) + \tfrac{1}{2}\left(\sigma'_2 + \sigma'_3\right)\sin\varphi - c\,\cos\varphi \le 0 \tag{3.7a}$$

$$f_{1b} = \tfrac{1}{2}\left(\sigma'_3 - \sigma'_2\right) + \tfrac{1}{2}\left(\sigma'_3 + \sigma'_2\right)\sin\varphi - c\,\cos\varphi \le 0 \tag{3.7b}$$

$$f_{2a} = \tfrac{1}{2}\left(\sigma'_3 - \sigma'_1\right) + \tfrac{1}{2}\left(\sigma'_3 + \sigma'_1\right)\sin\varphi - c\,\cos\varphi \le 0 \tag{3.7c}$$

$$f_{2b} = \tfrac{1}{2}\left(\sigma'_1 - \sigma'_3\right) + \tfrac{1}{2}\left(\sigma'_1 + \sigma'_3\right)\sin\varphi - c\,\cos\varphi \le 0 \tag{3.7d}$$

$$f_{3a} = \tfrac{1}{2}\left(\sigma'_1 - \sigma'_2\right) + \tfrac{1}{2}\left(\sigma'_1 + \sigma'_2\right)\sin\varphi - c\,\cos\varphi \le 0 \tag{3.7e}$$

$$f_{3b} = \tfrac{1}{2}\left(\sigma'_2 - \sigma'_1\right) + \tfrac{1}{2}\left(\sigma'_2 + \sigma'_1\right)\sin\varphi - c\,\cos\varphi \le 0 \tag{3.7f}$$
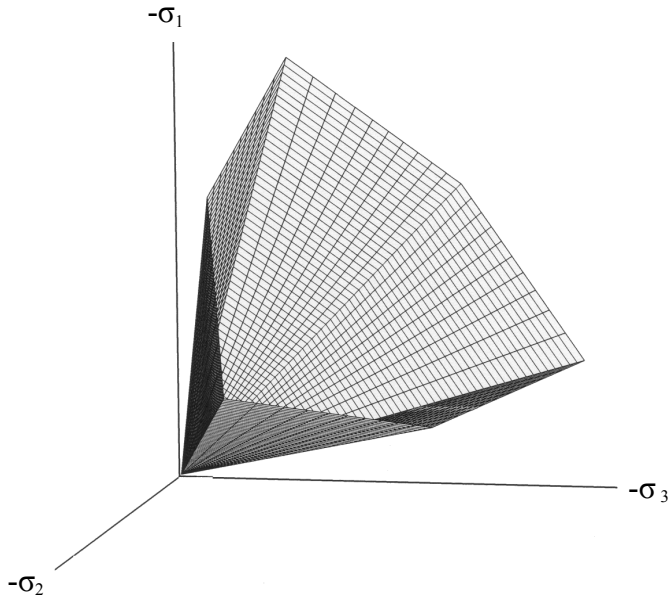

Figure 3.2 The Mohr-Coulomb yield surface in principal stress space ($c = 0$)

The two plastic model parameters appearing in the yield functions are the well-known friction angle φ and the cohesion c. These yield functions together represent a hexagonal cone in principal stress space as shown in Figure 3.2.

In addition to the yield functions, six plastic potential functions are defined for the Mohr-Coulomb model:

$$g_{1a} = \tfrac{1}{2}\left(\sigma'_2 - \sigma'_3\right) + \tfrac{1}{2}\left(\sigma'_2 + \sigma'_3\right)\sin\psi \tag{3.8a}$$

$$g_{1b} = \tfrac{1}{2}\left(\sigma'_3 - \sigma'_2\right) + \tfrac{1}{2}\left(\sigma'_3 + \sigma'_2\right)\sin\psi \tag{3.8b}$$

$$g_{2a} = \tfrac{1}{2}\left(\sigma'_3 - \sigma'_1\right) + \tfrac{1}{2}\left(\sigma'_3 + \sigma'_1\right)\sin\psi \tag{3.8c}$$

$$g_{2b} = \tfrac{1}{2}\left(\sigma'_1 - \sigma'_3\right) + \tfrac{1}{2}\left(\sigma'_1 + \sigma'_3\right)\sin\psi \tag{3.8d}$$

$$g_{3a} = \tfrac{1}{2}\left(\sigma'_1 - \sigma'_2\right) + \tfrac{1}{2}\left(\sigma'_1 + \sigma'_2\right)\sin\psi \tag{3.8e}$$

$$g_{3b} = \tfrac{1}{2}\left(\sigma'_2 - \sigma'_1\right) + \tfrac{1}{2}\left(\sigma'_2 + \sigma'_1\right)\sin\psi \tag{3.8f}$$

The plastic potential functions contain a third plasticity parameter, the dilatancy angle ψ. This parameter is required to model positive plastic volumetric strain increments (dilatancy) as actually observed for dense soils. A discussion of all of the model parameters used in the Mohr-Coulomb model is given at the end of this section.

When implementing the Mohr-Coulomb model for general stress states, special treatment is required for the intersection of two yield surfaces. Some programs use a smooth transition from one yield surface to another, i.e. the rounding-off of the corners (see for example Smith & Griffith, 1982). In PLAXIS, however, the exact form of the full Mohr-Coulomb model is implemented, using a sharp transition from one yield surface to another. For a detailed description of the corner treatment the reader is referred to the literature (Koiter, 1960; van Langen & Vermeer, 1990).

For $c > 0$, the standard Mohr-Coulomb criterion allows for tension. In fact, allowable tensile stresses increase with cohesion. In reality, soil can sustain none or only very small tensile stresses. This behaviour can be included in a PLAXIS analysis by specifying a tension cut-off. In this case, Mohr circles with positive principal stresses are not allowed. The tension cut-off introduces three additional yield functions, defined as:

$$f_4 = \sigma_1' - \sigma_t \leq 0 \tag{3.9a}$$

$$f_5 = \sigma_2' - \sigma_t \leq 0 \tag{3.9b}$$

$$f_6 = \sigma_3' - \sigma_t \leq 0 \tag{3.9c}$$

When this tension cut-off procedure is used, the allowable tensile stress, σ_t, is, by default, taken equal to zero. For these three yield functions an associated flow rule is adopted. For stress states within the yield surface, the behaviour is elastic and obeys Hooke's law for isotropic linear elasticity, as discussed in Section 2.2. Hence, besides the plasticity parameters c, φ, and ψ, input is required on the elastic Young's modulus E and Poisson's ratio v.

3.3   BASIC PARAMETERS OF THE MOHR-COULOMB MODEL

The Mohr-Coulomb model requires a total of five parameters, which are generally familiar to most geotechnical engineers and which can be obtained from basic tests on soil samples. These parameters with their standard units are listed below:

E : Young's modulus [kN/m^2]

v : Poisson's ratio [-]

φ : Friction angle [°]

c : Cohesion [kN/m^2]
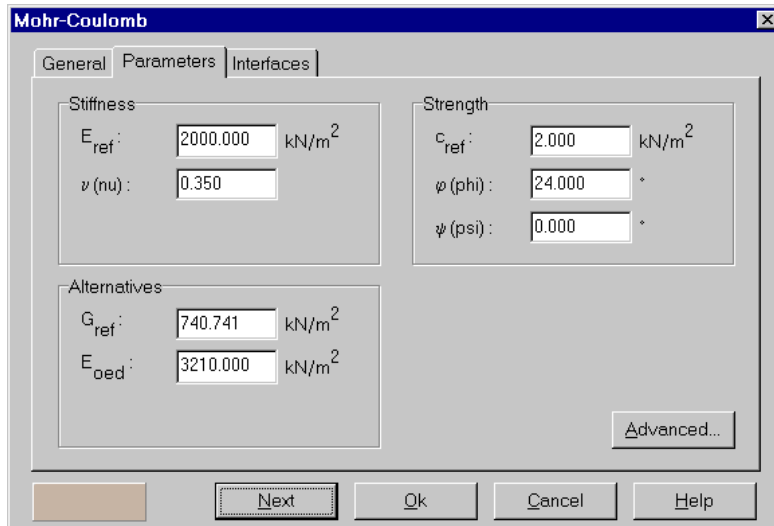
ψ : Dilatancy angle [°]

Figure 3.3 Parameter tab sheet for Mohr-Coulomb model

Young's modulus (E)

PLAXIS uses the Young's modulus as the basic stiffness modulus in the elastic model and the Mohr-Coulomb model, but some alternative stiffness moduli are displayed as well. A stiffness modulus has the dimension of stress. The values of the stiffness parameter adopted in a calculation require special attention as many geomaterials show a non-linear behaviour from the very beginning of loading. In soil mechanics the initial slope is usually indicated as E_0 and the secant modulus at 50% strength is denoted as E_{50} (see Figure 3.4). For materials with a large linear elastic range it is realistic to use E_0, but for loading of soils one generally uses E_{50}. Considering unloading problems, as in the case of tunnelling and excavations, one needs E_{ur} instead of E_{50}.
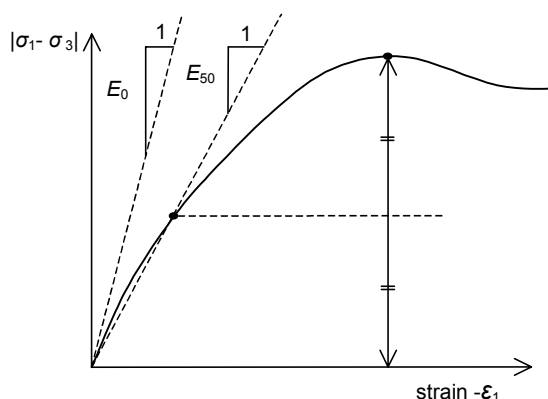
Figure 3.4 Definition of E_0 and E_{50} for standard drained triaxial test results

For soils, both the unloading modulus, E_{ur}, and the first loading modulus, E_{50}, tend to increase with the confining pressure. Hence, deep soil layers tend to have greater stiffness than shallow layers. Moreover, the observed stiffness depends on the stress path that is followed. The stiffness is much higher for unloading and reloading than for primary loading. Also, the observed soil stiffness in terms of a Young's modulus may be lower for (drained) compression than for shearing. Hence, when using a constant stiffness modulus to represent soil behaviour one should choose a value that is consistent with the stress level and the stress path development. Note that some stress-dependency of soil behaviour is taken into account in the advanced models in PLAXIS, which are described in Chapters 5 and 6. For the Mohr-Coulomb model, PLAXIS offers a special option for the input of a stiffness increasing with depth (see Section 3.4).

Poisson's ratio (ν)

Standard drained triaxial tests may yield a significant rate of volume decrease at the very beginning of axial loading and, consequently, a low initial value of Poisson's ratio (ν_0). For some cases, such as particular unloading problems, it may be realistic to use such a

low initial value, but in general when using the Mohr-Coulomb model the use of a higher value is recommended.

The selection of a Poisson's ratio is particularly simple when the elastic model or Mohr-Coulomb model is used for gravity loading (increasing $\Sigma Mweight$ from 0 to 1 in a plastic calculation). For this type of loading PLAXIS should give realistic ratios of $K_0 = \sigma_h / \sigma_v$. As both models will give the well-known ratio of $\sigma_h / \sigma_v = \nu / (1-\nu)$ for one-dimensional compression it is easy to select a Poisson's ratio that gives a realistic value of K_0. Hence, ν is evaluated by matching K_0. This subject is treated more extensively in Appendix A of the Reference Manual, which deals with initial stress distributions. In many cases one will obtain ν values in the range between 0.3 and 0.4. In general, such values can also be used for loading conditions other than one-dimensional compression. For unloading conditions, however, it is more common to use values in the range between 0.15 and 0.25.

Cohesion (c)

The cohesive strength has the dimension of stress. PLAXIS can handle cohesionless sands ($c = 0$), but some options will not perform well. To avoid complications, non-experienced users are advised to enter at least a small value (use $c > 0.2$ kPa).

PLAXIS offers a special option for the input of layers in which the cohesion increases with depth (see Section 3.4).

Friction angle (φ)

The friction angle, φ (phi), is entered in degrees. High friction angles, as sometimes obtained for dense sands, will substantially increase plastic computational effort.
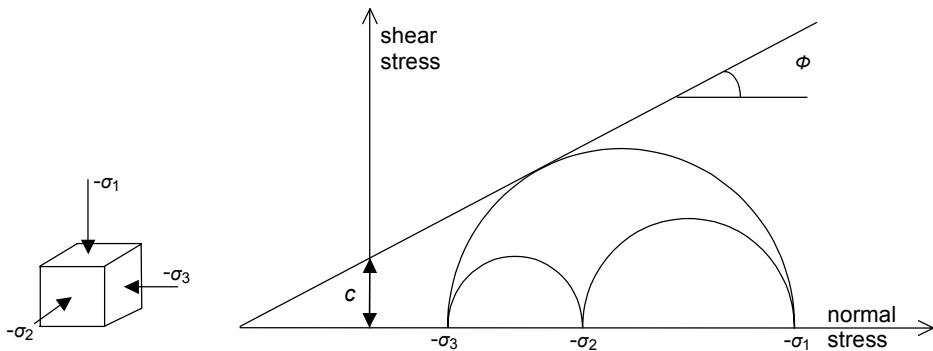

Figure 3.5 Stress circles at yield; one touches Coulomb's envelope

The computing time increases more or less exponentially with the friction angle. Hence, high friction angles should be avoided when performing preliminary computations for a particular project. The friction angle largely determines the shear strength as shown in

Figure 3.5 by means of Mohr's stress circles. A more general representation of the yield criterion is shown in Figure 3.2. The Mohr-Coulomb failure criterion proves to be better for describing soil behaviour than the Drucker-Prager approximation, as the latter failure surface tends to be highly inaccurate for axisymmetric configurations.

Dilatancy angle (ψ)

The dilatancy angle, ψ (psi), is specified in degrees. Apart from heavily over-consolidated layers, clay soils tend to show little dilatancy ($\psi \approx 0$). The dilatancy of sand depends on both the density and on the friction angle. For quartz sands the order of magnitude is $\psi \approx \varphi$ - 30°. For φ-values of less than 30°, however, the angle of dilatancy is mostly zero. A small negative value for ψ is only realistic for extremely loose sands. For further information about the link between the friction angle and dilatancy, see Bolton (1986).

3.4   ADVANCED PARAMETERS OF THE MOHR-COULOMB MODEL

When using the Mohr-Coulomb model, the <Advanced> button in the *Parameters* tab sheet may be clicked to enter some additional parameters for advanced modelling features. As a result, an additional window appears as shown in Figure 3.6. The advanced features comprise the increase of stiffness and cohesive strength with depth and the use of a tension cut-off. In fact, the latter option is used by default, but it may be deactivated here, if desired.
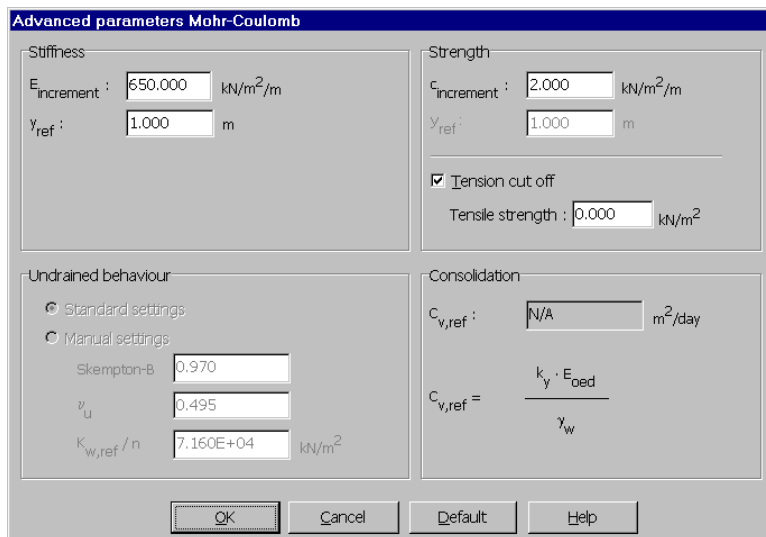

Figure 3.6 Advanced Mohr-Coulomb parameters window

Increase of stiffness ($E_{increment}$)

In real soils, the stiffness depends significantly on the stress level, which means that the stiffness generally increases with depth. When using the Mohr-Coulomb model, the stiffness is a constant value. In order to account for the increase of the stiffness with depth the $E_{increment}$-value may be used, which is the increase of the Young's modulus per unit of depth (expressed in the unit of stress per unit depth). At the level given by the y_{ref} parameter, the stiffness is equal to the reference Young's modulus, E_{ref}, as entered in the *Parameters* tab sheet. The actual value of Young's modulus in the stress points is obtained from the reference value and $E_{increment}$. Note that during calculations a stiffness increasing with depth does not change as a function of the stress state.

Increase of cohesion ($c_{increment}$)

PLAXIS offers an advanced option for the input of clay layers in which the cohesion increases with depth. In order to account for the increase of the cohesion with depth the $c_{increment}$-value may be used, which is the increase of cohesion per unit of depth (expressed in the unit of stress per unit depth). At the level given by the y_{ref} parameter, the cohesion is equal to the (reference) cohesion, c_{ref}, as entered in the *Parameters* tab sheet. The actual value of cohesion in the stress points is obtained from the reference value and $c_{increment}$.

Tension cut-off

In some practical problems an area with tensile stresses may develop. According to the Coulomb envelope shown in Figure 3.5 this is allowed when the shear stress (radius of Mohr circle) is sufficiently small. However, the soil surface near a trench in clay sometimes shows tensile cracks. This indicates that soil may also fail in tension instead of in shear. Such behaviour can be included in PLAXIS analysis by selecting the tension cut-off. In this case Mohr circles with positive principal stresses are not allowed. When selecting the tension cut-off the allowable tensile strength may be entered. For the Mohr-Coulomb model and the Hardening-Soil model the tension cut-off is, by default, selected with a tensile strength of zero.

4   THE JOINTED ROCK MODEL (ANISOTROPY)

Materials may have different properties in different directions. As a result, they may respond differently when subjected to particular conditions in one direction or another. This aspect of material behaviour is called anisotropy. When modelling anisotropy, distinction can be made between elastic anisotropy and plastic anisotropy. Elastic anisotropy refers to the use of different elastic stiffness properties in different directions. Plastic anisotropy may involve the use of different strength properties in different directions, as considered in the Jointed Rock model. Another form of plastic anisotropy is kinematic hardening. The latter is not considered in PLAXIS program.
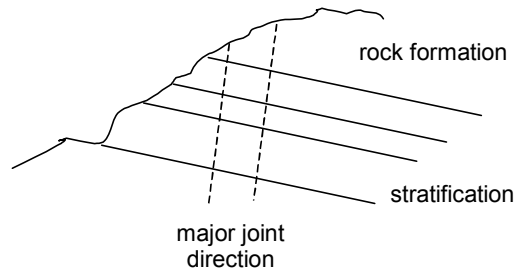

Figure 4.1 Visualization of concept behind the Jointed Rock model

The Jointed Rock model is an anisotropic elastic perfectly-plastic model, especially meant to simulate the behaviour of stratified and jointed rock layers. In this model it is assumed that there is intact rock with an eventual stratification direction and major joint directions. The intact rock is considered to behave as a transversly anisotropic elastic material, quantified by five parameters and a direction. The anisotropy may result from stratification or from other phenomena. In the major joint directions it is assumed that shear stresses are limited according to Coulomb's criterion. Upon reaching the maximum shear stress in such a direction, plastic sliding will occur. A maximum of three sliding directions ('planes') can be defined, of which the first plane is assumed to coincide with the direction of elastic anisotropy. Each plane may have different shear strength properties. In addition to plastic shearing, the tensile stresses perpendicular to the three planes are limited according to a predefined tensile strength (tension cut-off).

The application of the Jointed Rock model is justified when families of joints or joint sets are present. These joint sets have to be parallel, not filled with fault gouge, and their spacing has to be small compared to the characteristic dimension of the structure.

Some basic characteristics of the Jointed Rock model are:

- Anisotropic elastic behaviour for intact rock   Parameters E_1, E_2, v_1, v_2, G_2

- Shear failure according to Coulomb in three directions, i Parameters c_i, φ_i and ψ_i

- Limited tensile strength in three directions, i Parameters $\sigma_{t,i}$

4.1   ANISOTROPIC ELASTIC MATERIAL STIFFNESS MATRIX

The elastic material behaviour in the Jointed Rock model is described by an elastic material stiffness matrix, $\underline{D}^*$. In contrast to Hooke's law, the D^*-matrix as used in the Jointed Rock model is transversely anisotropic. Different stiffnesses can be used normal to and in a predefined direction ('plane 1'). This direction may correspond to the stratification direction or to any other direction with significantly different elastic stiffness properties.

Consider, for example, a horizontal stratification, where the stiffness in horizontal direction, E_1, is different from the stiffness in vertical direction, E_2. In this case the 'Plane 1' direction is parallel to the x-z-plane and the following constitutive relations exist (See: Zienkiewicz & Taylor: The Finite Element Method, 4th Ed.):

$$\dot{\varepsilon}_{xx} = \frac{\dot{\sigma}_{xx}}{E_1} - \frac{v_2\dot{\sigma}_{yy}}{E_2} - \frac{v_1\dot{\sigma}_{zz}}{E_1} \tag{4.1a}$$

$$\dot{\varepsilon}_{yy} = -\frac{v_2\dot{\sigma}_{xx}}{E_2} + \frac{\dot{\sigma}_{yy}}{E_2} - \frac{v_2\dot{\sigma}_{zz}}{E_2} \tag{4.1b}$$

$$\dot{\varepsilon}_{zz} = -\frac{v_1\dot{\sigma}_{xx}}{E_1} - \frac{v_2\dot{\sigma}_{yy}}{E_2} + \frac{\dot{\sigma}_{zz}}{E_1} \tag{4.1c}$$

$$\dot{\gamma}_{xy} = \frac{\dot{\sigma}_{xy}}{G_2} \tag{4.1d}$$

$$\dot{\gamma}_{yz} = \frac{\dot{\sigma}_{yz}}{G_2} \tag{4.1e}$$

$$\dot{\gamma}_{zx} = \frac{2(1+v_1)\dot{\sigma}_{zx}}{E_1} \tag{4.1f}$$

The inverse of the anisotropic elastic material stiffness matrix, $(\underline{D}^*)^{-1}$, follows from the above relations. This matrix is symmetric. The regular material stiffness matrix $\underline{D}^*$ can only be obtained by numerical inversion.

In general, the stratification plane will not be parallel to the global x-z-plane, but the above relations will generally hold for a local (n,s,t) coordinate system where the stratification plane is parallel to the s-t-plane. The orientation of this plane is defined by the *dip angle* and *dip direction* (see 4.3). As a consequence, the local material stiffness matrix has to be transformed from the local to the global coordinate system. Therefore we consider first a transformation of stresses and strains:

$$\underline{\sigma}_{nst} = \underline{\underline{R}}_{\sigma} \ \underline{\sigma}_{xyz} \qquad\qquad \underline{\sigma}_{xyz} = \underline{\underline{R}}_{\sigma}^{-1} \ \underline{\sigma}_{nst} \qquad\qquad (4.2a)$$

$$\underline{\varepsilon}_{nst} = \underline{\underline{R}}_{\varepsilon} \ \underline{\varepsilon}_{xyz} \qquad\qquad \underline{\varepsilon}_{xyz} = \underline{\underline{R}}_{\varepsilon}^{-1} \ \underline{\varepsilon}_{nst} \qquad\qquad (4.2b)$$

where

$$\underline{\underline{R}}_{\sigma} = \begin{bmatrix} n_x^2 & n_y^2 & n_z^2 & 2\ n_x\ n_y & 2\ n_y\ n_z & 2\ n_x\ n_z \\ s_x^2 & s_y^2 & s_z^2 & 2\ s_x\ s_y & 2\ s_y\ s_z & 2\ s_x\ s_z \\ t_x^2 & t_y^2 & t_z^2 & 2\ t_x\ t_y & 2\ t_y\ t_z & 2\ t_x\ t_z \\ n_x\ s_x & n_y\ s_y & n_z\ s_z & n_x\ s_y+n_y\ s_x & n_y\ s_z+n_z\ s_y & n_z\ s_x+n_x\ s_z \\ s_x\ t_x & s_y\ t_y & s_z\ t_z & s_x\ t_y+s_y\ t_x & s_y\ t_z+s_z\ t_y & s_x\ t_z+s_z\ t_x \\ n_x\ t_x & n_y\ t_y & n_z\ t_z & n_x\ t_y+n_y\ t_x & n_y\ t_z+n_z\ t_y & n_z\ t_x+n_x\ t_z \end{bmatrix} \qquad (4.3)$$

and

$$\underline{\underline{R}}_{\varepsilon} = \begin{bmatrix} n_x^2 & n_y^2 & n_z^2 & n_x\ n_y & n_y\ n_z & n_x\ n_z \\ s_x^2 & s_y^2 & s_z^2 & s_x\ s_y & s_y\ s_z & s_x\ s_z \\ t_x^2 & t_y^2 & t_z^2 & t_x\ t_y & t_y\ t_z & t_x\ t_z \\ 2\ n_x\ s_x & 2\ n_y\ s_y & 2\ n_z\ s_z & n_x\ s_y+n_y\ s_x & n_y\ s_z+n_z\ s_y & n_z\ s_x+n_x\ s_z \\ 2\ s_x\ t_x & 2\ s_y\ t_y & 2\ s_z\ t_z & s_x\ t_y+s_y\ t_x & s_y\ t_z+s_z\ t_y & s_x\ t_z+s_z\ t_x \\ 2\ n_x\ t_x & 2\ n_y\ t_y & 2\ n_z\ t_z & n_x\ t_y+n_y\ t_x & n_y\ t_z+n_z\ t_y & n_z\ t_x+n_x\ t_z \end{bmatrix} \ (4.4)$$

n_x, n_y, n_z, s_x, s_y, s_z, t_x, t_y and t_z are the components of the normalized n, s and t-vectors in global (x,y,z)-coordinates (i.e. 'sines' and 'cosines'; see 4.3). For plane condition $n_z = s_z = t_x = t_y = 0$ and $t_z = 1$.

It further holds that :

$$\underline{\underline{R}}_{\varepsilon}^{T} = \underline{\underline{R}}_{\sigma}^{-1} \qquad\qquad \underline{\underline{R}}_{\sigma}^{T} = \underline{\underline{R}}_{\varepsilon}^{-1} \qquad\qquad (4.5)$$

A local stress-strain relationship in (n,s,t)-coordinates can be transformed to a global relationship in (x,y,z)-coordinates in the following way:

$$\left. \begin{aligned} \underline{\sigma}_{nst} &= \underline{\underline{D}}_{nst}^{*} \ \underline{\varepsilon}_{nst} \\ \underline{\sigma}_{nst} &= \underline{\underline{R}}_{\sigma} \ \underline{\sigma}_{xyz} \\ \underline{\varepsilon}_{nst} &= \underline{\underline{R}}_{\varepsilon} \ \underline{\varepsilon}_{xyz} \end{aligned} \right\} \qquad \Rightarrow \qquad \underline{\underline{R}}_{\sigma} \ \underline{\sigma}_{xyz} = \underline{\underline{D}}_{nst}^{*} \ \underline{\underline{R}}_{\varepsilon} \ \underline{\varepsilon}_{xyz} \qquad (4.6)$$

Hence,

$$\underline{\sigma}_{xyz} = \underline{\underline{R}}_{\sigma}^{-1} \; \underline{\underline{D}}_{nst}^{*} \; \underline{\underline{R}}_{\varepsilon} \; \underline{\varepsilon}_{xyz} \tag{4.7}$$

Using to above condition (4.5):

$$\underline{\sigma}_{xyz} = \underline{\underline{R}}_{\varepsilon}^{T} \; \underline{\underline{D}}_{nst}^{*} \; \underline{\underline{R}}_{\varepsilon} \; \underline{\varepsilon}_{xyz} = \underline{\underline{D}}_{xyz}^{*} \; \underline{\varepsilon}_{xyz} \quad \text{or} \quad \underline{\underline{D}}_{xyz}^{*} = \underline{\underline{R}}_{\varepsilon}^{T} \; \underline{\underline{D}}_{nst}^{*} \; \underline{\underline{R}}_{\varepsilon} \tag{4.8}$$

Actually, not the D^{*}-matrix is given in local coordinates but the inverse matrix $(\underline{D}^{*})^{-1}$.

$$\left. \begin{array}{l} \underline{\varepsilon}_{nst} = \underline{\underline{D}}_{nst}^{*}{}^{-1} \; \underline{\sigma}_{nst} \\[4pt] \underline{\sigma}_{nst} = \underline{\underline{R}}_{\sigma} \; \underline{\sigma}_{xyz} \\[4pt] \underline{\varepsilon}_{nst} = \underline{\underline{R}}_{\varepsilon} \; \underline{\varepsilon}_{xyz} \end{array} \right\} \quad \Rightarrow \underline{\varepsilon}_{xyz} = \underline{\underline{R}}_{\varepsilon}^{-1} \; \underline{\underline{D}}_{nst}^{*}{}^{-1} \; \underline{\underline{R}}_{\sigma} \; \underline{\sigma}_{xyz} = \underline{\underline{R}}_{\sigma}^{T} \; \underline{\underline{D}}_{nst}^{*}{}^{-1} \; \underline{\underline{R}}_{\sigma} \; \underline{\sigma}_{xyz} \tag{4.9}$$

Hence,

$$\underline{\underline{D}}_{xyz}^{*}{}^{-1} = \underline{\underline{R}}_{\sigma}^{T} \; \underline{\underline{D}}_{nst}^{*}{}^{-1} \; \underline{\underline{R}}_{\sigma} \quad \text{or} \quad \underline{\underline{D}}_{xyz}^{*} = \left[\; \underline{\underline{R}}_{\sigma}^{T} \; \underline{\underline{D}}_{nst}^{*}{}^{-1} \; \underline{\underline{R}}_{\sigma} \; \right]^{-1} \tag{4.10}$$

Instead of inverting the $(\underline{D}_{nst}^{*})^{-1}$-matrix in the first place, the transformation is considered first, after which the total is numerically inverted to obtain the global material stiffness matrix $\underline{D}_{xyz}^{*}$.

4.2   PLASTIC BEHAVIOUR IN THREE DIRECTIONS

A maximum of 3 sliding directions (sliding planes) can be defined in the Jointed Rock model. The first sliding plane corresponds to the direction of elastic anisotropy. In addition, a maximum of two other sliding directions may be defined. However, the formulation of plasticity on all planes is similar. On each plane a local Coulomb condition applies to limit the shear stress, $|\tau|$. Moreover, a tension cut-off criterion is used to limit the tensile stress on a plane. Each plane, i, has its own strength parameters c_i, ϕ_i, ψ_i and $\sigma_{t,i}$.

In order to check the plasticity conditions for a plane with local (n,s,t)-coordinates it is necessary to calculate the local stresses from the Cartesian stresses. The local stresses involve three components, i.e. a normal stress component, σ_n, and two independent shear stress components, τ_s and τ_t.

$$\underline{\sigma}_i = \underline{\underline{T}}_i^{T} \; \underline{\sigma} \tag{4.11}$$

where

$$\underline{\sigma}_i = \begin{pmatrix} \sigma_n & \tau_s & \tau_t \end{pmatrix}^T \qquad (4.12a)$$

$$\underline{\sigma} = \begin{pmatrix} \sigma_{xx} & \sigma_{yy} & \sigma_{zz} & \sigma_{xy} & \sigma_{yz} & \sigma_{zx} \end{pmatrix}^T \qquad (4.12b)$$

$\underline{\underline{T}}_i^T$ = transformation matrix (3x6), for plane i

As usual in PLAXIS, tensile (normal) stresses are defined as positive whereas compression is defined as negative.
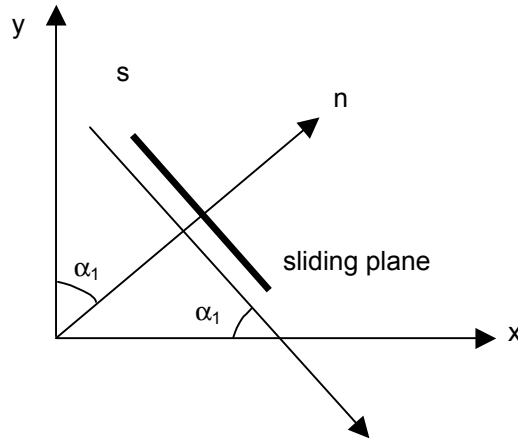
Figure 4.2 Plane strain situation with a single sliding plane and vectors n, s

Consider a plane strain situation as visualized in Figure 4.2. Here a sliding plane is considered under an angle α_1 (= *dip angle*) with respect to the *x*-axis. In this case the transformation matrix $\underline{\underline{T}}^T$ becomes:

$$T^T = \begin{bmatrix} s^2 & c^2 & 0 & -2sc & 0 & 0 \\ sc & -sc & 0 & -s^2+c^2 & 0 & 0 \\ 0 & 0 & 0 & 0 & -c & -s \end{bmatrix} \qquad (4.13)$$

where

$s = \sin \alpha_1$

$c = \cos \alpha_1$

In the general three-dimensional case the transformation matrix is more complex, since it involves both the *dip angle* and the *dip direction* (see 4.3):

$$\underline{\underline{T}}^T = \begin{bmatrix} n_x^2 & n_y^2 & n_z^2 & 2\ n_x\ n_y & 2\ n_y\ n_z & 2\ n_z\ n_x \\ n_x\ s_x & n_y\ s_y & n_z\ s_z & n_x\ s_y + n_y\ s_x & n_z\ s_y + n_y\ s_z & n_z\ s_x + n_x\ s_z \\ n_x\ t_x & n_y\ t_y & n_z\ t_z & n_y\ t_x + n_x\ t_y & n_y\ t_z + n_z\ t_y & n_z\ t_x + n_x\ t_z \end{bmatrix} \quad (4.14)$$

Note that the general transformation matrix, $\underline{\underline{T}}^T$, for the calculation of local stresses corresponds to rows 1, 4 and 6 of $\underline{R}_\sigma$ (see Eq. 4.3).

After having determined the local stress components, the plasticity conditions can be checked on the basis of yield functions. The yield functions for plane *i* are defined as:

$$f_i = |\tau_s| + \sigma_n \tan \varphi_i - c_i \qquad \text{(Coulomb)} \qquad (4.15a)$$

$$f_i^t = \sigma_n - \sigma_{t,i} \quad (\sigma_{t,i} \le c_i\ \cot \phi_i) \qquad \text{(Tension cut-off)} \qquad (4.15b)$$

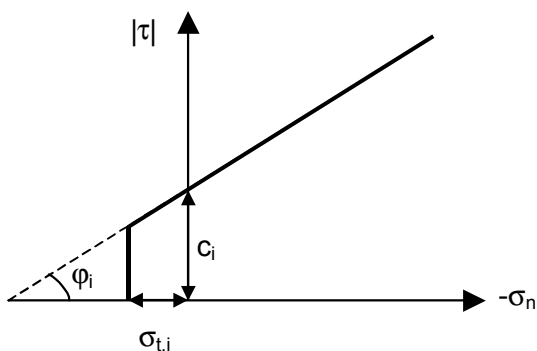Figure 4.3 visualizes the full yield criterion on a single plane.

Figure 4.3 Yield criterion for individual plane

The local plastic strains are defined by:

$$\Delta \underline{\varepsilon}_j^p = \lambda_j\ \frac{\partial g_j}{\partial \underline{\sigma}_j} \qquad (4.16)$$

where g_j is the local plastic potential function for plane j:

$$g_j = \left|\tau_j\right| + \sigma_n \tan\phi_j - c_j \qquad \text{(Coulomb)} \qquad (4.17a)$$

$$g_j^t = \sigma_n - \sigma_{t,j} \qquad \text{(Tension cut-off)} \qquad (4.17b)$$

The transformation matrix, $\underline{T}$, is also used to transform the local plastic strain increments of plane j, $\Delta\underline{\varepsilon}\,^p_j$, into global plastic strain increments, $\Delta\underline{\varepsilon}\,^p$:

$$\Delta\underline{\varepsilon}\,^p = \underline{\underline{T}}_j \ \Delta\underline{\varepsilon}\,^p_j \qquad (4.18)$$

The consistency condition requires that at yielding the value of the yield function must remain zero for all active yield functions. For all planes together, a maximum of 6 yield functions exist, so up to 6 plastic multipliers must be found such that all yield functions are at most zero and the plastic multipliers are non-negative.

$$f_c^i = f_c^{ie} - \sum_{j=1}^{np} <\lambda_c^j> \frac{\partial f_c^{i^T}}{\partial\sigma} T_i^T D \ T_j \frac{\partial g_c^j}{\partial\sigma} - \sum_{j=1}^{np} <\lambda_t^j> \frac{\partial f_c^{i^T}}{\partial\sigma} T_i^T D \ T_j \frac{\partial g_t^j}{\partial\sigma} \quad (4.19a)$$

$$f_t^i = f_t^{ie} - \sum_{j=1}^{np} <\lambda_c^j> \frac{\partial f_t^{i^T}}{\partial\sigma} T_i^T D \ T_j \frac{\partial g_c^j}{\partial\sigma} - \sum_{j=1}^{np} <\lambda_t^j> \frac{\partial f_t^{i^T}}{\partial\sigma} T_i^T D \ T_j \frac{\partial g_t^j}{\partial\sigma} \quad (4.19b)$$

This means finding up to 6 values of $\lambda_i \geq 0$ such that all $f_i \leq 0$ and $\lambda_i f_i = 0$

When the maximum of 3 planes are used, there are $2^6 = 64$ possibilities of (combined) yielding. In the calculation process, all these possibilities are taken into account in order to provide an exact calculation of stresses.

4.3   PARAMETERS OF THE JOINTED ROCK MODEL

Most parameters of the jointed rock model coincide with those of the isotropic Mohr-Coulomb model. These are the basic elastic parameters and the basic strength parameters.

Elastic parameters as in Mohr-Coulomb model (see Section 3.3):

E_1 :   Young's modulus for rock as a continuum   [kN/m^2]

ν_1 :   Poisson's ratio for rock as a continuum   [−]

Anisotropic elastic parameters 'Plane 1' direction (e.g. stratification direction):

E_2	:	Young's modulus in 'Plane 1' direction	[kN/m^2]
G_2	:	Shear modulus in 'Plane 1' direction	[kN/m^2]
v_2	:	Poisson's ratio in 'Plane 1' direction	[−]

Strength parameters in joint directions (Plane i=1, 2, 3):

c_i	:	Cohesion	[kN/m^2]
φ_i	:	Friction angle	[°]
ψ	:	Dilatancy angle	[°]
$\sigma_{t,i}$	:	Tensile strength	[kN/m^2]

Definition of joint directions (Plane i=1, 2, 3):

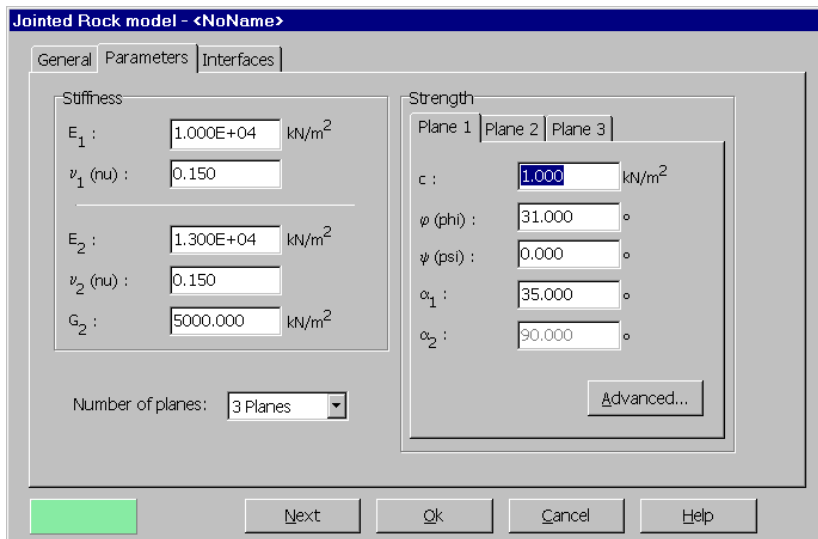|			
n	:	Numer of joint directions ($1 \leq n \leq 3$)	
$\alpha_{1,i}$	:	Dip angle	[°]
$\alpha_{2,i}$	:	Dip direction	[°]

Figure 4.4 Parameters for the Jointed Rock model

Elastic parameters

The elastic parameters E_1 and v_1 are the (constant) stiffness (Young's modulus) and Poisson's ratio of the rock as a continuum according to Hooke's law, i.e. as if it would not be anisotropic.

Elastic anisotropy in a rock formation may be introduced by stratification. The stiffness perpendicular to the stratification direction is usually reduced compared with the general stiffness. This reduced stiffness can be represented by the parameter E_2, together with a second Poisson's ratio, v_2. In general, the elastic stiffness normal to the direction of elastic anisotropy is defined by the parameters E_2 and v_2.

Elastic shearing in the stratification direction is also considered to be 'weaker' than elastic shearing in other directions. In general, the shear stiffness in the anisotropic direction can explicitly be defined by means of the elastic shear modulus G_2. In contrast to Hooke's law of isotropic elasticity, G_2 is a separate parameter and is not simply related to Young's modulus by means of Poisson's ratio (see Eq. 4.1d and e).

If the elastic behaviour of the rock is fully isotropic, then the parameters E_2 and v_2 can be simply set equal to E_1 and v_1 respectively, whereas G_2 should be set to $\frac{1}{2}E_1/(1+v_1)$.

Strength parameters

Each sliding direction (plane) has its own strength properties c_i, φ_i and $\sigma_{t,i}$ and dilatancy angle ψ_i. The strength properties c_i and φ_i determine the allowable shear strength according to Coulomb's criterion and σ_t determines the tensile strength according to the tension cut-off criterion. The latter is displayed after pressing <Advanced> button. By default, the tension cut-off is active and the tensile strength is set to zero. The dilatancy angle, ψ_i, is used in the plastic potential function g, and determines the plastic volume expansion due to shearing.

Definition of joint directions

It is assumed that the direction of elastic anisotropy corresponds with the first direction where plastic shearing may occur ('Plane 1'). This direction must always be specified. In the case the rock formation is stratified without major joints, the *number of sliding planes* (= sliding directions) is still 1, and strength parameters must be specified for this direction anyway. A maximum of three sliding directions can be defined. These directions may correspond to the most critical directions of joints in the rock formation.

The sliding directions are defined by means of two parameters: The *Dip angle* (α_1) (or shortly *Dip*) and the *Dip direction* (α_2). Instead of the latter parameter, it is also common in geology to use the *Strike*. However, care should be taken with the definition of *Strike*, and therefore the unambiguous *Dip direction* as mostly used by rock engineers is used in PLAXIS. The definition of both parameters is visualized in Figure 4.5.
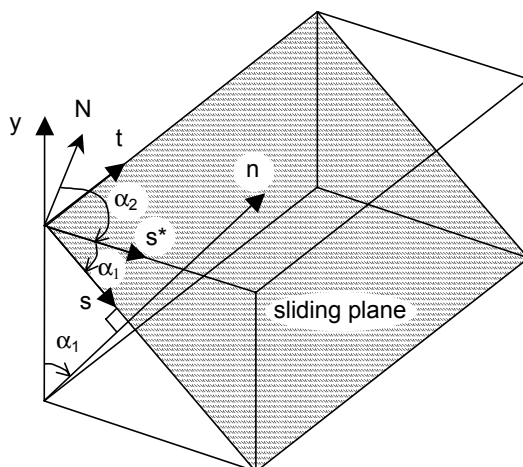
Figure 4.5 Definition of dip angle and dip direction

Consider a sliding plane, as indicated in Figure 4.5. The sliding plane can be defined by the vectors (s,t), which are both normal to the vector n. The vector n is the 'normal' to the sliding plane, whereas the vector s is the 'fall line' of the sliding plane and the vector t is the 'horizontal line' of the sliding plane. The sliding plane makes an angle α_1 with respect to the horizontal plane, where the horizontal plane can be defined by the vectors (s^*,t), which are both normal to the vertical y-axis. The angle α_1 is the *dip angle*, which is defined as the positive 'downward' inclination angle between the horizontal plane and the sliding plane. Hence, α_1 is the angle between the vectors s^* and s, measured clockwise from s^* to s when looking in the positive t-direction. The dip angle must be entered in the range [0°, 90°].

The orientation of the sliding plane is further defined by the *dip direction*, α_2, which is the orientation of the vector s^* with respect to the North direction (N). The dip direction is defined as the positive angle from the North direction, measured clockwise to the horizontal projection of the fall line ($=s^*$-direction) when looking downwards. The dip direction is entered in the range [0°, 360°].

In addition to the orientation of the sliding planes it is also known how the global (x,y,z) model coordinates relate to the North direction. This information is contained in the *Declination* parameter, as defined in the *General settings* in the Input program. The *Declination* is the positive angle from the North direction to the positive z-direction of the model.
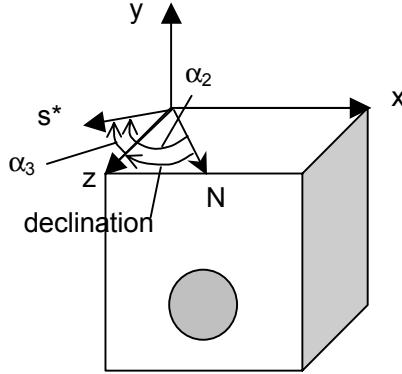
Figure 4.6 Definition of various directions and angles in the horiziontal plane

In order to transform the local (n,s,t) coordinate system into the global (x,y,z) coordinate system, an auxiliary angle α_3 is used internally, being the difference between the *Dip direction* and the *Declination*:

$$\alpha_3 = \alpha_2 - Declination \tag{4.19}$$

Hence, α_3 is defined as the positive angle from the positive *z*-direction clockwise to the *s**-direction when looking downwards.

From the definitions as given above, it follows that:

$$\underline{n} = \begin{bmatrix} n_x \\ n_y \\ n_z \end{bmatrix} = \begin{bmatrix} -\sin\alpha_1 \sin\alpha_3 \\ \cos\alpha_1 \\ \sin\alpha_1 \cos\alpha_3 \end{bmatrix} \tag{4.20a}$$

$$\underline{s} = \begin{bmatrix} s_x \\ s_y \\ s_z \end{bmatrix} = \begin{bmatrix} -\cos\alpha_1 \sin\alpha_3 \\ -\sin\alpha_1 \\ \cos\alpha_1 \cos\alpha_3 \end{bmatrix} \tag{4.20b}$$

$$\underline{t} = \begin{bmatrix} t_x \\ t_y \\ t_z \end{bmatrix} = \begin{bmatrix} \cos\alpha_3 \\ 0 \\ \sin\alpha_3 \end{bmatrix} \tag{4.20c}$$

Below some examples are shown of how sliding planes occur in a 3D models for different values of α_1, α_2 and *Declination*:

$\alpha_1 = 45^\circ$

$\alpha_2 = 0^\circ$

Declination = 0º
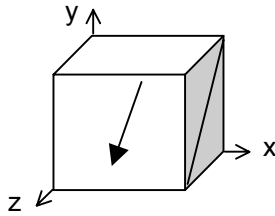
$\alpha_1 = 45^\circ$

$\alpha_2 = 90^\circ$

Declination = 0º
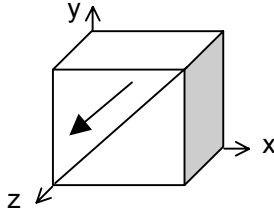
$\alpha_1 = 45^\circ$

$\alpha_2 = 0^\circ$

Declination = 90º
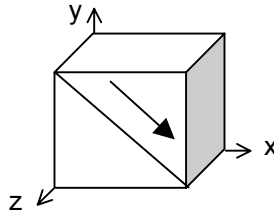
Figure 4.7 Examples of failure directions defined by α_1 , α_2 and *Declination*

As it can be seen, for plane strain conditions (the cases considered in Version 8) only α_1 is required. By default, α_2 is fixed at 90º and the declination is set to 0º.

5   THE HARDENING-SOIL MODEL (ISOTROPIC HARDENING)

In contrast to an elastic perfectly-plastic model, the yield surface of a hardening plasticity model is not fixed in principal stress space, but it can expand due to plastic straining. Distinction can be made between two main types of hardening, namely shear hardening and compression hardening. Shear hardening is used to model irreversible strains due to primary deviatoric loading. Compression hardening is used to model irreversible plastic strains due to primary compression in oedometer loading and isotropic loading. Both types of hardening are contained in the present model.

The Hardening-Soil model is an advanced model for simulating the behaviour of different types of soil, both soft soils and stiff soils, Schanz (1998). When subjected to primary deviatoric loading, soil shows a decreasing stiffness and simultaneously irreversible plastic strains develop. In the special case of a drained triaxial test, the observed relationship between the axial strain and the deviatoric stress can be well approximated by a hyperbola. Such a relationship was first formulated by Kondner (1963) and later used in the well-known hyperbolic model (Duncan & Chang, 1970). The Hardening-Soil model, however, supersedes the hyperbolic model by far. Firstly by using the theory of plasticity rather than the theory of elasticity. Secondly by including soil dilatancy and thirdly by introducing a yield cap. Some basic characteristics of the model are:

- Stress dependent stiffness according to a power law.   Input parameter m

- Plastic straining due to primary deviatoric loading.   Input parameter E_{50}^{ref}

- Plastic straining due to primary compression.   Input parameter E_{oed}^{ref}

- Elastic unloading / reloading.   Input parameters E_{ur}^{ref} , ν_{ur}

- Failure according to the Mohr-Coulomb model.   Parameters c, φ and ψ

A basic feature of the present Hardening-Soil model is the stress dependency of soil stiffness. For oedometer conditions of stress and strain, the model implies for example the relationship $E_{oed} = E_{oed}^{ref} \left(\sigma / p^{ref} \right)^{m}$. In the special case of soft soils it is realistic to use $m = 1$. In such situations there is also a simple relationship between the modified compression index λ^*, as used in the the Soft-Soil model and the oedometer loading modulus (see also Section 6.7)

$$E_{oed}^{ref} = \frac{p^{ref}}{\lambda^*} \qquad\qquad \lambda^* = \frac{\lambda}{(1+e_0)}$$

where p^{ref} is a reference pressure. Here we consider a tangent oedometer modulus at a particular reference pressure p^{ref}. Hence, the primary loading stiffness relates to the modified compression index λ^*.

Similarly, the unloading-reloading modulus relates to the modified swelling index κ^*. There is the approximate relationship:

$$E_{ur}^{ref} = \frac{3p^{ref}\left(1 - 2v_{ur}\right)}{\kappa^*} \qquad\qquad \kappa^* = \frac{\kappa}{\left(1 + e_0\right)}$$

Again, this relationship applies in combination with the input value $m = 1$.

5.1 HYPERBOLIC RELATIONSHIP FOR STANDARD DRAINED TRIAXIAL TEST

A basic idea for the formulation of the Hardening-Soil model is the hyperbolic relationship between the vertical strain, ε_1, and the deviatoric stress, q, in primary triaxial loading. Here standard drained triaxial tests tend to yield curves that can be described by:

$$-\varepsilon_1 = \frac{1}{2E_{50}}\frac{q}{1 - q / q_a} \qquad\qquad \text{for}: q < q_f \qquad\qquad (5.1)$$

Where q_a is the asymptotic value of the shear strength. This relationship is plotted in Figure 5.1. The parameter E_{50} is the confining stress dependent stiffness modulus for primary loading and is given by the equation:

$$E_{50} = E_{50}^{ref}\left(\frac{c\,\cos\varphi - \sigma_3'\sin\varphi}{c\,\cos\varphi + p^{ref}\sin\varphi}\right)^m \qquad\qquad (5.2)$$

where E_{50}^{ref} is a reference stiffness modulus corresponding to the reference confining pressure p^{ref}. In PLAXIS, a default setting $p^{ref} = 100$ stress units is used. The actual stiffness depends on the minor principal stress, σ_3', which is the confining pressure in a triaxial test. Please note that σ_3 is negative for compression. The amount of stress dependency is given by the power m. In order to simulate a logarithmic stress dependency, as observed for soft clays, the power should be taken equal to 1.0. Janbu (1963) reports values of m around 0.5 for Norwegian sands and silts, whilst Von Soos (1980) reports various different values in the range $0.5 < m < 1.0$.

The ultimate deviatoric stress, q_f, and the quantity q_a in Eq. (5.1) are defined as:

$$q_f = \left(c\cot\varphi - \sigma_3'\right)\frac{2\sin\varphi}{1 - \sin\varphi} \qquad \text{and}: \quad q_a = \frac{q_f}{R_f} \qquad\qquad (5.3)$$

Again it is remarked that σ'_3 is usually negative. The above relationship for q_f is derived from the Mohr-Coulomb failure criterion, which involves the strength parameters c and φ. As soon as $q = q_f$, the failure criterion is satisfied and perfectly plastic yielding occurs as described by the Mohr-Coulomb model.

The ratio between q_f and q_a is given by the failure ratio R_f, which should obviously be smaller than 1. In PLAXIS, $R_f = 0.9$ is chosen as a suitable default setting.

For unloading and reloading stress paths, another stress-dependent stiffness modulus is used:

$$E_{ur} = E_{ur}^{ref} \left(\frac{c \, \cos\varphi - \sigma'_3 \sin\varphi}{c \, \cos\varphi + p^{ref} \sin\varphi} \right)^m \tag{5.4}$$

where E_{ur}^{ref} is the reference Young's modulus for unloading and reloading, corresponding to the reference pressure p^{ref}. In many practical cases it is appropriate to set E_{ur}^{ref} equal to $3 E_{50}^{ref}$; this is the default setting used in PLAXIS.
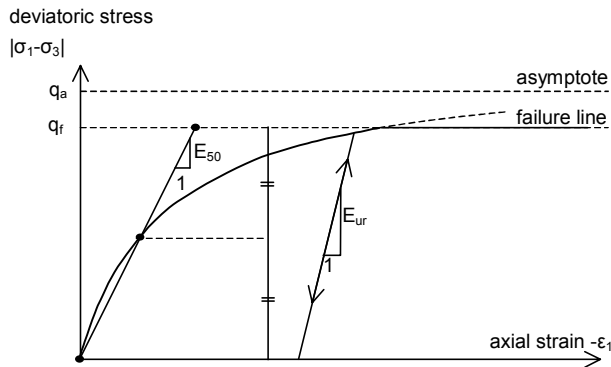
Figure 5.1   Hyperbolic stress-strain relation in primary loading for a standard drained triaxial test

5.2   APPROXIMATION OF HYPERBOLA BY THE HARDENING-SOIL MODEL

For the sake of convenience, restriction is again made to triaxial loading conditions with $\sigma'_2 = \sigma'_3$ and σ'_1 being the major compressive stress. Moreover, it is assumed that $q < q_f$, as also indicated in Figure 5.1. It should also be realised that compressive stress and strain are considered positive. For a more general presentation of the Hardening-Soil

model the reader is referred to Schanz et al (1999). In this section it will be shown that this model gives virtually the hyperbolic stress strain curve of Eq. (5.1) when considering stress paths of standard drained triaxial tests. Let us first consider the corresponding plastic strains. This stems from a yield function of the form:

$$f = \overline{f} - \gamma^p \tag{5.5}$$

where $\overline{f}$ is a function of stress and γ^p is a function of plastic strains:

$$\overline{f} = \frac{1}{E_{50}} \frac{q}{1 - q/q_a} - \frac{2q}{E_{ur}} \qquad \gamma^p = -\left(2\varepsilon_1^p - \varepsilon_v^p\right) \approx -2\varepsilon_1^p \tag{5.6}$$

with q, q_a, E_{50} and E_{ur} as defined by Eqs. (5.2) to (5.4), whilst the superscript p is used to denote plastic strains. For hard soils, plastic volume changes (ε_v^p) tend to be relatively small and this leads to the approximation $\gamma^p \approx -2\varepsilon_1^p$. The above definition of the strain-hardening parameter γ^p will be referred to later.

An essential feature of the above definitions for $\overline{f}$ is that it matches the well-known hyperbolic law (5.1). For checking this statement, one has to consider primary loading, as this implies the yield condition $f = 0$. For primary loading, it thus yields $\gamma^p = \overline{f}$ and it follows from Eqs. (5.6) that:

$$-\varepsilon_1^p \approx \tfrac{1}{2}\,\overline{f} = \frac{1}{2E_{50}} \frac{q}{1 - q/q_a} - \frac{q}{E_{ur}} \tag{5.7}$$

In addition to the plastic strains, the model accounts for elastic strains. Plastic strains develop in primary loading alone, but elastic strains develop both in primary loading and unloading / reloading. For drained triaxial test stress paths with $\sigma_2' = \sigma_3' = $ constant, the elastic Young's modulus E_{ur} remains constant and the elastic strains are given by the equations:

$$-\varepsilon_1^e = \frac{q}{E_{ur}} \qquad\qquad -\varepsilon_2^e = -\varepsilon_3^e = -\nu_{ur}\frac{q}{E_{ur}} \tag{5.8}$$

where ν_{ur} is the unloading / reloading Poisson's ratio. Here it should be realised that restriction is made to strains that develop during deviatoric loading, whilst the strains that develop during the very first stage of the test are not considered. For the first stage of isotropic compression (with consolidation), the Hardening-Soil model predicts fully elastic volume changes according to Hooke's law, but these strains are not included in Eq. (5.8).

For the deviatoric loading stage of the triaxial test, the axial strain is the sum of an elastic component given by Eq. (5.8) and a plastic component according to Eq. (5.7). Hence, it follows that:

$$-\varepsilon_1 = -\varepsilon_1^e - \varepsilon_1^p \approx \frac{1}{2E_{50}} \frac{q}{1 - q / q_a}$$

(5.9)

This relationship holds exactly in absence of plastic volume strains, i.e. when $\varepsilon_v^p = 0$.

In reality, plastic volumetric strains will never be precisely equal to zero, but for hard soils plastic volume changes tend to be small when compared with the axial strain, so that the approximation in Eq. (5.9) will generally be accurate. It is thus made clear that the present Hardening-Soil model yields a hyperbolic stress-strain curve under triaxial testing conditions.

For a given constant value of the hardening parameter, γ^p, the yield condition $f = 0$, can be visualised in p'-q-plane by means of a yield locus. When plotting such yield loci, one has to use Eq. (5.6) as well as Eqs. (5.2) and (5.4) for E_{50} and E_{ur} respectively. Because of the latter expressions, the shape of the yield loci depend on the exponent m. For $m = 1$, straight lines are obtained, but slightly curved yield loci correspond to lower values of the exponent. Figure 5.2 shows the shape of successive yield loci for $m = 0.5$, being typical for hard soils.
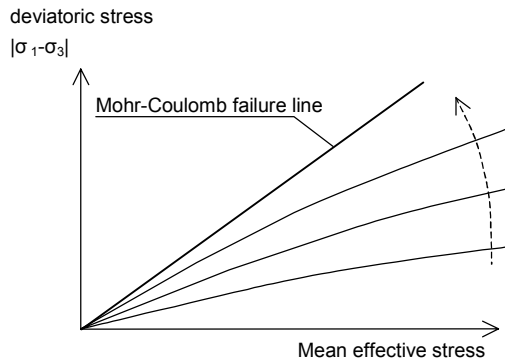

deviatoric stress
$|\sigma_1 - \sigma_3|$

Mohr-Coulomb failure line

Mean effective stress

Figure 5.2   Successive yield loci for various constant values of the hardening parameter γ^p

5.3 PLASTIC VOLUMETRIC STRAIN FOR TRIAXIAL STATES OF STRESS

Having presented a relationship for the plastic shear strain, γ^p, attention is now focused on the plastic volumetric strain, ε_v^p. As for all plasticity models, the Hardening-Soil model involves a relationship between rates of plastic strain, i.e. a relationship between $\dot{\varepsilon}_v^p$ and $\dot{\gamma}^p$. This flow rule has the linear form:

$$\dot{\varepsilon}_v^p = \sin\psi_m \; \dot{\gamma}^p \tag{5.10}$$

Clearly, further detail is needed by specifying the mobilised dilatancy angle ψ_m. For the present model, the expression:

$$\sin\psi_m = \frac{\sin\varphi_m - \sin\varphi_{cv}}{1 - \sin\varphi_m \, \sin\varphi_{cv}} \tag{5.11}$$

is adopted, where φ_{cv} is the critical state friction angle, being a material constant independent of density, and φ_m is the mobilised friction angle:

$$\sin\varphi_m = \frac{\sigma_1' - \sigma_3'}{\sigma_1' + \sigma_3' - 2\,c\cot\varphi} \tag{5.12}$$

The above equations correspond to the well-known stress-dilatancy theory by Rowe (1962), as explained by Schanz & Vermeer (1995). The essential property of the stress-dilatancy theory is that the material contracts for small stress ratios ($\varphi_m < \varphi_{cv}$), whilst dilatancy occurs for high stress ratios ($\varphi_m > \varphi_{cv}$). At failure, when the mobilised friction angle equals the failure angle, φ, it is found from Eq. (5.11) that:

$$\sin\psi = \frac{\sin\varphi - \sin\varphi_{cv}}{1 - \sin\varphi \sin\varphi_{cv}} \tag{5.13a}$$

or equivalently:

$$\sin\varphi_{cv} = \frac{\sin\varphi - \sin\psi}{1 - \sin\varphi \sin\psi} \tag{5.13b}$$

Hence, the critical state angle can be computed from the failure angles φ and ψ. PLAXIS performs this computation automatically and so users do not need to specify a value for φ_{cv}.

Instead, one has to provide input data on the ultimate friction angle, φ, and the ultimate dilatancy angle, ψ.

5.4   PARAMETERS OF THE HARDENING-SOIL MODEL

Some parameters of the present hardening model coincide with those of the non-hardening Mohr-Coulomb model. These are the failure parameters c, φ and ψ.
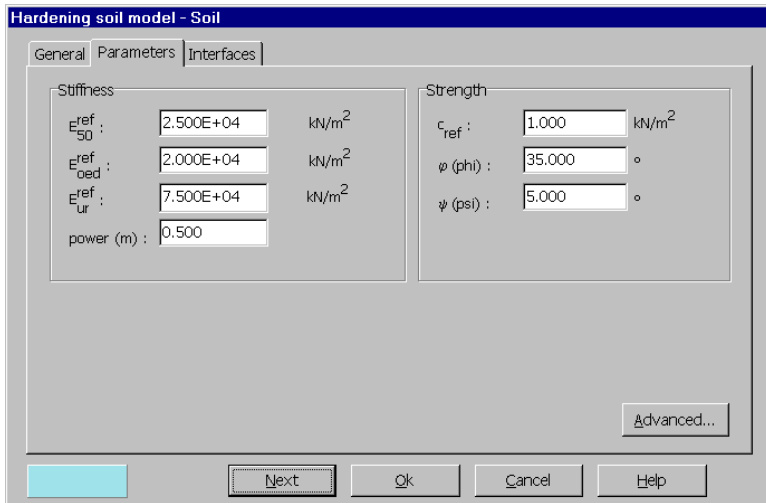
Figure 5.3 Basic parameters for the Hardening-Soil model

Failure parameters as in Mohr-Coulomb model (see Section 3.3):

c	: (Effective) cohesion	[kN/m^2]
φ	: (Effective) angle of internal friction	[°]
ψ	: Angle of dilatancy	[°]

Basic parameters for soil stiffness:

E_{50}^{ref}	: Secant stiffness in standard drained triaxial test	[kN/m^2]
E_{oed}^{ref}	: Tangent stiffness for primary oedometer loading	[kN/m^2]
m	: Power for stress-level dependency of stiffness	[-]

Advanced parameters (it is advised to use the default setting):

E_{ur}^{ref}	: Unloading / reloading stiffness (default $E_{ur}^{ref} = 3\,E_{50}^{ref}$)	[kN/m^2]
ν_{ur}	: Poisson's ratio for unloading-reloading (default $\nu_{ur} = 0.2$)	[-]

p^{ref} : Reference stress for stiffnesses (default $p^{ref} = 100$ stress units)   [kN/m^2]

K_0^{nc} : K_0-value for normal consolidation (default $K_0^{nc} = 1$-sinφ)   [-]

R_f : Failure ratio q_f / q_a (default $R_f = 0.9$) (see Figure 5.1)   [-]

$\sigma_{tension}$: Tensile strength (default $\sigma_{tension} = 0$ stress units)   [kN/m^2]

$c_{increment}$: As in Mohr-Coulomb model (default $c_{increment} = 0$)   [kN/m^3]

Stiffness moduli E_{50}^{ref} & E_{oed}^{ref} and power m

The advantage of the Hardening-Soil model over the Mohr-Coulomb model is not only the use of a hyperbolic stress-strain curve instead of a bi-linear curve, but also the control of stress level dependency. When using the Mohr-Coulomb model, the user has to select a fixed value of Young's modulus whereas for real soils this stiffness depends on the stress level. It is therefore necessary to estimate the stress levels within the soil and use these to obtain suitable values of stiffness. With the Hardening-Soil model, however, this cumbersome selection of input parameters is not required. Instead, a stiffness modulus E_{50}^{ref} is defined for a reference minor principal stress of $-\sigma_3' = p^{ref}$

As a default value, the program uses $p^{ref} = 100$ stress units.

As some PLAXIS users are familiar with the input of shear moduli rather than the above stiffness moduli, shear moduli will now be discussed. Within Hooke's theory of elasticity conversion between E and G goes by the equation $E = 2 (1+v) G$. As E_{ur} is a real elastic stiffness, one may thus write $E_{ur} = 2 (1+v) G_{ur}$, where G_{ur} is an elastic shear modulus. Please note that PLAXIS allows for the input of E_{ur} and v_{ur} but not for a direct input of G_{ur}. In contrast to E_{ur}, the secant modulus E_{50} is not used within a concept of elasticity. As a consequence, there is no simple conversion from E_{50} to G_{50}.

In contrast to elasticity based models, the elastoplastic Hardening-Soil model does not involve a fixed relationship between the (drained) triaxial stiffness E_{50} and the oedometer stiffness E_{oed} for one-dimensional compression. Instead, these stiffnesses can be inputted independently.

Having defined E_{50} by Eq. (5.2), it is now important to define the oedometer stiffness. Here we use the equation:

$$E_{oed} = E_{oed}^{ref} \left(\frac{c \, \cos\varphi - \sigma_3' \sin\varphi}{c \, \cos\varphi + p^{ref} \sin\varphi} \right)^m \tag{5.14}$$

where E_{oed} is a tangent stiffness modulus as indicated in Figure 5.4. Hence, E_{oed}^{ref} is a tangent stiffness at a vertical stress of $-\sigma_1' = p^{ref}$. Note that we use σ_1 rather than σ_3 and that we consider primary loading.
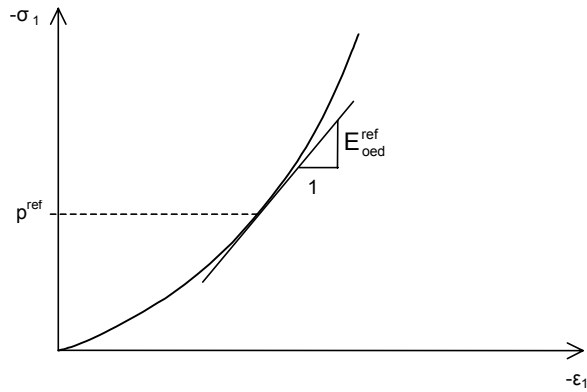
Figure 5.4 Definition of E_{oed}^{ref} in oedometer test results

Advanced parameters

Realistic values of ν_{ur} are about 0.2 and this value is thus used as a default setting, as indicated in Figure 5.5.

Figure 5.5 Advanced parameters window

In contrast to the Mohr-Coulomb model, K_0^{nc} is not simply a function of Poisson's ratio, but a proper input parameter. As a default setting PLAXIS uses the correlation $K_0^{nc} = 1 - \sin\varphi$. It is suggested to maintain this value as the correlation is highly realistic. However, users do have the possibility to select different values. All possible different input values for K_0^{nc} cannot be accommodated for. Depending on other parameters, such as E_{50}, E_{oed}, E_{ur} and ν_{ur}, there happens to be a certain range of valid K_0^{nc}-values. K_0^{nc} values outside this range are rejected by PLAXIS. On inputting values, the program shows the nearest possible value that will be used in the computations.

Dilatancy cut-off

After extensive shearing, dilating materials arrive in a state of critical density where dilatancy has come to an end, as indicated in Figure 5.6. This phenomenon of soil behaviour can be included in the Hardening-Soil model by means of a dilatancy cut-off. In order to specify this behaviour, the initial void ratio, e_{init}, and the maximum void ratio, e_{max}, of the material must be entered as general parameters. As soon as the volume change results in a state of maximum void, the mobilised dilatancy angle, ψ_{mob}, is automatically set back to zero, as indicated in Figure 5.6.
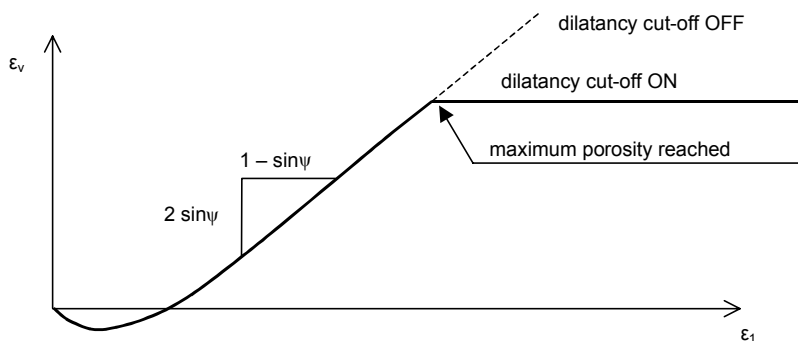
Figure 5.6   Resulting strain curve for a standard drained triaxial test when including dilatancy cut-off

$$\text{for} \quad e < e_{max}: \qquad \sin\psi_{mob} = \frac{\sin\varphi_{mob} - \sin\varphi_{cv}}{1 - \sin\varphi_{mob}\ \sin\varphi_{cv}}$$

$$\text{where:} \qquad \sin\varphi_{cv} = \frac{\sin\varphi - \sin\psi}{1 - \sin\varphi\ \sin\psi} \qquad\qquad (5.15a)$$

$$\text{for} \quad e \geq e_{max}: \qquad \psi_{mob} = 0 \qquad\qquad (5.15b)$$

The void ratio is related to the volumetric strain, ε_v by the relationship:

$$-\left(\varepsilon_v - \varepsilon_v^{init}\right) = \ln\left(\frac{1+e}{1+e_{init}}\right) \tag{5.16}$$

where an increment of ε_v is positive for dilatancy.

The initial void ratio, e_{init}, is the in-situ void ratio of the soil body. The maximum void ratio is the void ratio of the material in a state of critical void (critical state). As soon as the maximum void ratio is reached, the dilatancy angle is set to zero. The minimum void ratio, e_{min}, of a soil can also be inputted, but this general soil parameter is not used within the context of the Hardening-Soil model.

Please note that the selection of the dilatancy cut-off and the input of void ratios is done in the 'general' tab sheet of the material data set window and not in the 'parameters' tab sheet. The selection of the dilatancy cut-off is only available when the Hardening-Soil model has been selected. By default, the dilatancy cut-off is not active.
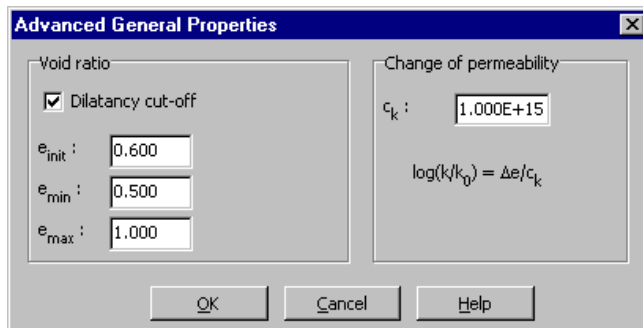
Figure 5.7 Advanced general properties window

5.5   ON THE CAP YIELD SURFACE IN THE HARDENING-SOIL MODEL

Shear yield surfaces as indicated in Figure 5.2 do not explain the plastic volume strain that is measured in isotropic compression. A second type of yield surface must therefore be introduced to close the elastic region in the direction of the p-axis. Without such a cap type yield surface it would not be possible to formulate a model with independent input of both E_{50}^{ref} and E_{oed}^{ref}. The triaxial modulus largely controls the shear yield surface and the oedometer modulus controls the cap yield surface. In fact, E_{50}^{ref} largely controls the magnitude of the plastic strains that are associated with the shear yield surface. Similarly, E_{oed}^{ref} is used to control the magnitude of plastic strains that originate

from the yield cap. In this section the yield cap will be described in full detail. To this end we consider the definition of the cap yield surface:

$$f^c = \frac{\tilde{q}^2}{\alpha^2} + p^2 - p_p^2 \tag{5.17}$$

where α is an auxiliary model parameter that relates to K_0^{nc} as will be discussed later. Further more we have $p = -(\sigma_1+\sigma_2+\sigma_3)/3$ and $\tilde{q} = \sigma_1+(\delta-1)\sigma_2-\delta\sigma_3$ with $\delta=(3+\sin\varphi)/(3-\sin\varphi)$. $\tilde{q}$ is a special stress measure for deviatoric stresses. In the special case of triaxial compression $(-\sigma_1>-\sigma_2=-\sigma_3)$ it yields $\tilde{q} = -(\sigma_1-\sigma_3)$ and for triaxial extension $(-\sigma_1=-\sigma_2>-\sigma_3)$ $\tilde{q}$ reduces to $\tilde{q} = -\delta(\sigma_1-\sigma_3)$. The magnitude of the yield cap is determined by the isotropic pre-consolidation stress p_p. We have a hardening law relating p_p to volumetric cap strain ε_v^{pc}:

$$\varepsilon_v^{pc} = \frac{\beta}{1-m}\left(\frac{p_p}{p^{ref}}\right)^{1-m} \tag{5.18}$$

The volumetric cap strain is the plastic volumetric strain in isotropic compression. In addition to the well known constants m and p^{ref} there is another model constant β. Both α and β are cap parameters, but we will not use them as direct input parameters. Instead, we have relationships of the form:

$$\alpha \leftrightarrow K_0^{nc} \qquad\qquad \text{(default: } K_0^{nc} = 1 - \sin\varphi \text{)}$$

$$\beta \leftrightarrow E_{oed}^{ref} \qquad\qquad \text{(default: } E_{oed}^{ref} = E_{50}^{ref} \text{)}$$

such that K_0^{nc} and E_{oed}^{ref} can be used as input parameters that determine the magnitude of α and β respectively. For understanding the shape of the yield cap, it should first of all be realised that it is an ellipse in p-$\tilde{q}$-plane, as indicated in Figure 5.8.

The ellipse has length p_p on the p-axis and αp_p on the $\tilde{q}$-axis. Hence, p_p determines its magnitude and α its aspect ratio. High values of α lead to steep caps underneath the Mohr-Coulomb line, whereas small α-values define caps that are much more pointed around the p-axis. The ellipse is used both as a yield surface and as a plastic potential. Hence:

$$\underline{\dot{\varepsilon}}^{pc} = \lambda \, \frac{\partial f^c}{\partial \underline{\sigma}} \qquad \text{with:} \qquad \lambda = \frac{\beta}{2\,p}\left(\frac{p_p}{p^{ref}}\right)^m \frac{\dot{p}_p}{p^{ref}} \tag{5.19}$$

This expression for λ derives from the yield condition $f^c = 0$ and Eq. (5.18) for p_p. Input data on initial p_p-values is provided by means of the PLAXIS procedure for initial stresses. Here, p_p is either computed from the entered overconsolidation ratio (OCR) or the pre-overburden pressure (POP) (see Section 2.6). For understanding the yield surfaces in full detail, one should consider both Figure 5.8 and Figure 5.9.
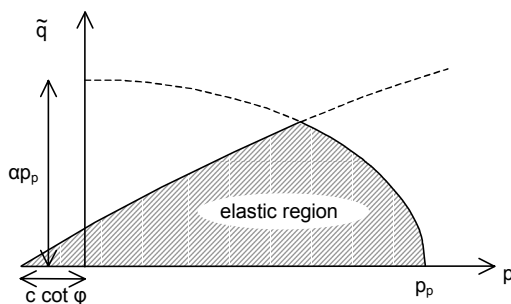
Figure 5.8   Yield surfaces of Hardening-Soil model in p-$\tilde{q}$ -plane. The elastic region can be further reduced by means of a tension cut-off
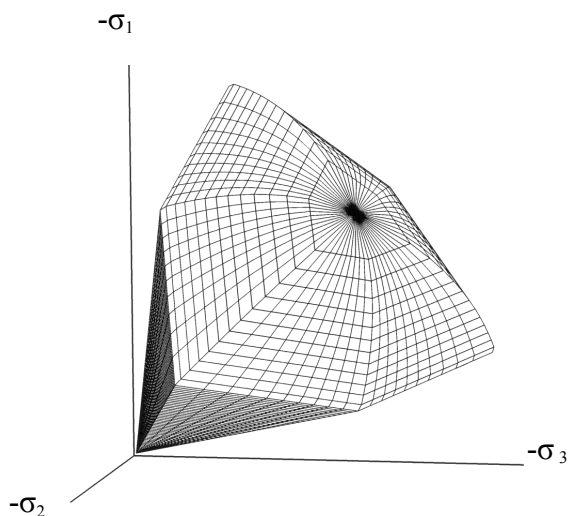
Figure 5.9   Representation of total yield contour of the Hardening-Soil model in principal stress space for cohesionless soil

The first figure shows simple yield lines, whereas the second one depicts yield surfaces in principal stress space. Both the shear locus and the yield cap have the hexagonal shape of the classical Mohr-Coulomb failure criterion. In fact, the shear yield locus can expand up to the ultimate Mohr-Coulomb failure surface. The cap yield surface expands as a function of the pre-consolidation stress p_p.

6   SOFT-SOIL-CREEP MODEL (TIME DEPENDENT BEHAVIOUR)

6.1   INTRODUCTION

As soft soils we consider near-normally consolidated clays, clayey silts and peat. The special features of these materials is their high degree of compressibility. This is best demonstrated by oedometer test data as reported for instance by Janbu in his Rankine lecture (1985). Considering tangent stiffness moduli at a reference oedometer pressure of 100 kPa, he reports for normally consolidated clays E_{oed} = 1 to 4 MPa, depending on the particular type of clay considered. The differences between these values and stiffnesses for NC-sands are considerable as here we have values in the range of 10 to 50 MPa, at least for non-cemented laboratory samples. Hence, in oedometer testing normally consolidated clays behave ten times softer than normally consolidated sands. This illustrates the extreme compressibility of soft soils.

Another feature of the soft soils is the linear stress-dependency of soil stiffness. According to the Hardening-Soil model we have:

$$E_{oed} = E_{oed}^{ref} \left(\sigma / p^{ref} \right)^m$$

at least for c = 0, and a linear relationship is obtained for m = 1. Indeed, on using an exponent equal to one, the above stiffness law reduces to:

$$E_{oed} = \sigma / \lambda^* \text{ where } \lambda^* = p^{ref} / E_{oed}^{ref}$$

For this special case of m = 1, the Hardening-Soil model yields $\dot{\varepsilon} = \lambda^* \dot{\sigma} / \sigma$, which can be integrated to obtain the well-known logarithmic compression law $\varepsilon = \lambda^* \ln \sigma$ for primary oedometer loading.

For many practical soft-soil studies, the modified compression index λ^* will be known and the PLAXIS user can compute the oedometer modulus from the relationship:

$$E_{oed}^{ref} = p^{ref} / \lambda^*$$

From the above considerations it would seem that the HS-model is perfectly suitable for soft soils. Indeed, most soft soil problems can be analysed using this model, but the HS-model is not suitable when considering creep, i.e. secondary compression. All soils exhibit some creep, and primary compression is thus always followed by a certain amount of secondary compression. Assuming the secondary compression (for instance during a period of 10 or 30 years) to be a percentage of the primary compression, it is clear that creep is important for problems involving large primary compression. This is for instance the case when constructing embankments on soft soils. Indeed, large primary settlements of dams and embankments are usually followed by substantial creep

settlements in later years. In such cases it is desirable to estimate the creep from FEM-computations.

Dams or buildings may also be founded on initially overconsolidated soil layers that yield relatively small primary settlements. Then, as a consequence of the loading, a state of normal consolidation may be reached and significant creep may follow. This is a treacherous situation as considerable secondary compression is not preceded by the warning sign of large primary compression. Again, computations with a creep model are desirable.

Buisman (1936) was probably the first to propose a creep law for clay after observing that soft-soil settlements could not be fully explained by classical consolidation theory. This work on 1D-secondary compression was continued by other researchers including, for example, Bjerrum (1967), Garlanger (1972), Mesri (1977) and Leroueil (1977). More mathematical lines of research on creep were followed by, for example, Sekiguchi (1977), Adachi and Oka (1982) and Borja et al. (1985). This mathematical 3D-creep modelling was influenced by the more experimental line of 1D-creep modelling, but conflicts exist.

3D-creep should be a straight forward extension of 1D-creep, but this is hampered by the fact that present 1D-models have not been formulated as differential equations. For the presentation of the Soft-Soil-Creep model we will first complete the line of 1D-modelling by conversion to a differential form. From this 1D differential equation an extension was made to a 3D-model. This Chapter gives a full description of the formulation of the Soft-Soil-Creep model. In addition, attention is focused on the model parameters. Finally, a validation of the 3D model is presented by considering both model predictions and data from triaxial tests. Here, attention is focused on constant strain rate triaxial tests and undrained triaxial creep tests. For more applications of the model the reader is referred to Vermeer et al. (1998) and Neher & Vermeer (1998).

Some basic characteristics of the Soft-Soil-Creep model are:

- Stress-dependent stiffness (logarithmic compression behaviour)

- Distinction between primary loading and unloading-reloading

- Secondary (time-dependent) compression

- Memory of pre-consolidation stress

- Failure behaviour according to the Mohr-Coulomb criterion

6.2 BASICS OF ONE-DIMENSIONAL CREEP

When reviewing previous literature on secondary compression in oedometer tests, one is struck by the fact that it concentrates on behaviour related to step loading, even though natural loading processes tend to be continuous or transient in nature. Buisman (1936)

was probably the first to consider such a classical creep test. He proposed the following equation to describe creep behaviour under constant effective stress:

$$\varepsilon = \varepsilon_c - C_B \log\left(\frac{t}{t_c}\right) \qquad \text{for:} \quad t > t_c \qquad (6.1)$$

where ε_c is the strain up to the end of consolidation, t the time measured from the beginning of loading, t_c the time to the end of primary consolidation and C_B is a material constant.

Please note that we do not follow the soil mechanics convention that compression is considered positive. Instead, compressive stresses and strains are taken to be negative. For further consideration, it is convenient to rewrite this equation as:

$$\varepsilon = \varepsilon_c - C_B \log\left(\frac{t_c + t'}{t_c}\right) \text{ for} \quad t' > 0 \qquad (6.2)$$

with $t' = t - t_c$ being the effective creep time.

Based on the work by Bjerrum on creep, as published for instance in 1967, Garlanger (1972) proposed a creep equation of the form:

$$e = e_c - C_\alpha \log\left(\frac{\tau_c + t'}{\tau_c}\right) \quad \text{with:} \quad C_\alpha = C_B\left(1 + e_0\right) \quad \text{for:} \quad t' > 0 \qquad (6.3)$$

Differences between Garlanger's and Buisman's forms are modest. The engineering strain ε is replaced by void ratio e and the consolidation time t_c is replaced by a parameter τ_c. Eqs. 6.2 and 6.3 are entirely identical when choosing $\tau_c = t_c$. For the case that $\tau_c \neq t_c$ differences between both formulations will vanish when the effective creep time t' increases.

For practical consulting, oedometer tests are usually interpreted by assuming $t_c = 24h$. Indeed, the standard oedometer test is a *Multiple Stage Loading Test* with loading periods of precisely one day. Due to the special assumption that this loading period coincides to the consolidation time t_c, it follows that such tests have no effective creep time. Hence one obtains $t' = 0$ and the log-term drops out of Eq. (6.3) It would thus seem that there is no creep in this standard oedometer test, but this suggestion is entirely false. Even highly impermeable oedometer samples need less than one hour for primary consolidation. Then all excess pore pressures are zero and one observes pure creep for the other 23 hours of the day. Therefore we will not make any assumptions about the precise values of τ_c and t_c.

Another slightly different possibility to describe secondary compression is the form adopted by Butterfield (1979):

$$\varepsilon^H = \varepsilon_c^H - C \ln\left(\frac{\tau_c + t'}{\tau_c}\right) \tag{6.4}$$

where ε^H is the logarithmic strain defined as:

$$\varepsilon^H = \ln\left(\frac{V}{V_0}\right) = \ln\left(\frac{1+e}{1+e_0}\right) \tag{6.5}$$

with the subscript '0' denoting the initial values. The subscript 'H' is used for denoting logarithmic strain. We use this particular symbol, as the logarithmic strain measure was originally used by Hencky. For small strains it is possible to show that:

$$C = \frac{C_\alpha}{(1+e_0)\cdot \ln 10} = \frac{C_B}{\ln 10} \tag{6.6}$$

because then logarithmic strain is approximately equal to the engineering strain. Both Butterfield (1979) and Den Haan (1994) showed that for cases involving large strain, the logarithmic small strain supersedes the traditional engineering strain.

6.3   ON THE VARIABLES τ_c AND ε_c

In this section attention will first be focussed on the variable τ_c. Here a procedure is to be described for an experimental determination of this variable. In order to do so we depart from Eq. (6.4) By differentiating this equation with respect to time and dropping the superscript 'H' to simplify notation, one finds:

$$-\dot{\varepsilon} = \frac{C}{\tau_c + t'} \qquad \text{or inversely:} \qquad -\frac{1}{\dot{\varepsilon}} = \frac{\tau_c + t'}{C} \tag{6.7}$$

which allows one to make use of the construction developed by Janbu (1969) for evaluating the parameters C and τ_c from experimental data. Both the traditional way, being indicated in Figure 6.1a, as well as the Janbu method of Figure 6.1b can be used to determine the parameter C from an oedometer test with constant load. The use of the Janbu method is attractive, because both τ_c and C follow directly when fitting a straight line through the data. In Janbu's representation of Figure 6.1b, τ_c is the intercept with the (non-logarithmic) time axis of the straight creep line. The deviation from a linear relation for $t < t_c$ is due to consolidation.
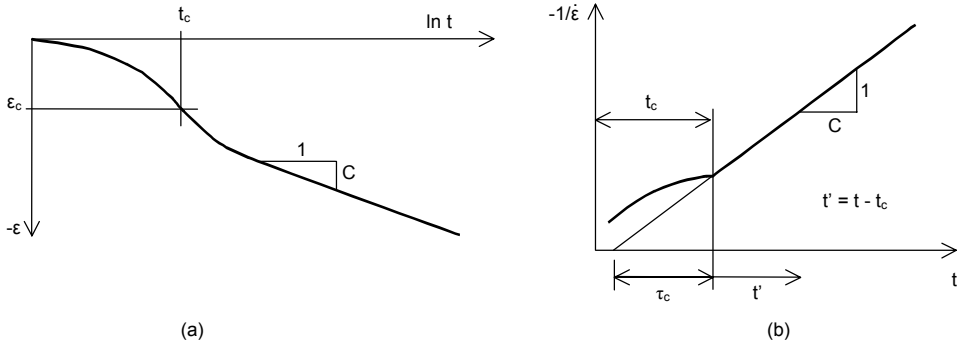
Figure 6.1 Consolidation and creep behaviour in standard oedometer test

Considering the classical literature it is possible to describe the end-of-consolidation strain ε_c, by an equation of the form:

$$\varepsilon_c = \varepsilon_c^e + \varepsilon_c^c = -A \ln\left(\frac{\sigma'}{\sigma_{0'}}\right) - B \ln\left(\frac{\sigma_{pc}}{\sigma_{p0}}\right) \tag{6.8}$$

Note that ε is a logarithmic strain, rather than a classical small strain although we conveniently omit the subscript 'H'. In the above equation σ_0' represents the initial effective pressure before loading and σ' is the final effective loading pressure. The values σ_{p0} and σ_{pc} representing the pre-consolidation pressure corresponding to before-loading and end-of-consolidation states respectively. In most literature on oedometer testing, one adopts the void ratio e instead of ε, and log instead of ln, and the swelling index C_r instead of A, and the compression index C_c instead of B. The above constants A and B relate to C_r and C_c as:

$$A = \frac{C_r}{(1+e_0)\cdot\ln 10} \qquad\qquad B = \frac{(C_c - C_r)}{(1+e_0)\cdot\ln 10} \tag{6.9}$$

Combining Eqs. 6.4 and 6.8 it follows that:

$$\varepsilon = \varepsilon^e + \varepsilon^c = -A\ln\left(\frac{\sigma'}{\sigma_{0'}}\right) - B\ln\left(\frac{\sigma_{pc}}{\sigma_{p0}}\right) - C\ln\left(\frac{\tau_c + t'}{\tau_c}\right) \tag{6.10}$$

where ε is the total logarithmic strain due to an increase in effective stress from σ_0' to σ' and a time period of $t_c + t'$. In Figure 6.2 the terms of Eq. (6.10) are depicted in a ε–$\ln\sigma$ diagram.
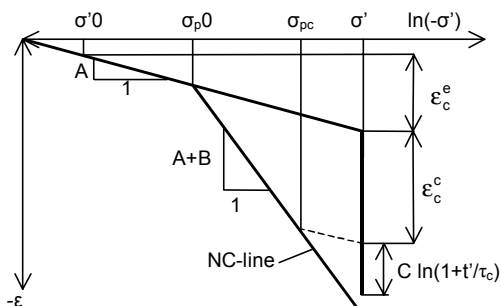
Figure 6.2   Idealised stress-strain curve from oedometer test with division of strain increments into an elastic and a creep component. For $t' + t_c = 1$ day, one arrives precisely on the NC-line

Up to this point, the more general problem of creep under transient loading conditions has not yet been addressed, as it should be recalled that restrictions have been made to creep under constant load. For generalising the model, a differential form of the creep model is needed. No doubt, such a general equation may not contain t' and neither τ_c as the consolidation time is not clearly defined for transient loading conditions.

6.4   DIFFERENTIAL LAW FOR 1D-CREEP

The previous equations emphasize the relation between accumulated creep and time, for a given constant effective stress. For solving transient or continuous loading problems, it is necessary to formulate a constitutive law in differential form, as will be described in this section. In a first step we will derive an equation for τ_c. Indeed, despite the use of logarithmic strain and ln instead of log, equation (6.10) is classical without adding new knowledge. Moreover, the question on the physical meaning of τ_c is still open. In fact, we have not been able to find precise information on τ_c in the literature, apart from Janbu's method of experimental determination.

In order to find an analytical expression for the quantity τ_c, we adopt the basic idea that all inelastic strains are time dependent. Hence total strain is the sum of an elastic part ε^e and a time-dependent creep part ε^c. For non-failure situations as met in oedometer loading conditions, we do not assume an instantaneous plastic strain component, as used in traditional elastoplastic modelling. In addition to this basic concept, we adopt Bjerrum's idea that the pre-consolidation stress depends entirely on the amount of creep strain being accumulated in the course of time. In addition to Eq. (6.10) we therefore introduce the expression:

$$\varepsilon = \varepsilon^e + \varepsilon^c = -A\ln\left(\frac{\sigma'}{\sigma_{0'}}\right) - B\ln\left(\frac{\sigma_p}{\sigma_{p0}}\right) \qquad \rightarrow$$

$$\rightarrow \quad \sigma_p = \sigma_{p0}\exp\left(\frac{-\varepsilon^c}{B}\right) \tag{6.11}$$

Please note that ε^c is negative, so that σ_p exceeds σ_{p0}. The longer a soil sample is left to creep the larger σ_p grows. The time-dependency of the pre-consolidation pressure σ_p is now found by combining Eqs. 6.10 and 6.11 to obtain:

$$\varepsilon^c - \varepsilon_c^c = -B\ln\left(\frac{\sigma_p}{\sigma_{pc}}\right) = -C\ln\left(\frac{\tau_c + t'}{\tau_c}\right) \tag{6.12}$$

This equation can now be used for a better understanding of τ_c, at least when adding knowledge from standard oedometer loading. In conventional oedometer testing the load is stepwise increased and each load step is maintained for a constant period of $t_c + t' = \tau$, where τ is precisely one day.

In this way of stepwise loading the so-called normal consolidation line (NC-line) with $\sigma_p = \sigma'$ is obtained. On entering $\sigma_p = \sigma'$ and $t' = \tau - t_c$ into Eq. (6.12) it is found that:

$$B\ln\left(\frac{\sigma'}{\sigma_{pc}}\right) = C\ln\left(\frac{\tau_c + \tau - t_c}{\tau_c}\right) \qquad \text{for:} \quad OCR = 1 \tag{6.13}$$

It is now assumed that $(\tau_c - t_c) \ll \tau$. This quantity can thus be disregarded with respect to τ and it follows that:

$$\frac{\tau}{\tau_c} = \left(\frac{\sigma'}{\sigma_{pc}}\right)^{\frac{B}{C}} \qquad \text{or:} \qquad \tau_c = \tau\left(\frac{\sigma_{pc}}{\sigma'}\right)^{\frac{B}{C}} \tag{6.14}$$

Hence τ_c depends both on the effective stress σ' and the end-of-consolidation pre-consolidation stress σ_{pc}. In order to verify the assumption $(\tau_c - t_c) \ll \tau$, it should be realised that usual oedometer samples consolidate for relatively short periods of less than one hour. Considering load steps on the normal consolidation line, we have OCR=1 both in the beginning and at the end of the load step. During such a load step σ_p increases from σ_{p0} up to σ_{pc} during the short period of (primary) consolidation. Hereafter σ_p increases further from σ_{pc} up to σ' during a relatively long creep period. Hence, at the end of the day the sample is again in a state of normal consolidation, but directly after the short consolidation period the sample is under-consolidated with $\sigma_p < \sigma'$. For the usually very high ratios of $B/C \geq 15$, we thus find very small τ_c-values from Eq. (6.14).

Hence not only t_c but also τ_c tend to be small with respect to τ. It thus follows that the assumption $(\tau_c - t_c) \ll \tau$ is certainly correct.

Having derived the simple expression 6.14 for τ_c, it is now possible to formulate the differential creep equation. To this end Eq. (6.10) is differentiated to obtain:

$$\dot{\varepsilon} = \dot{\varepsilon}^e + \dot{\varepsilon}^c = -A\frac{\dot{\sigma}'}{\sigma'} - \frac{C}{\tau_c + t'} \tag{6.15}$$

where $\tau_c + t'$ can be eliminated by means of Eq. (6.12) to obtain:

$$\dot{\varepsilon} = \dot{\varepsilon}^e + \dot{\varepsilon}^c = -A\frac{\dot{\sigma}'}{\sigma'} - \frac{C}{\tau_c}\left(\frac{\sigma_{pc}}{\sigma_p}\right)^{\frac{B}{C}}$$

with:

$$\sigma_p = \sigma_{p0}\ \exp\left(\frac{-\varepsilon^c}{B}\right) \tag{6.16}$$

Again it is recalled that ε^c is a compressive strain, being considered negative in this manual. Eq. (6.14) can now be introduced to eliminate τ_c and σ_{pc} and to obtain:

$$\dot{\varepsilon} = \dot{\varepsilon}^e + \dot{\varepsilon}^c = -A\frac{\dot{\sigma}'}{\sigma'} - \frac{C}{\tau}\left(\frac{\sigma'}{\sigma_p}\right)^{\frac{B}{C}} \tag{6.17}$$

6.5   THREE-DIMENSIONAL-MODEL

On extending the 1D-model to general states of stress and strain, the well-known stress invariants for pressure p and deviatoric stress q are adopted. These invariants are used to define a new stress measure named p^{eq}:

$$p^{eq} = p' + \frac{q^2}{M^2 p'} \tag{6.18}$$

In Figure 6.3 it is shown that the stress measure p^{eq} is constant on ellipses in p-q-plane. In fact we have the ellipses from the *Modified Cam-Clay-Model* as introduced by Roscoe and Burland (1968).
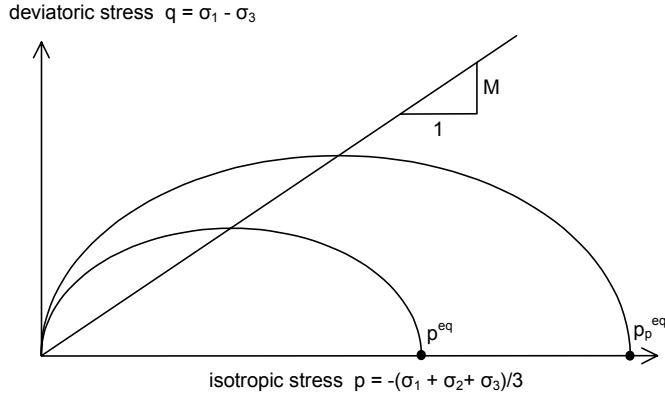
Figure 6.3 Diagram of p^{eq}-ellipse in a p-q-plane

The soil parameter M represents the slope of the so-called '*critical state line*' as also indicated in Figure 6.3. We use the general 3D-definition 2.7b for the deviatoric stress q and:

$$M = \frac{6 \sin \varphi_{cv}}{3 - \sin \varphi_{cv}} \tag{6.19}$$

where φ_{cv} is the critical-void friction angle, also referred to as critical-state friction angle. On using Eq. (2.7b) for q, the equivalent pressure p^{eq} is constant along ellipsoids in principal stress space. To extend the 1D-theory to a general 3D-theory, attention is now focused on normally consolidated states of stress and strain as met in oedometer testing. In such situations it yields $\sigma_2' = \sigma_3' = K_0^{NC} \sigma_1'$, and it follows from Eq. (6.18) that:

$$p^{eq} = \sigma' \left[\frac{1 + 2 K_0^{NC}}{3} + \frac{3\left(1 - K_0^{NC}\right)^2}{M^2 \left(1 + 2 K_0^{NC}\right)} \right] \quad ,$$

$$p_p^{eq} = \sigma_p \left[\frac{1 + 2 K_0^{NC}}{3} + \frac{3\left(1 - K_0^{NC}\right)^2}{M^2\left(1 + 2 K_0^{NC}\right)} \right] \tag{6.20}$$

where $\sigma' = K_0^{NC} \sigma_1'$, and p_p^{eq} is a generalised pre-consolidation pressure, being simply proportional to the one-dimensional one. For known values of K_0^{NC}, p^{eq} can thus be computed from σ', and p_p^{eq} can thus be computed from σ_p. Omitting the elastic strain in

the 1D-equation (6.17), introducing the above expressions for p^{eq} and $p_p{}^{eq}$ and writing ε_v instead of ε it is found that:

$$ -\dot{\varepsilon}_v^c = \frac{C}{\tau} \left(\frac{p^{eq}}{p_p^{eq}} \right)^{\frac{B}{C}} \qquad \text{where:} \qquad p_p^{eq} = p_{p0}^{eq} \exp \left(\frac{-\varepsilon_v^c}{B} \right) \tag{6.21} $$

For one-dimensional oedometer conditions, this equation reduces to Eq. (6.17), so that one has a true extension of the 1D-creep model. It should be noted that the subscript '0' is once again used in the equations to denote initial conditions and that $\varepsilon_v^c = 0$ for time $t = 0$.

Instead of the parameters A, B and C of the 1D-model, we will now change to the material parameters κ^*, λ^* and μ^*, who fit into the framework of critical-state soil mechanics. Conversion between constants follows the rules:

$$ \kappa^* = \frac{3(1 - v_{ur})}{(1 + v_{ur})} A \quad , \quad B = \lambda^* - \kappa^* \quad , \quad \mu^* = C \tag{6.22} $$

On using these new parameters, Eq. (6.21) changes to become:

$$ -\dot{\varepsilon}_v^c = \frac{\mu^*}{\tau} \left(\frac{p^{eq}}{p_p^{eq}} \right)^{\frac{\lambda^* - \kappa^*}{\mu^*}} \qquad \text{with:} \qquad p_p^{eq} = p_{p0}^{eq} \exp \left(\frac{-\varepsilon_v^c}{\lambda^* - \kappa^*} \right) \tag{6.23} $$

As yet the 3D-creep model is incomplete, as we have only considered a volumetric creep strain ε_v^c, whilst soft soils also exhibit deviatoric creep strains. For introducing general creep strains, we adopt the view that creep strain is simply a time-dependent plastic strain. It is thus logic to assume a flow rule for the rate of creep strain, as usually done in plasticity theory. For formulating such a flow rule, it is convenient to adopt the vector notation and considering principal directions:

$$ \underline{\sigma} = \left(\sigma_1 \ \sigma_2 \ \sigma_3 \right)^T \qquad \text{and:} \qquad \underline{\varepsilon} = \left(\varepsilon_1 \ \varepsilon_2 \ \varepsilon_3 \right)^T $$

where T is used to denote a transpose. Similar to the 1D-model we have both elastic and creep strains in the 3D-model. Using Hooke's law for the elastic part, and a flow rule for the creep part, one obtains:

$$ \underline{\dot{\varepsilon}} = \underline{\dot{\varepsilon}}^e + \underline{\dot{\varepsilon}}^c = \underline{\underline{D}}^{-1} \ \underline{\dot{\sigma}}' + \lambda \frac{\partial g^c}{\partial \underline{\sigma}'} \tag{6.24} $$

where the elasticity matrix and the plastic potential function are defined as:

$$\underline{\underline{D}}^{-1} = \frac{1}{E_{ur}} \begin{bmatrix} 1 & -v_{ur} & -v_{ur} \\ -v_{ur} & 1 & -v_{ur} \\ -v_{ur} & -v_{ur} & 1 \end{bmatrix} \quad \text{and:} \qquad g^c = p^{eq}$$

Hence we use the equivalent pressure p^{eq} as a plastic potential function for deriving the individual creep strain-rate components. The subscripts 'ur' are introduced to emphasize that both the elasticity modulus and Poisson's ratio will determine unloading-reloading behaviour. Now it follows from the above equations that:

$$\dot{\varepsilon}_v^c = \dot{\varepsilon}_1^c + \dot{\varepsilon}_2^c + \dot{\varepsilon}_3^c = \lambda = \left(\frac{\partial p^{eq}}{\partial \sigma_{1'}} + \frac{\partial p^{eq}}{\partial \sigma_{2'}} + \frac{\partial p^{eq}}{\partial \sigma_{3'}} \right) = \lambda = \frac{\partial p^{eq}}{\partial p'} = \lambda = \alpha \qquad (6.25)$$

Hence we define $\alpha = \partial p^{eq}/\partial p'$. Together with Eqs. 6.23 and 6.24 this leads to:

$$\dot{\underline{\varepsilon}} = \underline{\underline{D}}^{-1} \dot{\underline{\sigma}}' + \frac{\dot{\varepsilon}_v^c}{\alpha} \frac{\partial p^{eq}}{\partial \underline{\sigma}'} = \underline{\underline{D}}^{-1} \dot{\underline{\sigma}}' - \frac{1}{\alpha} \frac{\mu^*}{\tau} \left(\frac{p^{eq}}{p_p^{eq}} \right)^{\frac{\lambda^* - \kappa^*}{\mu^*}} \frac{\partial p^{eq}}{\partial \underline{\sigma}'} \qquad (6.26)$$

where:

$$p_p^{eq} = p_{p0}^{eq} \exp\left(\frac{-\varepsilon_v^c}{\lambda^* - \kappa^*} \right) \quad \text{or inversely: } - \varepsilon_v^c = \left(\lambda^* - \kappa^* \right) \ln \left(\frac{p_p^{eq}}{p_{p0}^{eq}} \right)$$

6.6 FORMULATION OF ELASTIC 3D-STRAINS

Considering creep strains, it has been shown that the 1D-model can be extended to obtain the 3D-model, but as yet this has not been done for the elastic strains.

To get a proper 3D-model for the elastic strains as well, the elastic modulus E_{ur} has to been defined as a stress-dependent tangent stiffness according to:

$$E_{ur} = 3(1 - 2v_{ur})K_{ur} = 3(1 - 2v_{ur}) \frac{p'}{\kappa^*} \qquad (6.27)$$

Hence, E_{ur} is not a new input parameter, but simply a variable quantity that relates to the input parameter κ^*. On the other hand v_{ur} is an additional true material constant. Hence similar to E_{ur}, the bulk modulus K_{ur} is stress dependent according to the rule $K_{ur} = p'/\kappa^*$. Now it can be derived for the volumetric elastic strain that:

$$\dot{\varepsilon}_v^e = \frac{\dot{p}'}{K_{ur}} = -\kappa^* \frac{\dot{p}'}{p'} \quad \text{or by integration:} \quad -\varepsilon_v^e = \kappa^* \ln\left(\frac{p'}{p_{0'}}\right) \quad (6.28)$$

Hence in the 3D-model the elastic strain is controlled by the mean stress p', rather than by principal stress σ' as in the 1D-model. However mean stress can be converted into principal stress. For one-dimensional compression on the normal consolidation line, we have both $-3p' = (1 + 2K_0^{NC})\sigma'$ and $-3p_0' = (1 + 2K_0^{NC})\sigma_0'$ and it follows that $p'/p_0 = \sigma'/\sigma_0$. As a consequence we derive the simple rule $-\varepsilon_v^c = \kappa^* \ln(\sigma'/\sigma_0')$, whereas the 1D-model involves $-\varepsilon_v^c = A \ln(\sigma'/\sigma_0')$. It would thus seem that κ^* coincides with A. Unfortunately this line of thinking cannot be extended towards overconsolidated states of stress and strain. For such situations, it can be derived that:

$$\frac{\dot{p}'}{p'} = \frac{1 + \nu_{ur}}{1 - \nu_{ur}} \frac{1}{1 + 2K_0} \frac{\dot{\sigma}'}{\sigma'} \quad (6.29)$$

and it follows that:

$$-\dot{\varepsilon}_v^e = \kappa^* \frac{\dot{p}'}{p'} = \frac{1 + \nu_{ur}}{1 - \nu_{ur}} \frac{\kappa^*}{1 + 2K_0} \frac{\dot{\sigma}'}{\sigma'} \quad (6.30)$$

where K_0 depends to a great extent on the degree of overconsolidation. For many situations, it is reasonable to assume $K_0 \approx 1$ and together with $\nu_{ur} \approx 0.2$ one obtains $-2\varepsilon_v^c \approx \kappa^* \ln(\sigma'/\sigma_0')$. Good agreement with the 1D-model is thus found by taking $\kappa^* \approx 2A$.

6.7   REVIEW OF MODEL PARAMETERS

As soon as the failure yield criterion $f(\underline{\sigma}', c, \varphi) = 0$ is met, instantaneous plastic strain rates develop according to the flow rule $\underline{\dot{\varepsilon}}^p = \lambda \, \partial g / \partial \underline{\sigma}'$ with $g = g(\sigma', \psi)$. This gives as additional soil parameters the effective cohesion, c, the Mohr-Coulomb friction angle, φ, and the dilatancy angle ψ. For fine grained, cohesive soils, the dilatancy angle tends to be small, it may often be assumed that ψ is equal to zero. In conclusion, the Soft-Soil-Creep model requires the following material constants:

Failure parameters as in the Mohr-Coulomb model:

c	: Cohesion	[kN/m²]
φ	: Friction angle	[°]
ψ	: Dilatancy angle	[°]

Basic stiffness parameters:

κ^*	: Modified swelling index	[-]
λ^*	: Modified compression index	[-]
μ^*	: Modified creep index	[-]

Advanced parameters (it is advised to use the default setting):

ν_{ur}	: Poisson's ratio for unloading-reloading (default 0.15)	[-]
K_0^{NC}	: $\sigma'_{xx} / \sigma'_{yy}$ stress ratio in a state of normal consolidation	[-]
M	: K_0^{NC} -related parameter (see below)	[-]
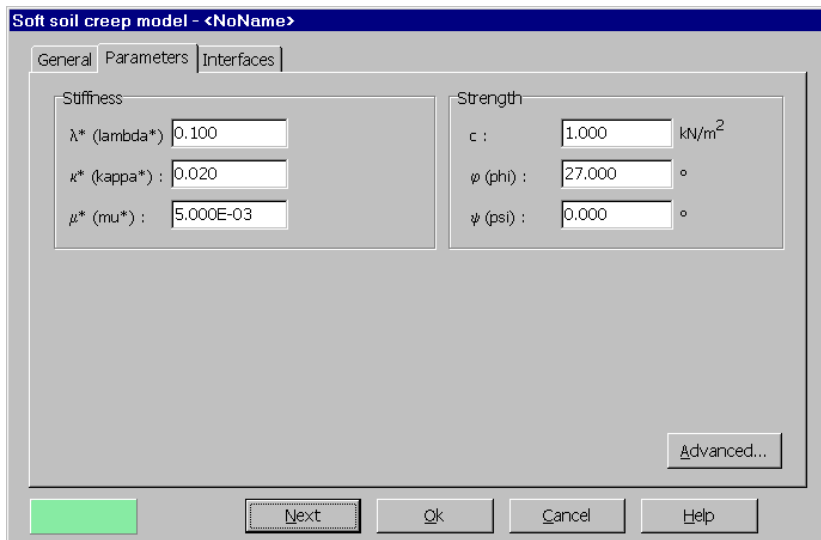
Figure 6.4 Parameters tab for the Soft-Soil-Creep model

By default, *M* is calculated from Eq. (6.19), using $\varphi_{cv} = \varphi + 0.1°$, this is not an experimental finding, but just a practical default value. In addition, PLAXIS displays the approximate value of K_0^{NC} that corresponds to the default setting of *M*. In general, resulting default values of K_0^{NC} tend to be somewhat higher than the ones that follow from Jaky's formula $K_0^{NC} = 1-\sin\varphi$. Alternatively, values of K_0^{NC} may be entered after which the corresponding value of *M* is calculated from the relation (Brinkgreve, 1994):

$$M = 3\sqrt{\frac{\left(1-K_0^{NC}\right)^2}{\left(1+2K_0^{NC}\right)^2} + \frac{\left(1-K_0^{NC}\right)\left(1-2\nu_{ur}\right)\left(\lambda^*/\kappa^*-1\right)}{\left(1+2K_0^{NC}\right)\left(1-2\nu_{ur}\right)\lambda^*/\kappa^*-\left(1-K_0^{NC}\right)\left(1+\nu_{ur}\right)}} \qquad (6.31)$$

Hence the user can not enter directly a particular value of M. Instead he can choose values for K_0^{NC}.
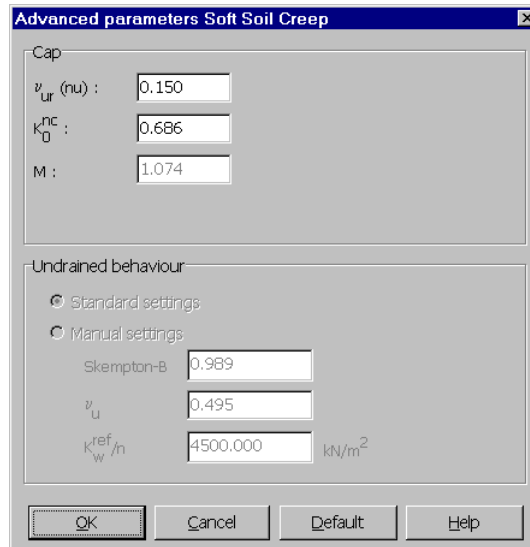
Figure 6.5 Advanced parameters for Soft-Soil-Creep model

Modified swelling index, modified compression index and modified creep index

These parameters can be obtained both from an isotropic compression test and an oedometer test. When plotting the logarithm of stress as a function of strain, the plot can be approximated by two straight lines (see Figure 6.2). The slope of the normal consolidation line gives the modified compression index λ^*, and the slope of the unloading (or swelling) line can be used to compute the modified swelling index κ^*, as explained in section 6.6. Note that there is a difference between the modified indices κ^* and λ^* and the original Cam-Clay parameters κ and λ. The latter parameters are defined in terms of the void ratio e instead of the volumetric strain ε_v. The parameter μ^* can be obtained by measuring the volumetric strain on the long term and plotting it against the logarithm of time (see Figure 6.1).

Table 6.1a Relationship to Cam-Clay parameters

$\lambda^* = \dfrac{\lambda}{1 + e}$	$\kappa^* = \dfrac{\kappa}{1 + e}$	- - -

Table 6.1b Relationship to Dutch engineering practice

$\lambda^* = \dfrac{1}{C_p}{}'$	$\kappa^* \approx \dfrac{2}{A_p}$	$\mu^* \approx \dfrac{1}{2.3\,C_s{}'}$

Table 6.1c Relationship to internationally normalized parameters

$\lambda^* = \dfrac{C_c}{2.3(1 + e)}$	$\kappa^* \approx \dfrac{2}{2.3}\dfrac{C_r}{1+e}$	$\mu^* = \dfrac{C_\alpha}{2.3(1 + e)}$

In Table 6.1b, A_p represents the slope of the one-dimensional unloading curve in the $\ln p'$-ε_v plot.

As already indicated in section 6.6, there is no exact relation between the isotropic compression indices κ and κ^* and the one-dimensional swelling indices A_p and C_r, because the ratio of horizontal and vertical stress changes during one-dimensional unloading. For the approximation it is assumed that the average stress state during unloading is an isotropic stress state, i.e. the horizontal and vertical stresses are equal.

For a rough estimate of the model parameters, one might use the correlation $\lambda^* \approx I_p(\%)/500$, the fact that λ^* / μ^* is in the range between 15 to 25 and the general observation λ^*/κ^* is in the range between 5 to 10.

For characterising a particular layer of soft soil, it is also necessary to know the initial pre-consolidation pressure σ_{p0}. This pressure may, for example, be computed from a given value of the overconsolidation ratio (OCR). Subsequently σ_{p0} can be used to compute the initial value of the generalised pre-consolidation pressure p_p^{eq} (see Section 2.6).

Poisson's ratio

In the case of the Soft-Soil-Creep model, Poisson's ratio is purely an elasticity constant rather than a pseudo-elasticity constant as used in the Mohr-Coulomb model. Its value will usually be in the range between 0.1 and 0.2. If the standard setting for the Soft-Soil-Creep model parameters is selected, then the value $\nu_{ur} = 0.15$ is automatically adopted. For loading of normally consolidated materials, Poisson's ratio plays a minor role, but it becomes important in unloading problems. For example, for unloading in a one-dimensional compression test (oedometer), the relatively small Poisson's ratio will result in a small decrease of the lateral stress compared with the decrease in vertical stress. As

a result, the ratio of horizontal and vertical stress increases, which is a well-known phenomenon for overconsolidated materials. Hence, Poisson's ratio should not be based on the normally consolidated K_0^{NC}-value, but on the ratio of difference in horizontal stress to difference in vertical stress in oedometer unloading and reloading:

$$\frac{v_{ur}}{1-v_{ur}} = \frac{\Delta\sigma_{xx}}{\Delta\sigma_{yy}} \quad \text{(unloading and reloading)} \quad (6.32)$$

6.8   VALIDATION OF THE 3D-MODEL

This section briefly compares the simulated response of undrained triaxial creep behaviour of Haney clay with test data provided by Vaid and Campanella (1977), using the material parameters summarized below. An extensive validation of the Soft-Soil-Creep model is also provided in Stolle et al. (1997). All triaxial tests considered were completed by initially consolidating the samples under an effective isotropic confining pressure of 525 kPa for 36 hours and then allowing them to stand for 12 hours under undrained conditions before starting a shearing part of the test.

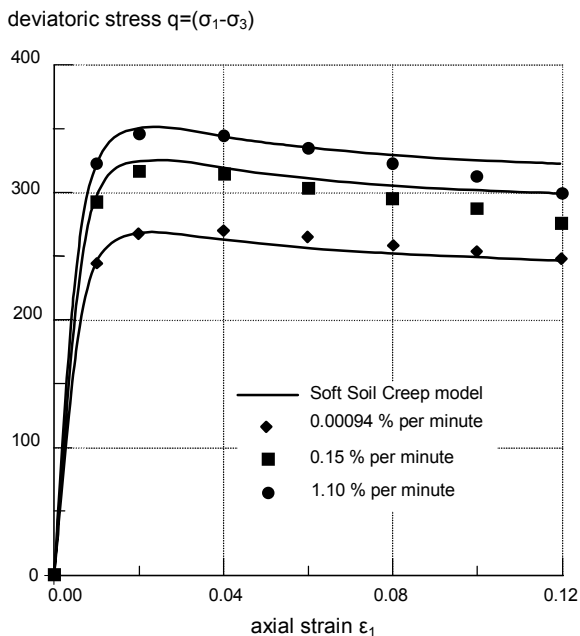deviatoric stress q=(σ_1-σ_3)

Figure 6.6   Results of the undrained triaxial tests (CU-tests) with different rates of strain The faster the test the higher the undrained shear strength

The material properties for Haney Clay are:

$\kappa^* = 0.016$ $\qquad$ $\lambda^* = 0.105$ $\qquad$ $\mu^* = 0.004$

$\phi_{mc} = 32^o$ $\qquad$ $\psi = 0^o$ $\qquad$ $c = 0$ kPa

$\phi_{cs} = 32.1^o$ $\qquad$ $K_0^{NC} = $ default $\qquad$ $v = 0.25$

The end-of-consolidation pre-consolidation pressure, p_p^{eq}, was found to be 373 kPa. This value was determined by simulating the consolidation part of the test. The pre-consolidation pressure p_p^{eq} of 373 kPa is less than 525 kPa, which would have been required for an OCR_o of 1. It is clear that the pre-consolidation pressure not only depends on the applied maximum consolidation stress, but also on creep time as discussed in previous sections. In Figure 6.6 we can see the results of Vaid and Campanella's tests (1977) for different strain rates and the computed curves, that were calculated with the present creep model. It is observed that the model describes the tests very well.

Constant strain rate shear tests

Undrained triaxial compression tests, as considered in Figure 6.6, performed under constant rates of vertical strain $\dot{\varepsilon}_1$ and constant horizontal pressure σ_3 where the shear stress q can move. This behaviour is shown in Figure 6.7.

deviatoric stress q = σ₁ - σ₃

"Fast" tests

"Slow" tests

isotropic stress p = -(σ₁ + 2σ₃)/3
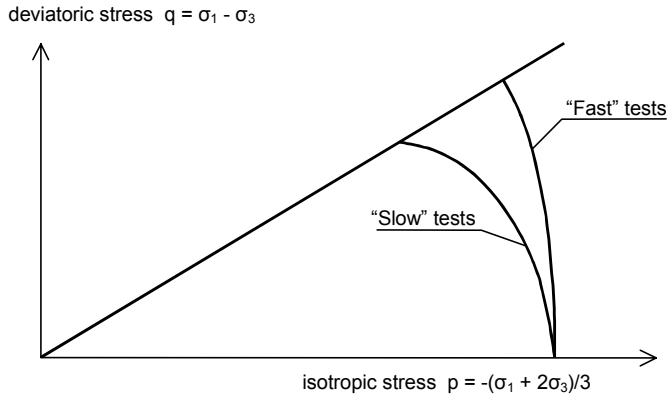
Figure 6.7 Strain rate dependency of the effective stress path in undrained triaxial tests

During these undrained tests it yields $\dot{\varepsilon}_v = \dot{\varepsilon}_v^{\,e} + \dot{\varepsilon}_v^{\,c} = 0$ or equivalently $\dot{\varepsilon}_v^{\,e} = -\dot{\varepsilon}_v^{\,c}$. Hence, creep compaction is balanced by elastic swelling of the sample. The slower a test is performed, the larger the creep compaction is and finally the elastic swelling. The

expression $\dot{p}' = K_{ur}\dot{\varepsilon}_v^e$, where K_{ur} is the elastic bulk modulus, shows that elastic swelling implies a decrease of the mean stress.

For extremely fast tests there is no time for creep; it yields $\dot{\varepsilon}_v^c = 0$ and consequently also $\dot{\varepsilon}_v^e = 0$. Hence in this extreme case there is no elastic volume change and consequently neither a change of the mean stress. This implies a straight vertical path for the effective stress in *p-q*-plane. On inspecting all numerical results, it appears that the undrained shear strength, c_u, may be approximated by the equation:

$$\frac{c_u}{c_u^*} \approx 1.02 + 0.09 \ \log \ \dot{\varepsilon} \tag{6.33}$$

where c_u^* is the undrained shear strength in an undrained triaxial test with a strain rate of 1% per hour. This agrees well with the experimental data summarized by Kulhawy and Mayne (1990).

Undrained triaxial creep tests

These tests begin with isotropic consolidation up to a mean stress of 525 kPa. Then a deviatoric stress *q* is applied in undrained loading. Finally all external stresses are kept constant and the sample is subjected to undrained creep.
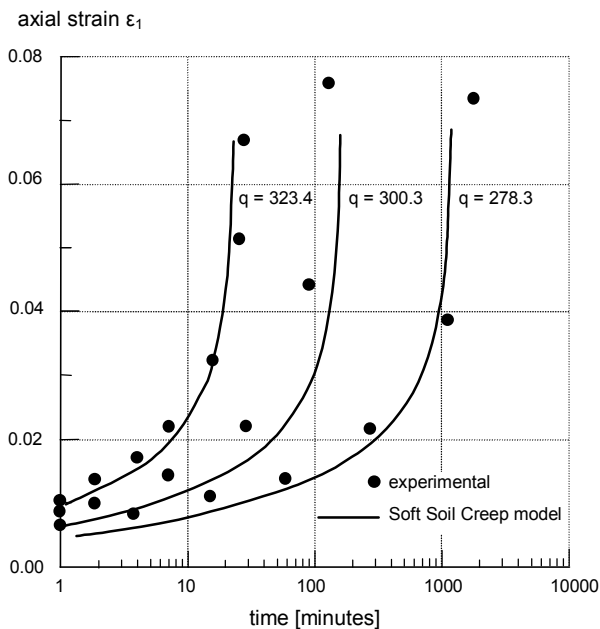

Figure 6.8 Results of triaxial creep tests.

Samples were first consolidated under the same isotropic stress. Then undrained samples were loaded up to different deviatoric stresses. Creep under constant deviatoric stress is observed, being well predicted by the Soft-Soil-Creep model.

The amount of creep depends on the applied deviatoric stress q or rather on the applied stress ratio q/p. For relatively small stress ratios, creep rates are small and they decrease in course of time. For large stress ratios, however, creep rates increase with time and samples will finally fail, i.e. strain rates become infinitely large.

Figure 6.8 shows the actual creep strain evolution for samples with three different deviatoric stresses.
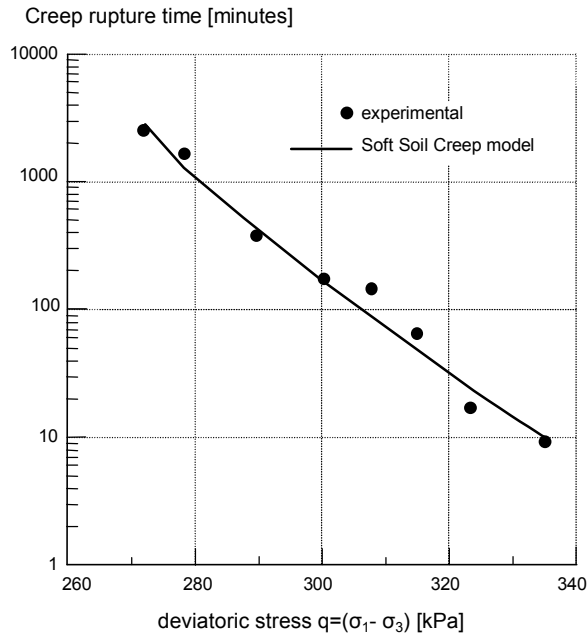
Creep rupture time [minutes]

Figure 6.9 Results of triaxial creep tests.

All tests have different constant deviatoric stress. The creep rupture time is the creep time up to a creep rate $\dot{\varepsilon} = \infty$, as indicated by the asymptotes in Figure 6.8.

7 THE SOFT SOIL MODEL

To highlight the significance of the Soft-Soil model, it is worth mentioning that starting from Version 7 some changes to the soil modelling strategy of PLAXIS have been introduced. Up to Version 6 PLAXIS material models had consisted of Mohr-Coulomb model, Soft-Soil model and Hard-Soil model. In Version 7, however, the idea of using separate models for soft soil and hard soil has been excluded. Instead, the Hard-Soil model was further developed to become an advanced model for soils ranging from soft to hard. This has resulted into the current Hardening-Soil model. At the same time the Soft-Soil-Creep model was implemented to capture some of the very special features of soft soil. As a result, the Soft-Soil model can be substituted by the new Hardening-Soil model or the Soft-Soil-Creep model. However, in order not to deny users' preferences to use models that they have got to know well, it was decided to keep the Soft-Soil model in PLAXIS Version 8. Some features of the Soft-Soil model are:

- Stress dependent stiffness (logarithmic compression behaviour).

- Distinction between primary loading and unloading-reloading.

- Memory for pre-consolidation stress.

- Failure behaviour according to the Mohr-Coulomb criterion.

7.1 ISOTROPIC STATES OF STRESS AND STRAIN ($\sigma_1' = \sigma_2' = \sigma_3'$)

In the Soft-Soil model, it is assumed that there is a logarithmic relation between the volumetric strain, ε_v, and the mean effective stress, p', which can be formulated as:

$$\varepsilon_v - \varepsilon_v^0 = -\lambda^* \ln\left(\frac{p'}{p^0}\right) \qquad \text{(virgin compression)} \qquad (7.1)$$

In order to maintain the validity of Expression (7.1) a minimum value of p' is set equal to a unit stress. The parameter λ^* is the modified compression index, which determines the compressibility of the material in primary loading. Note that λ^* differs from the index λ as used by Burland (1965).

The difference is that Eq. (7.1) is a function of volumetric strain instead of void ratio. Plotting Eq. (7.1) gives a straight line as shown in Figure 7.1.
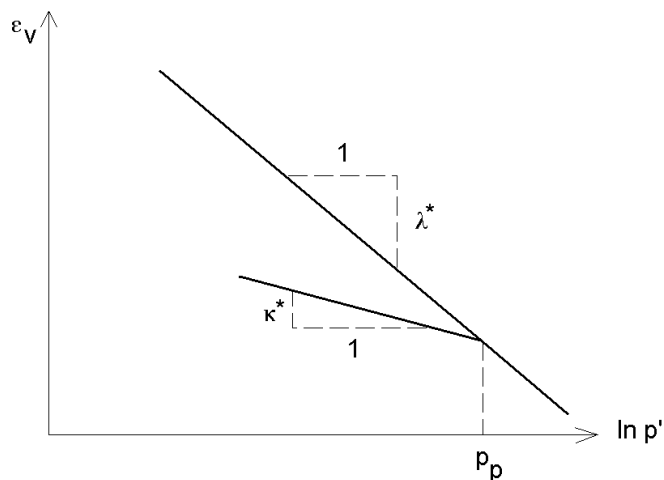
Figure 7.1 Logarithmic relation between volumetric strain and mean stress

During isotropic unloading and reloading a different path (line) is followed, which can be formulated as:

$$\varepsilon_v^e - \varepsilon_v^{e0} = -\kappa^* \ln\left(\frac{p'}{p^0}\right) \quad \text{(unloading and reloading)} \tag{7.2}$$

Again, a minimum value of p' is set equal to a unit stress. The parameter κ^* is the modified swelling index, which determines the compressibility of the material in unloading and subsequent reloading. Note that κ^* differs from the index κ as used by Burland. The ratio λ^*/κ^* is, however, equal to Burland's ratio λ/κ. The soil response during unloading and reloading is assumed to be elastic as denoted by the superscript e in Eq. (7.2). The elastic behaviour is described by Hooke's law (see Section 2.2) and Eq. (7.2) implies linear stress dependency on the tangent bulk modulus such that:

$$K_{ur} \equiv \frac{E_{ur}}{3\,(1 - 2\,\nu_{ur})} = \frac{p'}{\kappa^*} \tag{7.3}$$

in which the subscript ur denotes unloading / reloading. Note that effective parameters are considered rather than undrained soil properties, as might be suggested by the subscripts ur. Neither the elastic bulk modulus, K_{ur}, nor the elastic Young's modulus, E_{ur}, is used as an input parameter. Instead, ν_{ur} and κ^* are used as input constants for the part of the model that computes the elastic strains.

An infinite number of unloading / reloading lines may exist in Figure 7.1, each corresponding to a particular value of the isotropic pre-consolidation stress p_p. The pre-

consolidation stress represents the largest stress level experienced by the soil. During unloading and reloading, this pre-consolidation stress remains constant. In primary loading, however, the pre-consolidation stress increases with the stress level, causing irreversible (plastic) volumetric strains.

7.2   YIELD FUNCTION FOR TRIAXIAL STRESS STATE ($\sigma_2' = \sigma_3'$)

The Soft-Soil model is capable to simulate soil behaviour under general states of stress. However, for clarity, in this section, restriction is made to triaxial loading conditions under which $\sigma_2' = \sigma_3'$. For such a state of stress the yield function of the Soft-Soil model is defined as:

$$f = \overline{f} - p_p \tag{7.4}$$

where $\overline{f}$ is a function of the stress state (p',q) and p_p, the pre-consolidation stress, is a function of plastic strain such that:

$$\overline{f} = \frac{q^2}{M^2\ (p'+c\cot\varphi)} + p' \tag{7.5}$$

$$p_p = p_p^0 \exp\left(\frac{-\varepsilon_v^p}{\lambda^* - \kappa^*}\right) \tag{7.6}$$

The yield function f describes an ellipse in the p'-q-plane, as illustrated in Figure 7.2. The parameter M in Eq. (7.5) determines the height of the ellipse. The height of the ellipse is responsible for the ratio of horizontal to vertical stresses in primary one-dimensional compression. As a result, the parameter M determines largely the coefficient of lateral earth pressure, K_0^{nc}. In view of this, the value of M can be chosen such that a known value of K_0^{nc} is matched in primary one-dimensional compression. Such an interpretation and use of M differs from the original critical state line idea, but it ensures a proper matching of K_0^{nc}.

The tops of all ellipses are located on a line with slope M in the p'-q-plane. In the Modified Cam-Clay model (Burland 1965, 1967) the M-line is referred to as the critical state line and represents stress states at post peak failure. The parameter M is then based on the critical state friction angle. In the Soft-Soil model, however, failure is not necessarily related to critical state. The Mohr-Coulomb failure criterion is a function of the strength parameters φ and c, which might not correspond to the M-line.

The isotropic pre-consolidation stress, p_p, determines the extent of the ellipse along p' axis. During loading, infinitely many ellipses may exist (see Figure 7.2) each corresponds to a particular value of p_p. In tension ($p' < 0$), the ellipse extends to $c\cot\varphi$

(Eq. (7.5) and Figure 7.2). In order to make sure that the right hand side of the ellipse (i.e. the 'cap') will remain in the 'compression' zone ($p' > 0$) a minimum value of $c \cot\varphi$ is adopted for p_p. For $c = 0$, a minimum value of p_p equal to a stress unit is adopted. Hence, there is a 'threshold' ellipse as illustrated in Figure 7.2.
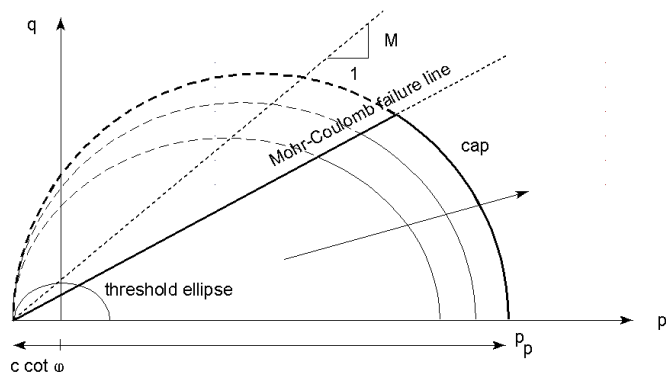

Figure 7.2 Yield surface of the Soft-Soil model in p'-q-plane

The value of p_p is determined by volumetric plastic strain following the hardening relation, Eq. (7.6). This equation reflects the principle that the pre-consolidation stress increases exponentially with decreasing volumetric plastic strain (compaction). p_p^0 can be regarded as the initial value of the pre-consolidation stress. The determination of p_p^0 is treated in Section 2.6. According to Eq. (7.6) the initial volumetric plastic strain is assumed to be zero.

In the Soft-Soil model, the yield function, Eq. (7.4), describes the irreversible volumetric strain in primary compression, and forms the cap of the yield contour. To model the failure state, a perfectly-plastic Mohr-Coulomb type yield function is used. This yield function represents a straight line in p'-q-plane as shown in Figure 7.2. The slope of the failure line is smaller than the slope of the M-line.

The total yield contour, as shown by the bold lines in Figure 7.2, is the boundary of the elastic stress area. The failure line is fixed, but the cap may increase in primary compression. Stress paths within this boundary give only elastic strain increments, whereas stress paths that tend to cross the boundary generally give both elastic and plastic strain increments.

For general states of stress, the plastic behaviour of the Soft-Soil model is defined by a total of six yield functions; three compression yield functions and three Mohr-Coulomb yield functions. The total yield contour in principal stress space, resulting from these six yield functions, is indicated in Figure 7.3.
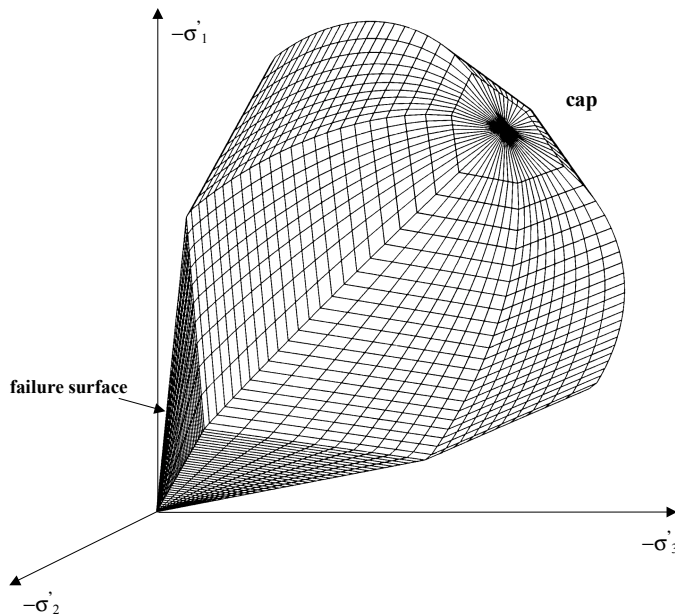
Figure 7.3   Representation of total yield contour of the Soft-Soil model in principal stress space

7.3   PARAMETERS OF THE SOFT-SOIL MODEL

The parameters of the Soft-Soil model coincide with those of the Soft-Soil-Creep model. However, since the Soft-Soil model does not include time, the modified creep index μ^* is not considered. Thus, the Soft-Soil model requires the following material constants:

Basic parameters:

λ^*	:	Modified compression index	[-]
κ^*	:	Modified swelling index	[-]
c	:	Cohesion	[kN/m^2]
φ	:	Friction angle	[°]
ψ	:	Dilatancy angle	[°]

Advanced parameters (use default settings):

ν_{ur}	:	Poisson's ratio for unloading / reloading	[-]
K_0^{NC}	:	Coefficient of lateral stress in normal consolidation	[-]
M	:	K_0^{NC}-parameter	[-]

Figure 7.4 shows PLAXIS window for inputting the values of the model parameters. M is calculated automatically from the coefficient of the lateral earth pressure, K_0^{NC}, by means of Eq. (7.8). Note that, physically, in the current model M differs from that in the Modified Cam-Clay model where it is related to the material friction.
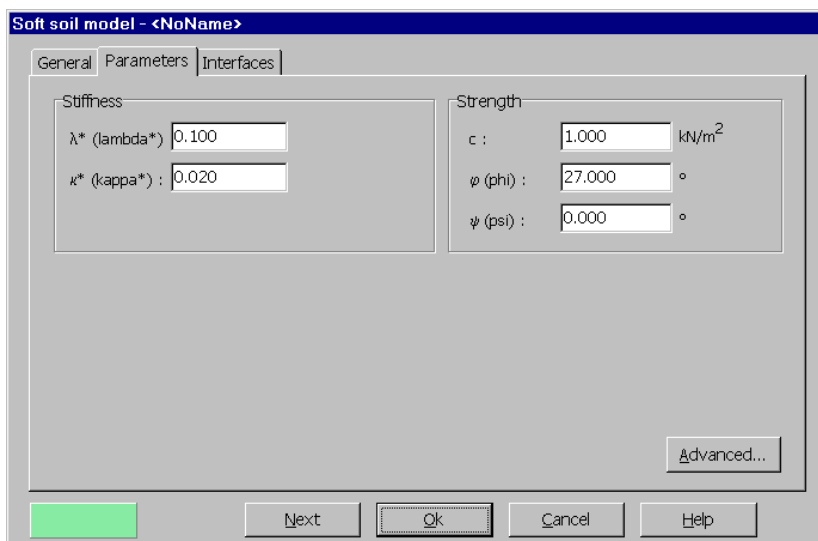

Figure 7.4 Parameters tab for the Soft-Soil model

Modified swelling index and modified compression index

These parameters can be obtained from an isotropic compression test including isotropic unloading. When plotting the logarithm of the mean stress as a function of the volumetric strain for clay-type materials, the plot can be approximated by two straight lines (see Figure 7.1). The slope of the primary loading line gives the modified compression index, and the slope of the unloading (or swelling) line gives the modified swelling index. Note that there is a difference between the modified indices κ^* and λ^* and the original Cam-Clay parameters κ and λ. The latter parameters are defined in terms of the void ratio e instead of the volumetric strain ε_v.

Apart from the isotropic compression test, the parameters κ^* and λ^* can be obtained from the one-dimensional compression test. Here a relationship exists with the internationally recognized parameters for one-dimensional compression and recompression, C_c and C_r. Another relationship exists with the Dutch parameters for one-dimensional compression, C_p' and A_p. These relationships are summarized in Table 7.1.

Table 7.1a Relationship to Cam-Clay parameters

1. $\qquad \lambda^* = \dfrac{\lambda}{1 + e}$	2 $\qquad \kappa^* = \dfrac{\kappa}{1 + e}$

Table 7.1b Relationship to Dutch engineering practice

3. $\qquad \lambda^* = \dfrac{1}{C_p}{}'$	4. $\qquad \kappa^* \approx \dfrac{2}{A_p}$

Table 7.1c Relationship to internationally normalized parameters

5. $\qquad \lambda^* = \dfrac{C_c}{2.3\,(1 + e)}$	6. $\qquad \kappa^* \approx \dfrac{2\,C_r}{2.3(1 + e)}$

Remarks on Table 7.1:

- In relations 1 and 2, the void ratio, e, is assumed to be constant. In fact, e will change during a compression test, but this will give a relatively small difference in void ratio. For e one can use the average void ratio that occurs during the test or just the initial value.

- In relations 4 and 6 there is no exact relation between κ^* and the one-dimensional swelling indices, because the ratio of horizontal and vertical stresses changes during one-dimensional unloading. For approximation it is assumed that the average stress state during unloading is an isotropic stress state, i.e. the horizontal and vertical stresses are equal.

- The factor 2.3 in relation 5 is obtained from the ratio between the logarithm of base 10 and the natural logarithm.

- The ratio λ^*/κ^* ($=\lambda/\kappa$) ranges, in general, between 3 and 7.

Cohesion

The cohesion has the dimension of stresses. Any effective cohesion may be used, including a cohesion of zero. When using the standard setting the cohesion is set equal to 1 kPa. Entering a cohesion will result in an elastic region that is partly located in the 'tension' zone, as illustrated in Figure 7.2. The left hand side of the ellipse crosses the p'-axis at a value of $-c\cot\varphi$. In order to maintain the right hand side of the ellipse (i.e. the cap) in the 'pressure' zone of the stress space, the isotropic pre-consolidation stress p_p has a minimum value of $c\cot\varphi$. This means that entering a cohesion larger than zero may result in a state of 'over-consolidation', depending on the magnitude of the cohesion and the initial stress state. As a result, a stiffer behaviour is obtained during the onset of loading. It is not possible to specify undrained shear strength by means of high cohesion

and a friction angle of zero. Input of model parameters should always be based on effective values.

Friction angle

The effective angle of internal friction represents the increase of shear strength with effective stress level. It is specified in degrees. Zero friction angle is not allowed. On the other hand, care should be taken with the use of high friction angles. It is often recommended to use φ_{cv}, i.e. the critical state friction angle, rather than a higher value based on small strains.

Moreover, using a high friction angle will substantially increase the computational requirements.

Dilatancy angle

For the type of materials, which can be described by the Soft-Soil model, the dilatancy can generally be neglected. A dilatancy angle of zero degrees is considered in the standard settings of the Soft-Soil model.

Poisson's ratio

In the Soft-Soil model, the Poisson's ratio is the well known pure elastic constant rather than the pseudo-elasticity constant as used in the Mohr-Coulomb model. Its value will usually be in the range between 0.1 and 0.2. If the standard setting for the Soft-Soil model parameters is selected, then $v_{ur} = 0.15$ is automatically used. For loading of normally consolidated materials, Poisson's ratio plays a minor role, but it becomes important in unloading problems. For example, for unloading in a one-dimensional compression test (oedometer), the relatively small Poisson's ratio will result in a small decrease of the lateral stress compared with the decrease in vertical stress. As a result, the ratio of horizontal and vertical stress increases, which is a well-known phenomenon in overconsolidated materials. Hence, Poisson's ratio should not be based on the normally consolidated K_0^{NC}-value, but on the ratio of the horizontal stress increment to the vertical stress increment in oedometer unloading and reloading test such that:

$$\frac{v_{ur}}{1 - v_{ur}} = \frac{\Delta\sigma_{xx}}{\Delta\sigma_{yy}} \qquad \text{(unloading and reloading)} \qquad (7.7)$$

K_0^{NC}-parameter

The parameter M is automatically determined based on the coefficient of lateral earth pressure in normally consolidated condition, K_0^{NC}, as entered by the user. The exact relation between M and K_0^{NC} gives (Brinkgreve, 1994):

$$M \approx 3 \sqrt{\frac{\left(1 - K_0^{NC}\right)^2}{\left(1 + 2K_0^{NC}\right)^2} + \frac{\left(1 - K_0^{NC}\right)\left(1 - 2v_{ur}\right)\left(\lambda^*/\kappa^* - 1\right)}{\left(1 + 2K_0^{NC}\right)\left(1 - 2v_{ur}\right)\lambda^*/\kappa^* - \left(1 - K_0^{NC}\right)\left(1 + v_{ur}\right)}} \quad (7.8)$$

The value of M is indicated in the input window. As can be seen from Eq. (7.8), M is also influenced by the Poisson's ratio v_{ur} and by the ratio λ^*/κ^*. However, the influence of K_0^{NC} is dominant. Eq. (7.8) can be approximated by:

$$M \approx 3.0 - 2.8 K_0^{NC} \tag{7.9}$$

8   APPLICATIONS OF ADVANCED SOIL MODELS

In this chapter, advanced soil models will be utilised in various applications in order to illustrate the particular features of these models. For applications on the standard Mohr-Coulomb model, the reader is referred to the *Tutorial Manual*.

8.1   HS MODEL: RESPONSE IN DRAINED AND UNDRAINED TRIAXIAL TESTS

In this Section, the Hardening-Soil model is utilised for the simulations of drained and undrained triaxial tests. Arbitrary sets of model parameters, Table 8.1, representing sands of different properties, are considered.

Table 8.1 Arbitrary Hardening-Soil parameters for sands of different densities

Parameter	Loose	Medium	Dense	Unit
E_{50}^{ref} (for p_{ref} = 100 kPa)	20000	30000	40000	kN/m^2
E_{ur}^{ref} (for p_{ref} = 100 kPa)	60000	90000	120000	kN/m^2
E_{oed}^{ref} (for p_{ref} = 100 kPa)	20000	30000	40000	kN/m^2
Cohesion c	0.0	0.0	0.0	kN/m^2
Friction angle φ	30	35	40	°
Dilatance angle ψ	0	5	10	°
Poisson's ratio v_{ur}	0.2	0.2	0.2	-
Power m	0.5	0.5	0.5	-
K_0^{nc} (using Cap)	0.5	0.43	0.36	-
Tensile strength	0.0	0.0	0.0	kN/m^2
Failure ratio	0.9	0.9	0.9	-

A triaxial test can simply be modelled by means of an axisymmetric geometry of unit dimensions (1m x 1m), that represent a quarter of the soil specimen, Figure 8.1. These dimensions are not realistic, but they are selected for simplicity. The dimension of the model does not influence the results, provided that the soil weight is not taken into account. In this configuration the stresses and strains are uniformly distributed over the geometry. The deformation magnitudes in x- and y-direction of the top right hand corner correspond to the horizontal and vertical strains respectively.

The left hand side and the bottom of the geometry are axes of symmetry. At these boundaries the displacements normal to the boundary are fixed and the tangential displacements are kept free to allow for 'smooth' movements. The remaining boundaries are fully free to move.

As in Version 7 the value of the applied loads can be controlled by the load multipliers such as *ΣMloadA* and *ΣMloadB*. However, in Version 8, and as described in the Reference manual, the load configurations and magnitudes can be specified in the Input program. Then in the calculation program these loads can be activated or deactivated by means of the *Staged construction* option. For this case, and to simulate the confining pressure p', distributed loads of -100 kN/m^2 representing the principal stresses σ_1' (load A) and σ_3' (load B) are applied in the Input program, as shown in Figure 8.1.

A very course mesh is sufficient for this simple geometry. Initial stresses and steady pore pressures are not taken into account.
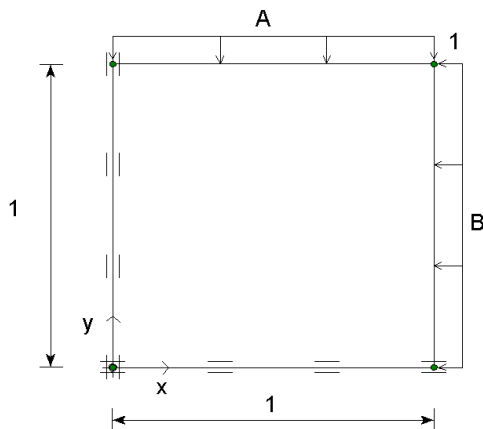

Figure 8.1 Simplified configuration of a triaxial test

In the Calculation program, the calculation of all phases can be done by means of the *Staged construction* process. In the first phase, the confinement pressure p' is applied by activating load A and B. In the second phase the displacements are reset to zero and the sample is vertically loaded up to failure while the horizontal load is kept constant. This implies modification of load A by double clicking the load in the geometry model. As a result a load window appears in which the input values of the load can be changed. (Details of the procedure can be found in the Reference and Tutorial manuals.) The latter phase is carried out for drained as well as undrained conditions.

These calculations are performed for the three different sets of material parameters, Table 8.1. The computational results are presented in the figures on the following pages.

Figure 8.2 shows the principal stress difference versus the axial strain for the drained condition. This shows a hyperbolic relationship between the stress and the strain, which is typical for the Hardening-Soil model. Obviously, the failure level is higher when the sand is denser. The HS model does not include softening behaviour, so after reaching failure the stress level does not reduce, at least in the drained tests.
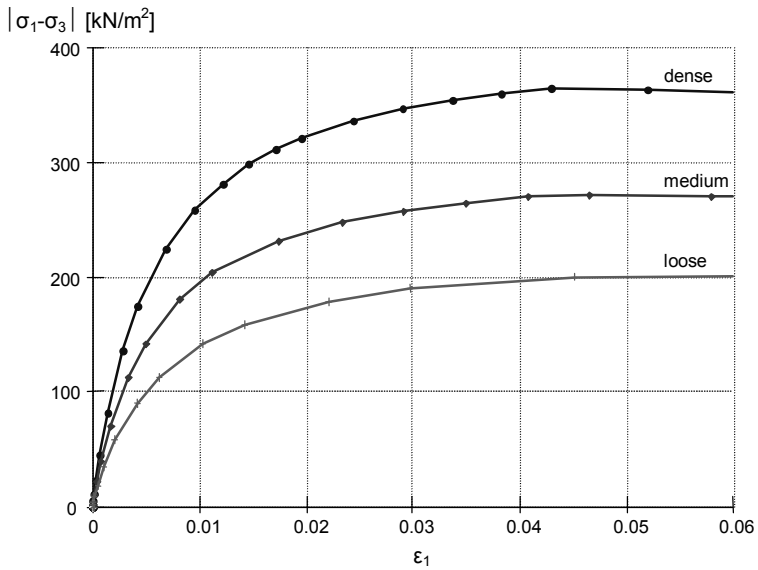
Figure 8.2   Results of drained triaxial tests using the Hardening-Soil model, Principal stress difference versus axial strain

Figure 8.3   Results of drained triaxial tests using the Hardening-Soil model, Volumetric strain versus axial strain

Figure 8.3 shows the axial strain versus the volumetric strain for the drained test. This graph clearly shows the influence of dilatancy in the denser sands. In contrast to the Mohr-Coulomb model, the transition from elastic behaviour to failure is much more gradual when using the Hardening-Soil model. In fact, in the HS model, plastic strain occurs immediately after load application.

Figure 8.4   Results of undrained triaxial tests using the Hardening-Soil model, Principal stress difference versus axial strain

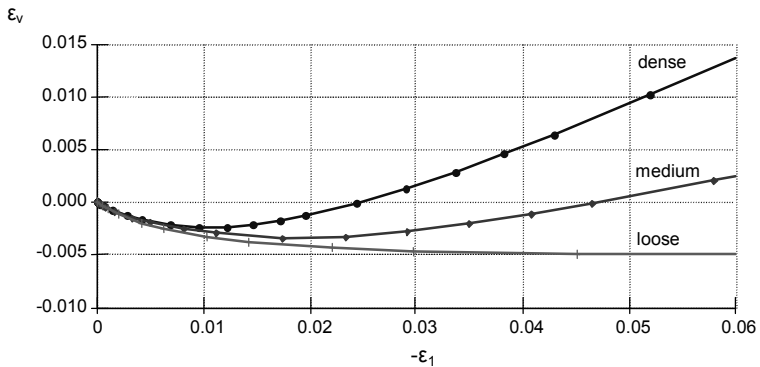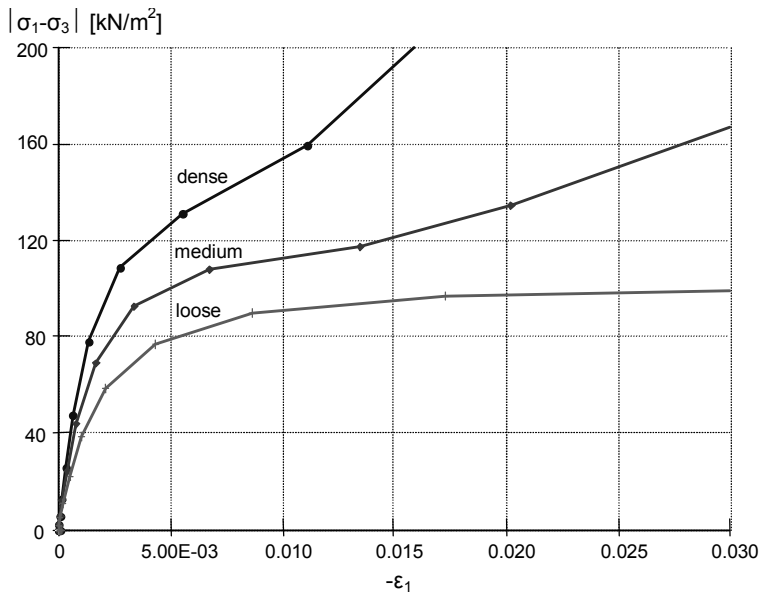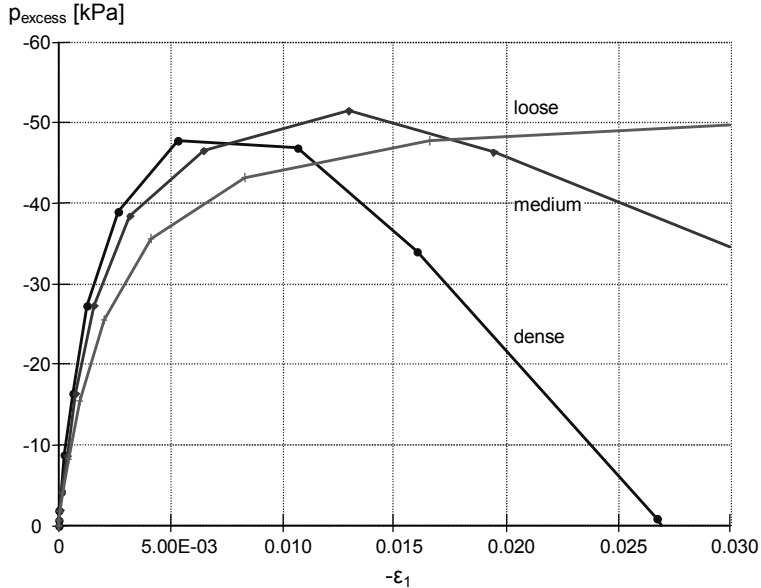Figure 8.5   Results of undrained triaxial tests using the Hardening-Soil model, Excess pore pressure vs axial strain

In the undrained tests, Figure 8.4, the failure level is, in principle, lower than that of the drained tests. However, for the medium and dense sands the stress level continues to increase after reaching the failure level due to the fact that dilatancy occurs which causes reduction of excess pore pressures and thus increase of the effective stresses. This can be seen in Figure 8.5.
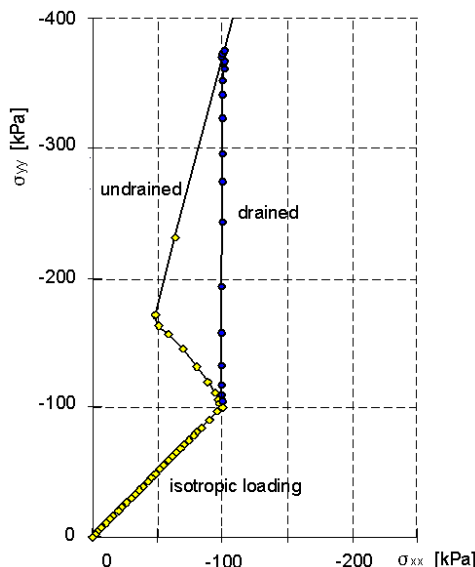
Figure 8.6 Stress paths for drained and undrained triaxial tests using the HS model

Figure 8.6 shows the effective stress paths, for the medium sand, during both the drained and undrained tests. During first phase (isotropic loading), both tests were drained. In the second phase there is a clear distinction between the two tests. In the undrained test the effective horizontal stress reduces while the vertical stress increases due to the development of excess pore pressures. The decrease in horizontal effective stress is more than when if the Mohr-Coulomb model would have been used. This is attributed to the plastic compaction (Cap hardening) that occurs in the HS model.

8.2   APPLICATION OF THE HARDENING-SOIL MODEL ON REAL SOIL TESTS

In this section the ability of the Hardening-Soil model to simulate laboratory tests on sand is examined by comparing PLAXIS calculation results with those obtained from laboratory tests. Extensive laboratory tests were conducted on loose and dense Hostun sand. On the basis of these tests the model parameters for the Hardening-Soil model were determined, Table 8.2.

Table 8.2 Hardening-Soil parameters for loose and dense Hostun sand

Parameter	Loose sand	Dense sand	Unit
Volumetric weight γ	17	17.5	kN/m^3
E_{50}^{ref} (p_{ref} = 100 kPa)	20000	37000	kN/m^2
E_{ur}^{ref} (p_{ref} = 100 kPa)	60000	90000	kN/m^2
E_{oed}^{ref} (p_{ref} = 100 kPa)	16000	29600	kN/m^2
Cohesion c	0.0	0.0	kN/m^2
Friction angle φ	34	41	°
Dilatancy angle ψ	0	14	°
Poisson's ratio ν_{ur}	0.20	0.20	-
Power m	0.65	0.50	-
K_0^{nc}	0.44	0.34	-
Tensile strength	0.0	0.0	kN/m^2
Failure ratio	0.9	0.9	-

Triaxial test

Standard drained triaxial tests were performed on loose and dense sand specimens. In PLAXIS the procedure for the simulation of the triaxial tests has been described in Section 8.1. In the first phase the sample is isotropically compressed up to a confining pressure of p' = -300 kN/m^2. In the second phase the sample is vertically loaded up to failure while the horizontal stress (confining pressure) is kept constant. The computational results and the measured data are presented in Figure 8.7, Figure 8.8 and 8-8.

The figures show that the computational results match reasonably with the test data. It can be seen that the material response (measured and computed) show gradual transition from elastic to plastic behaviour. As such the relation between the deviatoric stress and the axial strain can be approximated by a hyperbola.

The failure level is fully controlled by the friction angle (the cohesion is zero). The test results on dense sand show softening behaviour after the peak load has been reached. Modelling of the softening behaviour, however, is not incorporated in the Hardening-Soil model, and thus, the deviatoric stress remains constant. It can also be seen from the test data that the dilatancy reduces during softening. However, in the Hardening-Soil model the dilatancy continues to infinity, unless the dilatancy cut-off option has been used.
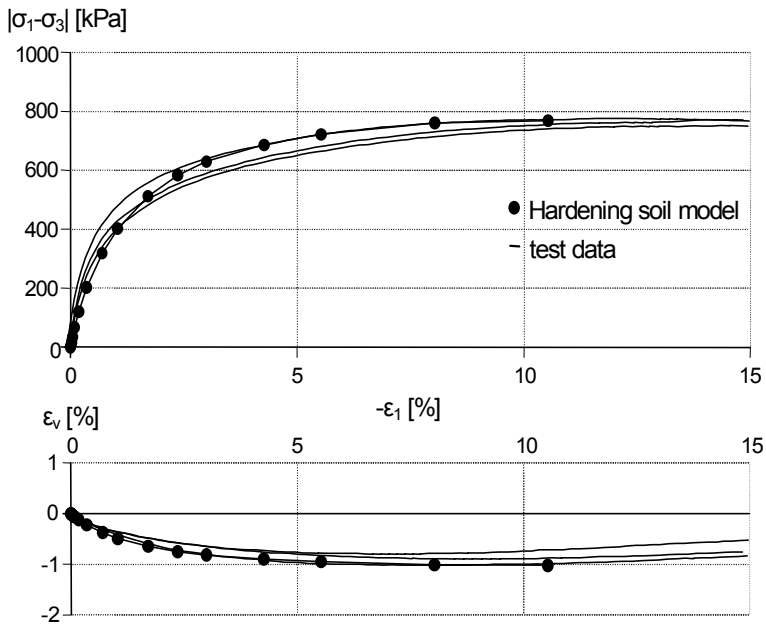
Figure 8.7   Results of drained triaxial tests on loose Hostun sand, principal stress ratio versus axial strain
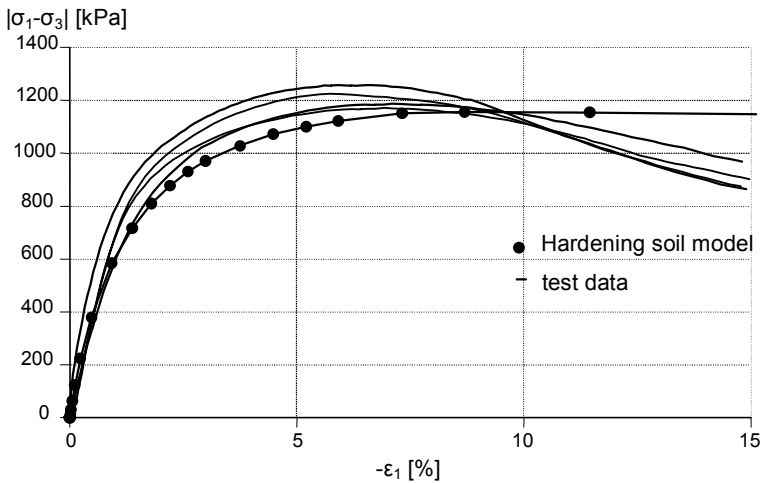
Figure 8.8   Results of drained triaxial tests on dense Hostun sand, principal stress ratio versus axial strain
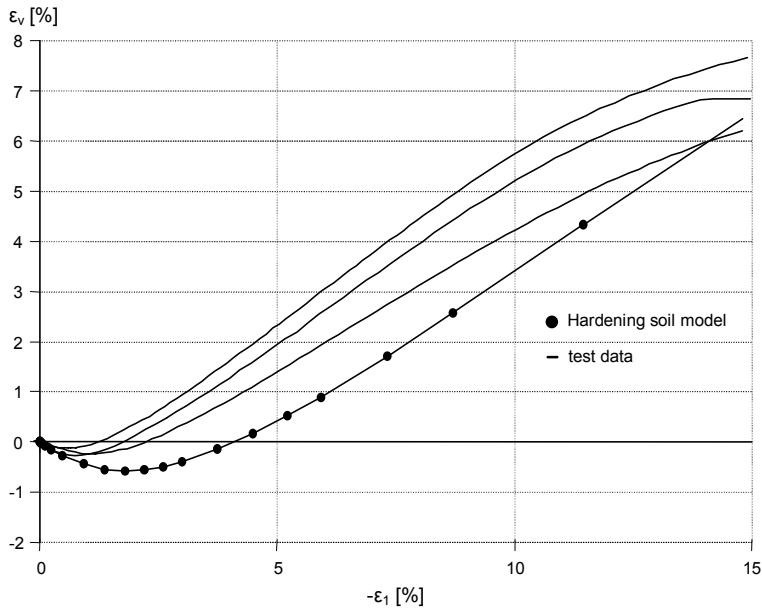
Figure 8.9   Results of drained triaxial tests on dense Hostun sand, volumetric strain versus axial strain

Oedometer test

As for the triaxial test, a set of oedometer test on both loose and dense sands, Table 8.2, was conducted. In PLAXIS the oedometer test is simulated as an axisymmetric geometry with unit dimensions, Figure 8.10. A coarse mesh is sufficient for this case.

Figure 8.10 Simplified configuration of an oedometer test

The computational results as compared with those obtained from the laboratory tests are shown in Figure 8.11 and Figure 8.12.

Figure 8.11 Results of oedometer test on loose Hostun sand, axial stress versus axial strain

Figure 8.12 Results of oedometer test on dense Hostun sand, axial stress versus axial strain

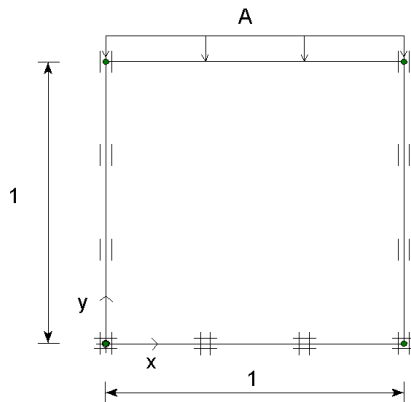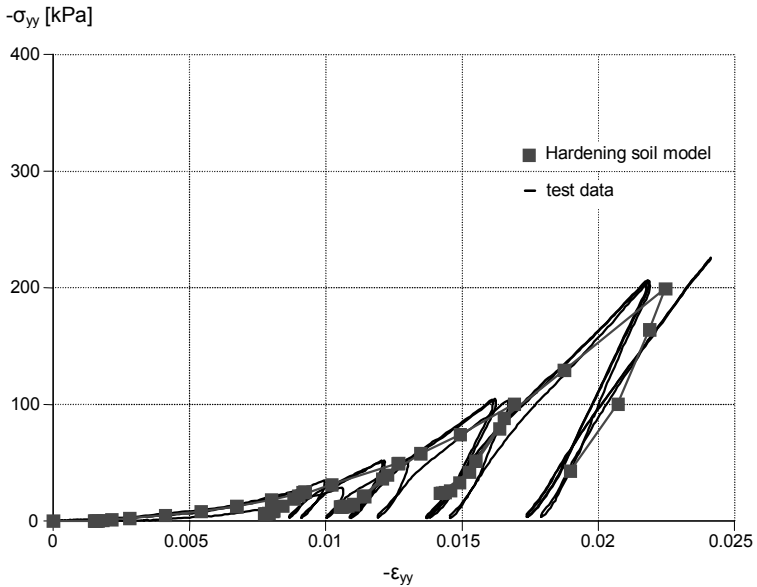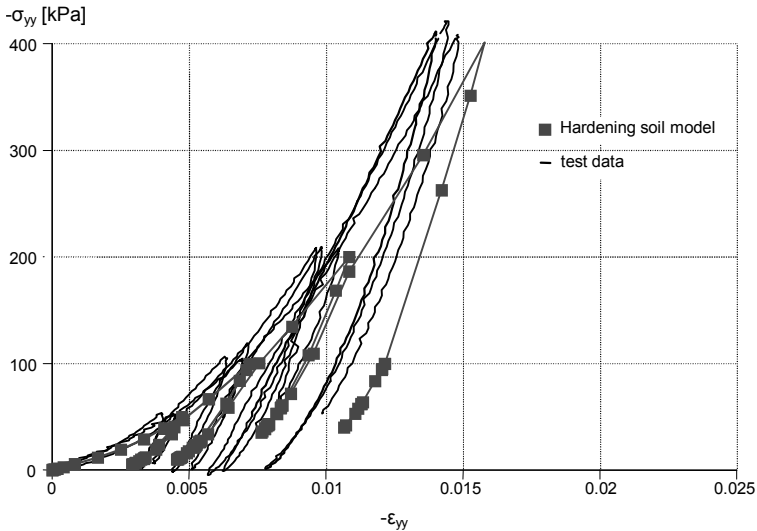From a stress free state the loose sand sample is loaded consecutively to 25 kPa, 50 kPa, 100 kPa and 200 kPa with intermediate unloading. The dense sand sample is loaded to 50 kPa, 100 kPa, 200 kPa and 400 kPa with intermediate unloading.

As it can be seen, the computational results show a reasonable agreement with the test data. No doubt, distinction should be made between loose and dense soil, but it seems that for a soil with a certain density the stiffness behaviour under different stress paths can be well captured with a single set of model parameters. (A small offset of 0.15% has been applied to the computational results of the loose sample in order to account for the relative soft response at the beginning of the test.)

Pressiometer test

In this Section the Pressiometer test is simulated and results from PLAXIS and laboratory experimentation are compared. Laboratory testing results on dense sand with material parameters listed in Table 8.2 are used.

In the field, the pressiometer with 44 mm in diameter covered with a membrane with 160 mm in height is attached to the Cone penetration shaft. In the laboratory, the pressiometer is attached to a 44 mm pipe and placed in a circular calibration chamber with a diameter of 1.2 m and a height of 0.75 m. A large overburden pressure of 500 kPa is applied at the surface to simulate the stress state at larger depths. In PLAXIS only half of the geometry is simulated by an axisymmetric model, Figure 8.13. The overburden pressure is simulated by load A, and the expansion of the pressiometer is simulated by imposing a horizontal distributed load, load B. Therefore the initial standard boundary conditions have to be changed near the pressiometer in order to allow for free horizontal displacements.
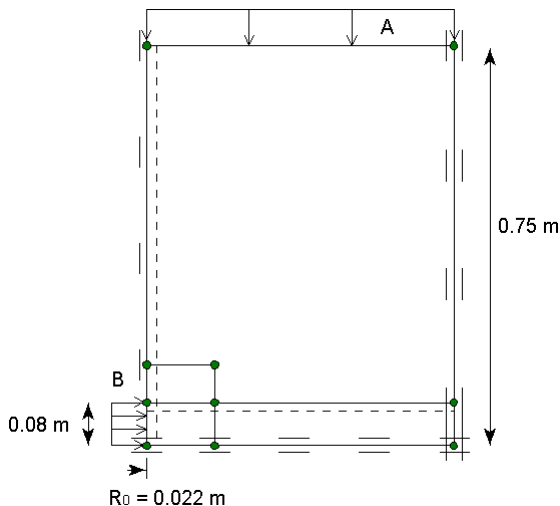
Figure 8.13 Geometry model for pressiometer test

To allow for a discontinuity in horizontal displacements, a vertical interface along the shaft of the pressiometer borehole and a horizontal interface just above the pressiometer are introduced. Both interfaces are set rigid (R_{inter} = 1.0). Extra geometry lines are created around the pressiometer to locally generate a finer mesh.

After the generation of initial stresses, the vertical overburden load (load A) is applied using the standard boundary fixities. From the calculations, the lateral stress around the pressiometer appears to be 180 kPa. Subsequently, the horizontal fixity near the pressiometer is removed, in the Input program, and replaced by Load B with a magnitude of 180 kPa. In the next calculation the pressure (load B) is further increased by use of *Staged construction* in an Updated Mesh analysis. The results of this calculation are presented in Figure 8.14 and Figure 8.15.
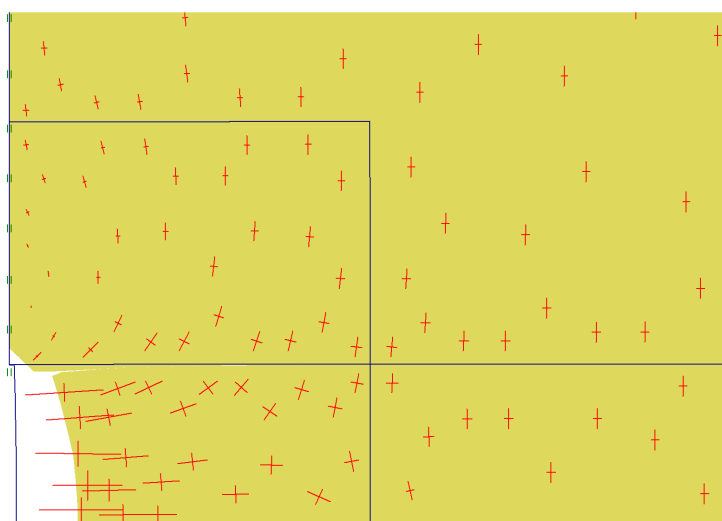
Figure 8.14 Stress distribution in deformed geometry around the pressiometer at a pressure of 2350 kPa

Figure 8.14 shows details of the deformations and the stress distribution when the pressure in the pressiometer was 2350 kPa. The high passive stresses appear very locally near the pressiometer. Just above the pressiometer the vertical stress is very low due to arching effects. Away from the pressiometer, a normal K_0-like stress state exists.

Figure 8.15 shows a comparison of the numerical results with those obtained from the laboratory test. In the figure the pressiometer pressure is presented as a function of the relative volume change. The latter quantity cannot directly be obtained from PLAXIS and was calculated from the original radius R_0 and the lateral expansion u_x of the pressiometer:

$$\frac{\Delta V}{V_0} = \frac{(R_0 + u_x)^2 - R_0^2}{R_0^2}$$

Up to a pressure of 1600 kPa the results match quite well. Above 1600 kPa there is a sudden decrease in stiffness in the real test data, which cannot be explained. Nevertheless, the original set of parameters for the dense sand that were derived from triaxial testing also seem to match the pressiometer data quite well.
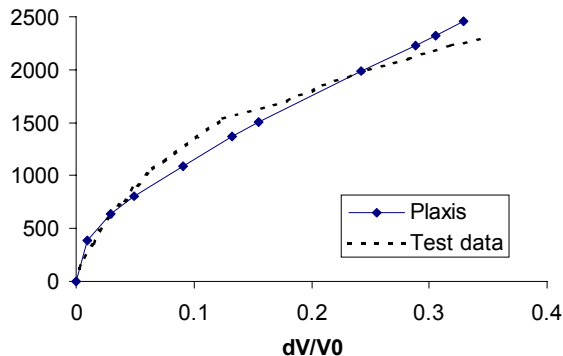
Figure 8.15 Comparison of numerical results and pressiometer test data

Conclusion

The above results indicate that by use of the Hardening Soil model it is possible to simulate different laboratory tests with different stress paths. This cannot be obtained with simple models such as Mohr-Coulomb without changing input parameters. Hence, the parameters in the Hardening-Soil model are consistent and more or less independent from the particular stress path. This makes the HS model a powerful and an accurate model, which can be used in many applications.

8.3   SSC MODEL: RESPONSE IN ONE-DIMENSIONAL COMPRESSION TEST

In this section the behaviour of the Soft-Soil-Creep model is illustrated on the basis of a one-dimensional compression test on clay. Two types of analysis are performed. First, the test is simulated assuming drained conditions in order to demonstrate the logarithmic stress-strain relationship and the logarithmic time-settlement behaviour on the long term (secondary compression). Second, the test is simulated more realistically by including undrained conditions and consolidation. Since the consolidation process depends on the drainage length, it is important to use actual dimensions of the test set-up. In this case an

axisymmetric configuration with specimen height of 0.01 m, Figure 8.16, is used. The material parameters are shown in Table 8.3. The parameter values are selected arbitrarily, but they are realistic for normally consolidated clay. The vertical preconsolidation stress is fixed at 50 kPa (POP = 50 kPa).
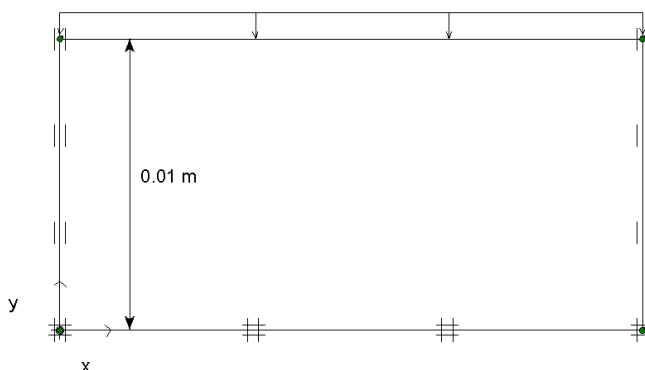
Figure 8.16 One-dimensional compression test

Drained analysis

In the first analysis successive plastic loading steps are applied using drained conditions. The load is doubled in every step using *Staged construction* with time increments of 1 day. After the last loading step an additional creep period of 100 days is applied. The calculation scheme is listed in Table 8.4. All calculations are performed with a tolerance of 1%.

Table 8.3 Soft-Soil-Creep model parameters for one-dimensional compression test

Parameter	Symbol	Value	Unit
Unit weight	γ	19	kN/m^3
Permeability	k$_x$, k_y	0.0001	m/day
Modified compression index	λ^*	0.10	-
Modified swelling index	κ^*	0.02	-
Secondary compression index	μ^*	0.005	-
Poisson's ratio	ν_{ur}	0.15	-
Cohesion	c	1.0	kN/m^2
Friction angle	φ	30	°
Dilatancy angle	ψ	0.0	°
Coeffient of lateral stress	K_0^{nc}	0.5	-

Table 8.4 Calculation scheme for the drained case

Phase	Calculation type	Load input: *Staged construction* [kPa]	Time increment [day]	End time [day]
1	Plastic	10	1	1
2	Plastic	20	1	2
3	Plastic	40	1	3
4	Plastic	80	1	4
5	Plastic	160	1	5
6	Plastic	320	1	6
7	Plastic	640	1	7
8	Plastic	640	100	107

Undrained analysis

In the second analysis the loading steps are instantaneously applied using undrained conditions. After each loading step a consolidation of 1 day is applied to let the excess pore pressures fully dissipate. After the last loading step, an additional creep period of 100 days is again introduced. The calculation scheme for this analysis is listed in Table 8.5. All calculations are performed with a reduced tolerance of 1%.

Table 8.5 Calculation scheme for second analysis

Phase	Calculation type	Loading input: *Staged construction* [kPa]	Time increment [day]	End time [day]
1	Plastic	10	0	0
2	Consolidation	10	1	1
3	Plastic	20	0	1
4	Consolidation	20	1	2
5	Plastic	40	0	2
6	Consolidation	40	1	3
7	Plastic	80	0	3
8	Consolidation	80	1	4
9	Plastic	160	0	4
10	Consolidation	160	1	5
11	Plastic	320	0	5
12	Consolidation	320	1	6
13	Plastic	640	0	6
14	Consolidation	640	1	7
15	Consolidation	640	100	107

Figure 8.17 Load-settlement curve of oedometer test with Soft-Soil-Creep model. A) Transient loading with doubling of loading within one day. B) Instantaneous loading with doubling of load at the beginning of a new day. C) As 'A' using Updated Mesh calculation

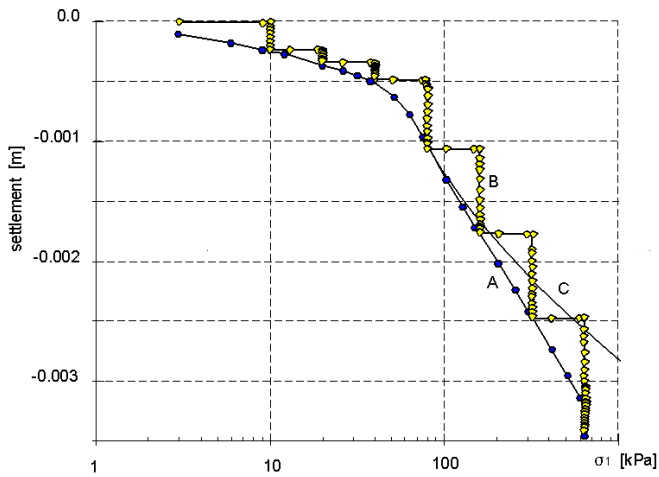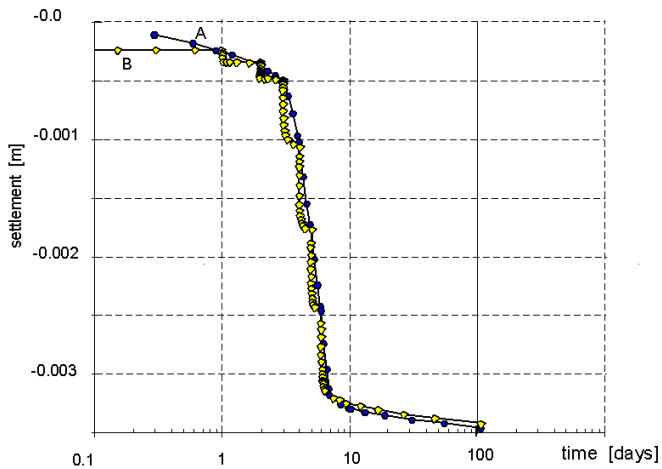

Figure 8.18 Time-settlement curve of oedometer test with Soft-Soil-Creep model. A) Transient loading with doubling of loading within one day. B) Instantaneous loading with doubling of load at the beginning of a new day

Figure 8.17 shows the load-settlement curves of both analyses. It can be seen that, after consolidation, the results of the undrained test match those of the drained test. The

influence of the preconsolidation stress can clearly be seen, although the transition between reloading and primary loading is not as sharp as when using the Soft-Soil model. In fact, the results presented here are more realistic. The transition is indeed around 50 kPa.

From the slope of the primary loading line one can back-calculate the modified compression index $\lambda^* = \Delta\varepsilon_1 / \ln((\sigma_1+\Delta\sigma_1)/\sigma_1) \approx 0.10$. Note that 1 mm settlement corresponds to $\varepsilon_1 = 10\%$. For an axial strain of 30% one would normally use an Updated Mesh analysis, which has not been done in this simple analysis. If, however, the Soft-Soil-Creep model would have been used in an Updated Mesh analysis with axial strains over 15% one would observe a stiffening effect as indicated by line *C* in Figure 8.17.

Figure 8.18 shows the time-settlement curves of the drained and the undrained analyses. From the last part of the curve one can back-calculate the secondary compression index $\mu^* = \Delta\varepsilon_1 / \ln(\Delta t/t_0) \approx 0.005$ (with $t_0 = 1$ day).

Another interesting phenomenon is the development of lateral stresses. During primary loading, the lateral stress is determined by K_0^{NC}, appropriate for normally consolidated soil. During unloading, the lateral stress decreases much less than the vertical stress, so that the ratio $\sigma'_{xx} / \sigma'_{yy}$ increases.

To show these effects the calculation is continued after with a new drained unloading phase that starts from phase 7 (see Table 8.4) in which the vertical stress is reduced to -80 kPa.
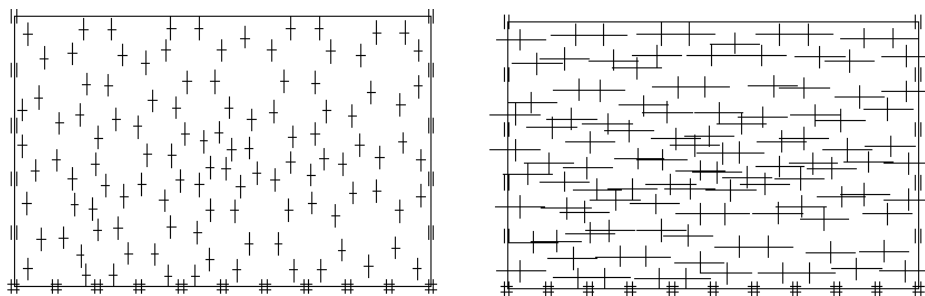
Figure 8.19 Stress states at a vertical stress level of -80 kPa. Left, after primary loading $\sigma_{xx}' \approx -40$ kPa. Right, after unloading from -640 kPa $\sigma_{xx}' \approx -220$ kPa

Figure 8.19 shows the stress state for two different calculation phases, both at a vertical stress level of 80 kPa. The plot in the left hand side shows the stress state after primary loading. As expected the horizontal stress is found to be approximately -40 kPa (corresponding to $K_0^{NC} = 0.5$). The plot in the right hand side shows the final situation after unloading down to -80 kPa. In this case the horizontal stress is decreased from -320 kPa to approximately -220 kPa, ($\Delta\sigma'_{xx} = 100$ kPa), i.e, much less than the decrease of the

vertical stress ($\Delta\sigma'_{yy}$ = 560 kPa). Thus, a situation where σ'_{xx} is larger than σ'_{yy} is obtained.

During sudden unloading in a one-dimensional compression test, the behaviour is purely elastic. Hence, the ratio of the horizontal and vertical stress increments can be determined as:

$$\frac{\Delta\sigma'_{xx}}{\Delta\sigma'_{yy}} = \frac{v_{ur}}{1 - v_{ur}} \tag{8.2}$$

It is easy to verify that the results correspond to Poisson's ratio v_{ur} = 0.15 as listed in Table 8.3.

8.4   SSC MODEL: UNDRAINED TRIAXIAL TESTS AT DIFFERENT LOADING RATES

In this section the Soft-Soil-Creep model is utilised for the simulation of clay in an undrained triaxial test at different strain rates. The model parameters are obtained from test results on Haney Clay (see Chapter 6) and are listed in Table 8.6.

Table 8.6 Soft-Soil-Creep model parameters for Haney clay

Parameter	Symbol	Value	Unit
Modified compression index	λ^*	0.105	-
Modified swelling index	κ^*	0.016	-
Secondary compression index	μ^*	0.004	-
Poisson's ratio	v_{ur}	0.15	-
Cohesion	c	0.0	kN/m^2
Friction angle	φ	32	°
Dilatancy angle	ψ	0.0	°
Coeffient of lateral stress	K_0^{nc}	0.61	-
Permeability	K_x , k_y	0.0001	m/day

Modelling of the triaxial test is as described in Section 8.1. However, here, the real dimension of the test set-up is simulated (17.5 x 17.5 mm^2), Figure 8.20. The specimen surfaces (top and right hand side in Figure 8.20) are assumed drained whereas the other boundaries are assumed closed. In addition to isotropic loading, prescribed displacements are also applied. Both types of loading are simulated using the *Staged construction* option. During isotropic loading, horizontal and vertical loads (both System

A) are applied. The calculation phases for isotropic loading consist of undrained plastic and consolidation analyses.
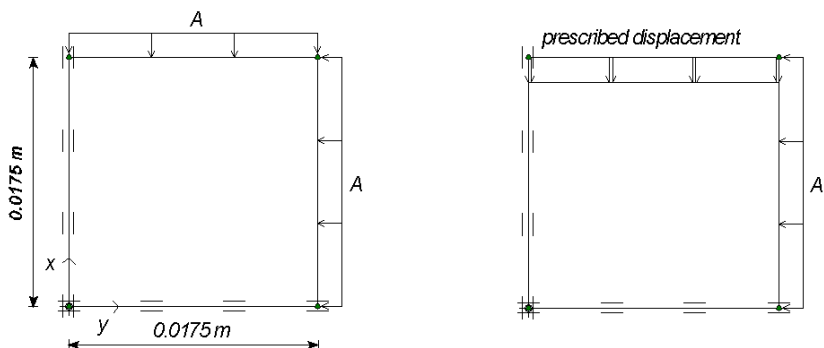
Figure 8.20 Modelling of triaxial test on Haney clay. Left, Initial configuration. Right, configuration for phase 9 - 11

After the isotropic loading phases, the displacements are reset to zero. The vertical load is deactivated and the prescribed displacement is activated. Rate of loading is simulated by applying prescribed displacements at different velocities. As such a total of 12% axial strain (2.1 mm) is applied in 8.865 days (0.00094%/minute), 0.0556 days (0.15%/minute) and 0.00758 days (1.10%/minute) respectively. Each of the prescribed displacement loading phase starts from the end of the isotropic loading phase. The calculation scheme is listed in Table 8.7.

Table 8.7 Loading scheme for triaxial tests at different loading rates

Phase	Calculation	Applied Load [kPa]	Applied displacement [mm]	Time increment [day]
1	Plastic	65	Inactive	0.00
2	Consolidation	65	Inactive	0.01
3	Plastic	130	Inactive	0.00
4	Consolidation	130	Inactive	0.01
5	Plastic	260	Inactive	0.00
6	Consolidation	260	Inactive	0.01
7	Plastic	520	Inactive	0.00
8	Consolidation	520	Inactive	0.01
9	Plastic	520	0.0021	8.865
10 (start from 8)	Plastic	520	0.0021	0.0556
11 (start from 8)	Plastic	520	0.0021	0.00758

The computational results are presented in Figure 8.21 and Figure 8.22. Figure 8.21 shows the stress-strain curves of the prescribed displacement loading phases. It can be seen that the shear strength highly depends on the strain rate; the higher strain rate the higher the shear strength.

Figure 8.22 shows the p-q stress paths from the prescribed displacement loading phases. For higher strain rates there is a smaller reduction of the mean effective stress, which allows for a larger ultimate deviatoric stress. It should be noted that the stress state is not homogeneous at all, because of the inhomogeneous (excess) pore pressure distribution. This is due to the fact that points close to draining boundaries consolidate faster than points at a larger distance.
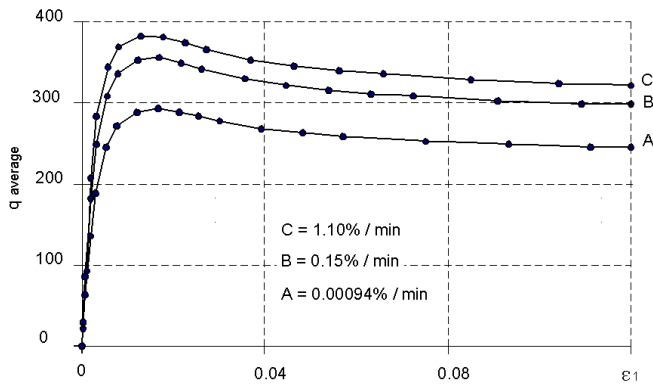

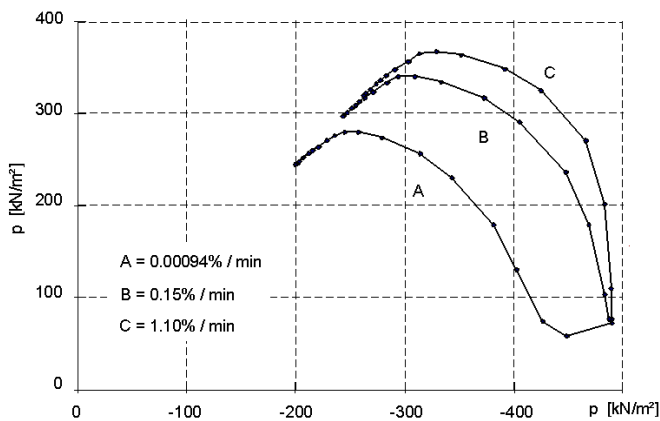Figure 8.21 Average deviatoric stress versus axial strain for different rates of straining

Figure 8.22 p-q stress paths for different rates of straining for a point at position (0.01 , 0.01)

8.5 SS MODEL: RESPONSE IN ISOTROPIC COMPRESSION TEST

In this Section it will be demonstrated that the Soft-Soil model obeys a logarithmic relationship between the volumetric strain and the mean stress in isotropic compression. For this purpose the test set up is simulated as that presented in Figure 8.1. The vertical load (A) and the horizontal load (B) are simultaneously applied to the same level so that a fully isotropic stress state occurs. The parameters of the Soft-Soil model are chosen arbitrarily, but the values are realistic for normally consolidated clay. The parameters are presented in Table 8.8.

Table 8.8 SS Model parameters for isotropic compression test

Modified compression index	λ^*	0.10
Modified swelling index	κ^*	0.02
Poisson's ratio	ν_{ur}	0.15
Friction angle	φ	30°
Cohesion	c	1.0 kPa
Normally consolidated K_0	K_0^{NC}	0.5

From a stress-free state, the model is isotropically loaded to a mean stress of $p' = 100$ kPa, after which the displacements are reset to zero. As a result, the material becomes 'normally consolidated', i.e., the preconsolidation stress is equivalent to the current state-of-stress. After that, the isotropic pressure is increased to $p' = 1000$ kPa. This loading path is denoted as 'primary loading'. Then, the sample is isotropically 'unloaded' to $p' = 100$ kPa. Finally, the sample is loaded up to $p' = 10000$ kPa. In the last loading path, the maximum preload of 1000 kPa is exceeded. and hence, it consists of two parts: the part of the loading path for which $p' < 1000$ kPa is referred to as 'reloading', and the part of the loading path for $p' > 1000$ kPa consists of further primary loading. The calculation phases are indicated in Table 8.9.

Table 8.9 Calculation phases for isotropic compression test on clay

Stage		Initial stress	Final stress
0	Initial situation		$p^0 = 100$ kPa
1	Primary loading	$p^0 = 100$ kPa	$p^1 = 1000$ kPa
2	Unloading	$p^1 = 1000$ kPa	$p^2 = 100$ kPa
3	Reloading	$p^2 = 100$ kPa	$p^3 = 1000$ kPa
4	Primary loading	$p^3 = 1000$ kPa	$p^4 = 10000$ kPa

The computational results are presented in Figure 8.23, which shows the relation between the vertical strain ε_{yy} and the vertical stress σ'_{yy}.
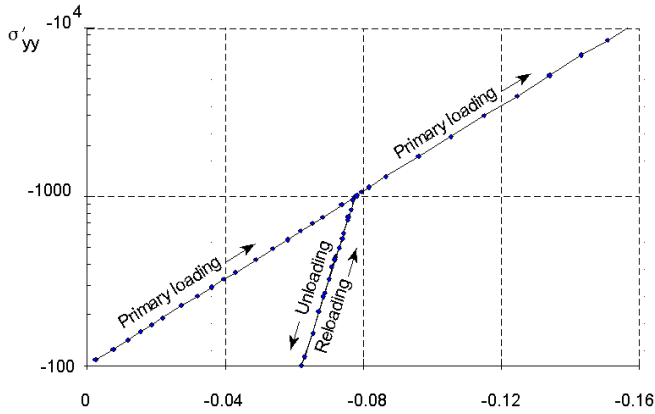
Figure 8.23 Results of isotropic compression test

The latter quantity is plotted on a logarithmic scale. The plot shows two straight lines, which indicates that there is indeed a logarithmic relation for loading and unloading. The vertical strain is 1/3 of the volumetric strain, ε_v, and the vertical stress is equal to the mean stress, p'. The volumetric strains obtained from the calculation are given in Table 8.10.

Table 8.10 Volumetric strains from various calculation phases

Phase	Initial strain	Final strain
0		$\varepsilon_v^0 = 0.000$
1	$\varepsilon_v^0 = 0.000$	$\varepsilon_v^1 = -0.235$
2	$\varepsilon_v^1 = -0.235$	$\varepsilon_v^2 = -0.188$
3	$\varepsilon_v^2 = -0.188$	$\varepsilon_v^3 = -0.235$
4	$\varepsilon_v^3 = -0.235$	$\varepsilon_v^4 = -0.471$

From these strains and corresponding stresses, the parameters λ^* and κ^* can be back-calculated using Eqs. (7.1) and (7.2).

$$\text{Phase 1} \quad \lambda^* = -\frac{\varepsilon_v^1 - \varepsilon_v^0}{\ln\left(p^1 / p^0\right)} = \frac{0.235}{\ln(1000/100)} = 0.102$$

Phase 2 $\quad \kappa^* = -\dfrac{\varepsilon_v^2 - \varepsilon_v^1}{\ln\left(p^2 / p^1\right)} = \dfrac{0.188 - 0.235}{\ln\left(100 / 1000\right)} = 0.020$

Phase 3 $\quad \kappa^* = -\dfrac{\varepsilon_v^3 - \varepsilon_v^2}{\ln\left(p^3 / p^2\right)} = \dfrac{0.235 - 0.188}{\ln\left(1000 / 100\right)} = 0.020$

Phase 4 $\quad \lambda^* = -\dfrac{\varepsilon_v^4 - \varepsilon_v^3}{\ln\left(p^4 / p^3\right)} = \dfrac{0.471 - 0.235}{\ln\left(10000 / 1000\right)} = 0.102$

The back-calculated values correspond to the input values as given in Table 8.8.

Note that the Soft-Soil model does not include time effects such as in the secondary compression. Such behaviour is included in the Soft-Soil-Creep model. An example of an application with this model is described in Section 8.7.

8.6 SUBMERGED CONSTRUCTION OF AN EXCAVATION WITH HS MODEL

In this example a particular advantage of the Hardening-Soil model is demonstrated, namely the distinction between loading and unloading stiffness. This feature becomes particularly important in quasi unloading problems like excavations and tunnels.
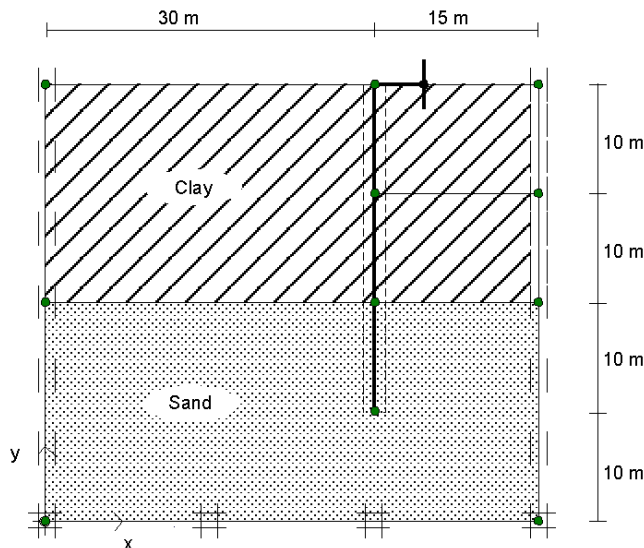

Figure 8.24 Geometry model of submerged excavation

In the submerged excavation example, presented in the Tutorial Manual, the heave at the bottom of the excavation is unrealistically large. In order to show that the results can be improved by using the Hardening-Soil model, a similar example is used here again.

The geometry model is similar to the one used in Lesson 2, Figure 8.24 but slightly simplified. The two soil layers are modelled here with the Hardening-Soil model instead of the Mohr-Coulomb model. The model parameters are listed in Table 8.11.

Table 8.11 HS model parameters for the two layers in the excavation project

Parameter	Clay layer	Sand layer	Unit
Unit weight above/below phreatic level	16 / 18	17 / 20	kN/m^3
E_{50}^{ref} (p_{ref} = 100 kPa)	8000	30000	kN/m^2
E_{ur}^{ref} (p_{ref} = 100 kPa)	24000	90000	kN/m^2
E_{oed}^{ref} (p_{ref} = 100 kPa)	4000	30000	kN/m^2
Cohesion c	5.0	1.0	kN/m^2
Friction angle φ	25	32	°
Dilatancy angle ψ	0	2	°
Poisson's ratio v_{ur}	0.2	0.2	-
Power m	0.8	0.5	-
K_0^{nc}	0.5	0.47	-
Tensile strength	0.0	0.0	kN/m^2
Failure ratio	0.9	0.9	-

After the generation of the initial pore pressures and effective stresses, the excavation is executed in two phases. The results of the excavation are shown in Figure 8.25.

The deformed mesh clearly shows that there is a limited heave at the bottom of the excavation. Most of the deformation is caused by the horizontal movement of the diaphragm wall, which pushes the soil up. The vertical heave at the bottom further away from the wall is very low as compared to the results presented in the Tutorial Manual.

The difference can be explained by the fact that, in contrast to the Mohr-Coulomb model, the Hardening-Soil model distinguishes between loading and unloading stiffness. The unloading stiffness is set here as three times higher than the loading stiffness, which is the default setting in PLAXIS.
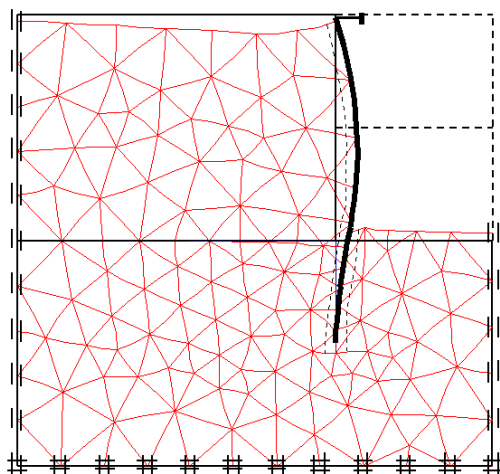
Figure 8.25 Deformed mesh after excavation

8.7   ROAD EMBANKMENT CONSTRUCTION WITH THE SSC MODEL

This example demonstrates some of the features of the Soft-Soil-Creep model in simulating soils for engineering problems. One of these features is the reduction of the mean effective stress during undrained loading due to compaction of the soil. This feature becomes particularly important in embankment construction projects, since it highly influences the stability of the embankment during construction. For example, in the first part of Lesson 5 of the Tutorial Manual (construction of a road embankment) the safety factor was relatively low during construction.
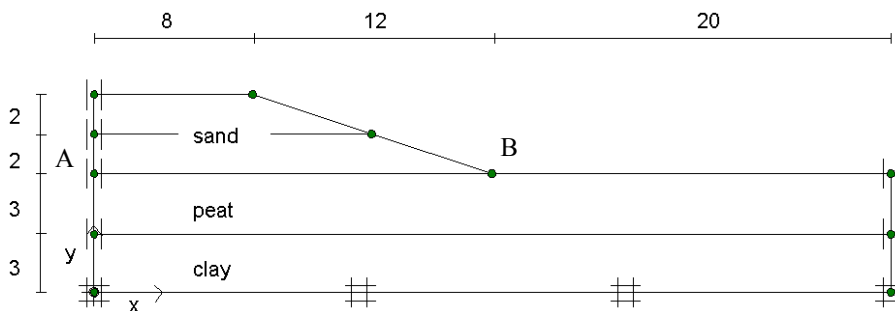
Figure 8.26 Geometry model of road embankment project

When using the Soft-Soil-Creep model for the clay layer with effective strength properties similar to those of the Mohr-Coulomb model, the safety factor will become even lower. To illustrate these effects, the embankment in Lesson 5, Figure 8.26, is reanalysed here.

In this section a similar geometry model as that of Lesson 5 is used, however, the clay layer is simulated by means of the Soft-Soil-Creep model. The model parameters for this layer are listed in Table 8.12. The peat layer and the sand embankment are simulated by means of Mohr-Coulomb using the same parameters as given in Lesson 5 of the Tutorial Manual.

Table 8.12 Soft-Soil-Creep model parameters for undrained clay layer

| Parameter	Clay layer	Unit
Unit soil weight above phreatic level γ_{unsat}	15	kN/m^3
Unit soil weight below phreatic level γ_{sat}	18	kN/m^3
Horizontal permeability k_x	$1 \cdot 10^{-4}$	m/day
Vertical permeability k_y	$1 \cdot 10^{-4}$	m/day
Modified compression index λ^*	0.035	-
Modified swelling index κ^*	0.007	-
Secondary compression index μ^*	0.002	-
Poisson's ratio ν_{ur}	0.15	-
Cohesion c	2	kN/m^2
Friction angle φ	24	°
Dilatancy angle ψ	0	°
Coeffient of lateral stress K_0^{NC}	0.59	-
OCR	1.4	-

The calculation phases are shown in Table 8.13. The first three phases are conducted using Staged construction. The fourth phase is conducted using the Minimum pore pressure loading input and the Safety analysis phase is conducted using the Incremental multipliers loading input.

It is worth mentioning here that if a Safety factor analysis is required, the Updated mesh option should not be used. This is attributed to the fact that with this option the *phi-c reduction* analysis will produce an infinite safety. Please note that if for some reason a normal calculation phase (such as Staged construction or *phi-c reduction*) is needed after an Updated mesh phase, the displacement must be reset to zero.

Table 8.13 Overview of calculation phases

Phase	Start from	Type	Loading input:	Time interval
1	0	Consolidation, Ultimate time	1st embankment part	5 day
2	1	Consolidation, Ultimate time	Desired maximum 50, First time incr. = 1 day	200 days
3	2	Consolidation, Ultimate time	2nd embankment part	5 days
4	3	Consolidation, Minimum pore pressure	Desired maximum 30, First time incr. = 1 day	
5	1	Safety analysis	$Msf = 0.1$	

Figure 8.27 shows the results of the Safety factor analysis after the construction of the first layer of the embankment (after 5 days). Also, the figure shows the results of the Safety factor analysis when using the Mohr-Coulomb model (see the Tutorial Manual).
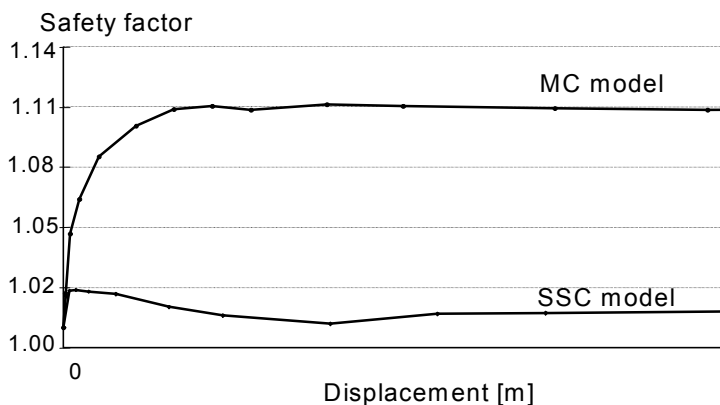
Figure 8.27 Safety factor analysis using MC model and SSC model.

It can be seen that the safety factor produced by the Soft Soil Creep model is 1.01, while by the Mohr-Coulomb model is 1.11. This difference is due to the reduction of the mean effective stress as a result of the accumulation of the irreversible compaction (volume creep strain) in the SSC model. Apparently due to this low safety factor, the calculation of the other phases is not possible because the structure has already reached to its failure state.
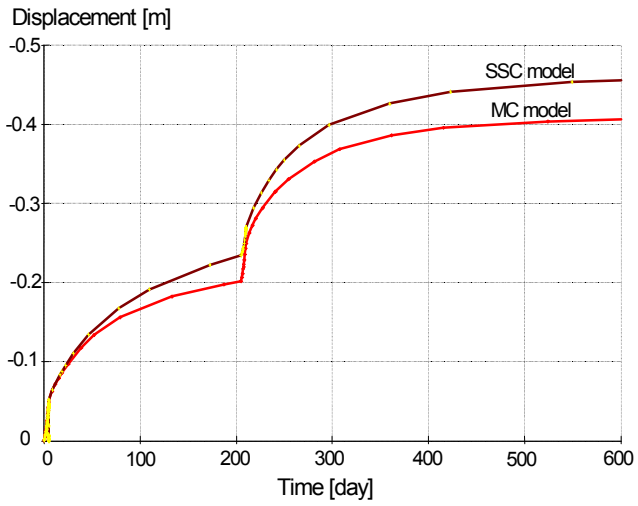
(a)
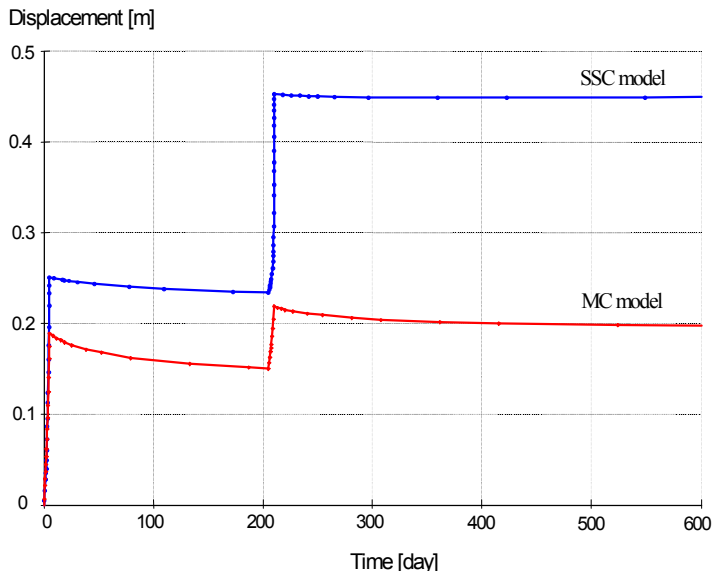
(b)

Figure 8.28 SSC model vs. MC model (a) vertical displacements at A, (b) horizontal displacements at B.

In order to study the influence of the SSC model on the response of the embankment, an Updated mesh analysis is conducted. The results are compared with those obtained by using Mohr-Coulomb model. Figure 8.28(a) shows the vertical displacements at point A and Figure 8.28(b) shows the horizontal displacements at point B, (see Figure 8.26). It can be seen that the SSC model exhibits little differences in the vertical displacement but much larger differences in the horizontal displacement. The later can be attributed to the fact that the material here is close to failure due to the creep effect. Figure 8.29 shows the tendency towards failure after the construction of the second layer.
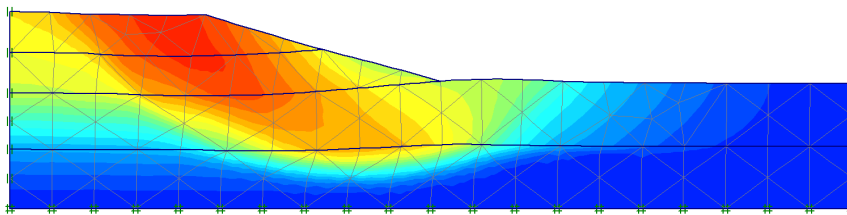
Figure 8.29 Tendency towards failure mechanism after the construction of second part of the embankment

Conclusion

The reduction of mean effective stress during undrained loading is a known phenomenon in soil engineering. This phenomenon has a negative influence on the strength and stability of the soil structure. When using simple soil models, like the Mohr-Coulomb model, this effect is not taken into account and leads to an over prediction of the stability when using effective strength properties. In such cases it is better to use undrained strength properties in the Mohr-Coulomb model ($c = c_u$ and $\varphi = 0$).

The Soft-Soil-Creep model does include the effect of reducing mean effective stress during undrained loading. This model gives a more realistic prediction of soft-soil behaviour, including time-dependent behaviour (secondary compression and consolidation). The disadvantage of this model, however, stems from the fact that no undrained strength properties can be specified (only c' and φ') and that the numerical procedure becomes more complicated (less robust) when soil failure is approached.

9   USER-DEFINED SOIL MODELS

9.1   INTRODUCTION

PLAXIS Version 8 has a facility for user-defined (UD) soil models. This facility allows users to implement a wide range of constitutive soil models (stress-strain-time relationship) in PLAXIS. Such models must be programmed in FORTRAN (or another programming language), then compiled as a Dynamic Link Library (DLL) and then added to the PLAXIS program directory.

In principle the user provides information about the current stresses and state variables and PLAXIS provides information about the previous ones and also the strain and time increments. In the material data base of the PLAXIS input program, the required model parameters can be entered in the material data sets.

$\sigma_{ij}^{t+\Delta t}, \kappa^{t+\Delta t}$ current stresses and state variables

$\sigma_{ij}^{t}, \kappa^{t}$ previous stresses and state variables

$\Delta \varepsilon_{ij}, \Delta t$ strain and time increments

As an example, a UD subroutine based on the Drucker-Prager material model is provided in the user-defined soil models directory, which is included in the program CD. In this section, a step-by-step description on how a user-defined soil model can be formed and utilised in PLAXIS is presented.

> >   Please note that the PLAXIS organization cannot be held responsible for any malfunctioning or wrong results due to the implementation and/or use of user-defined soil models.

9.2   IMPLEMENTATION   OF   UD   MODELS   IN   CALCULATIONS PROGRAM

The PLAXIS calculations program has been designed to allow for user-defined soil models. There are mainly four tasks (functionalities) to be performed in the calculations program:

*   Initialisation of state variables

*   Calculation of constitutive stresses (stresses computed from the material model at certain step)

*   Creation of effective material stiffness matrix

- Creation of elastic material stiffness matrix

These main tasks (and other tasks) have to be defined by the user in a subroutine called 'User_Mod'. In this subroutine more than one UD soil model can be defined. If a UD soil model is used in an application, the calculation program calls the corresponding task from the subroutine User_Mod. To create a UD soil model, the User_Mod subroutine must have the following structure:

```
Subroutine User_Mod      (IDTask, iMod, IsUndr, iStep, iTer, Iel,
                          Int, X, Y, Z, Time0, dTime, Props, Sig0,
                          Swp0, StVar0, dEps, D, Bulk_W, Sig, Swp,
                          StVar, ipl, nStat, NonSym, iStrsDep,
                          iTimeDep, iTang, iPrjDir, iPrjLen,
                          iAbort)
```

where:

IDTask	=	Identification of the task (1 = Initialise state variables; 2 = Calculate constitutive stresses; 3 = Create effective material stiffness matrix; 4 = Return the number of state variables; 5 = Return matrix attributes (NonSym, iStrsDep, iTimeDep); 6 = Create elastic material stiffness matrix)
iMod	=	User-defined soil model number (This option allows for more than one UD model.)
IsUndr	=	Drained condition (IsUndr = 0) or undrained condition (IsUndr = 1)
iStep	=	Current calculation step number
iter	=	Current iteration number
Iel	=	Current element number
Int	=	Current local stress point number (1..3 for 6-noded elements, or 1..12 for 15-noded elements)
X,Y,Z	=	Global coordinates of current stress point
Time0	=	Time at the start of the current step
dTime	=	Time increment of current step
Props	=	Array(1..50) with User-defined model parameters for the current stress point
Sig0	=	Array(1..6) with previous (= at the start of the current step) effective stress components of the current stress point ($\sigma'_{xx}{}^0$, $\sigma'_{yy}{}^0$, $\sigma'_{zz}{}^0$, $\sigma'_{xy}{}^0$, $\sigma'_{yz}{}^0$, $\sigma'_{zx}{}^0$).
		In 2D calculations σ_{yz} and σ_{zx} should be zero.
Swp0	=	Previous excess pore pressure of the current stress point

StVar0	=	Array(1..nStat) with previous values of state variables of the current stress point
dEps	=	Array(1..6) with strain increments of the current stress point in the current step ($\Delta\varepsilon_{xx}$, $\Delta\varepsilon_{yy}$, $\Delta\varepsilon_{zz}$, $\Delta\gamma_{xy}$, $\Delta\gamma_{yz}$, $\Delta\gamma_{zx}$)
D	=	Effective material stiffness matrix of the current stress point (1..6, 1..6)
Bulk_W	=	Bulk modulus of water for the current stress point (for undrained calculations and consolidation)
Sig	=	Array (1..6) with resulting constitutive stresses of the current stress point (σ'_{xx}, σ'_{yy}, σ'_{zz}, σ'_{xy}, σ'_{yz}, σ'_{zx})
Swp	=	Resulting excess pore pressure of the current stress point
StVar	=	Array(1..nStat) with resulting values of state variables for the current stress point
ipl	=	Plasticity indicator:
		0 = no plasticity,
		1 = Mohr-Coulomb (failure) point;
		2 = Tension cut-off point,
		3 = Cap hardening point,
		4 = Cap friction point,
		5 = Friction hardening point.
nStat	=	Number of state variables (unlimited)
NonSym	=	Parameter indicating whether the material stiffness matrix is non-symmetric (NonSym = 1) or not (NonSym = 0) (required for matrix storage and solution).
iStrsDep	=	Parameter indicating whether the material stiffness matrix is stress-dependent (iStrsDep = 1) or not (iStrsDep = 0).
iTimeDep	=	Parameter indicating whether the material stiffness matrix is time-dependent (iTimeDep = 1) or not (iTimeDep = 0).
iTang	=	Parameter indicating whether the material stiffness matrix is a tangent stiffness matrix, to be used in a full Newton-Raphson iteration process (iTang = 1) or not (iTang = 0).
iPrjDir	=	Project directory (for debugging purposes)
iPrjLen	=	Length of project directory name (for debugging purposes)
iAbort	=	Parameter forcing the calculation to stop (iAbort = 1).

In the above, 'increment' means 'the total contribution within the current step' and <u>not</u> per iteration. 'Previous' means 'at the start of the current step', which is equal to the value at the end of the previous step.

In the terminology of the above parameters it is assumed that the standard type of parameters is used, i.e. parameters beginning with the characters A-H and O-Z are double (8-byte) floating point values and the remaining parameters are 4-byte integer values.

The parameters `IDTask` to `dEps` and `iPrjDir` and `iPrjLen` are input parameters; The values of these parameters are provided by PLAXIS and can be used within the subroutine. These input parameters should not be modified (except for `StVar0` in case `IDTask` = 1). The parameters `D` to `iTang` and `iAbort` are output parameters. The values of these parameters are to be determined by the user. In case `IDTask` = 1, `StVar0` becomes output parameter.

The user subroutine should contain program code for listing the tasks and output parameters (`IDTask` = 1 to 6). After the declaration of variables, the User_Mod subroutine must have the following structure (here specified in pseudo code):

```
Case IDTask of
  1  Begin
       { Initialise state variables StVar0 }
     End
  2  Begin
       { Calculate constitutive stresses Sig (and Swp) }
     End
  3  Begin
       { Create effective material stiffness matrix D }
     End
  4  Begin
       { Return the number of state variables nStat }
     End
  5  Begin
       { Return matrix attributes NonSym, iStrsDep,
    iTimeDep}
     End
  6  Begin
       { Create elastic material stiffness matrix De }
     End
End Case
```

If more than one UD model is considered, distinction should be made between different models, indicated by the UD model number `iMod`.

Initialise state variables (`IDTask = 1`)

State variables (also called the hardening parameters) are, for example, used in hardening models to indicate the current position of the yield loci. The update of state variables is considered in the calculation of constitutive stresses based on the previous value of the state variables and the new stress state. Hence, it is necessary to know about the initial value of the state variables, i.e. the value at the beginning of the calculation step. Within a continuous calculation phase, state variables are automatically transferred from one calculation step to another. The resulting value of the state variable in the previous step, StVar, is stored in the output files and automatically used as the initial value in the current step, StVar0. When starting a new calculation phase, the initial value of the state variables is read from the output file of the previous calculation step and put in the StVar0 array. In this case it is not necessary to modify the StVar0 array.

However, if the previous calculation step does not contain information on the state variables (for example in the very first calculation step), the StVar0 array would contain zeros. For this case the initial value has to be calculated based on the actual conditions (actual stress state) at the beginning of the step. Consider, for example, the situation where the first state variable is the minimum mean effective stress, p' (considering that compression is negative). If the initial stresses have been generated using the K_0-procedure, then the initial effective stresses are non-zero, but the initial value of the state variable is zero, because the initialization of this user-defined variable is not considered in the K_0-procedure. In this case, part 1 of the user subroutine may look like:

```
1  Begin
     { Initialise state variables StVar0}
      p = (Sig0[1] + Sig0[2] + Sig0[3]) / 3.0
      StVar0[1] = Min(StVar0[1],p)
   End
```

Calculate constitutive stresses (`IDTask = 2`)

This task constitutes the main part of the user subroutine in which the stress integration and correction are performed according to the user-defined soil model formulation. Let us consider a simple example using a linear elastic *D*-matrix as created under IDTask = 3.

In this case the stress components, Sig, can directly be calculated from the initial stresses, Sig0, the material `stiffness` matrix, *D*, and the strain increments, dEps: Sig[i] = Sig0[i] + $\sum$(D[i, j]*dEps[j]). In this case, part 2 of the user subroutine may look like:

```
2  Begin
     { Calculate constitutive stresses Sig (and Swp) }
     For i=1 to 6 do
       Sig[i] = Sig0[i]
       For j=1 to 6 do
         Sig[i] = Sig[i] + D[i,j]*dEps[j]
       End for {j}
     End for   {i}
   End
```

Create effective material stiffness matrix (`IDTask = 3`)

The material stiffness matrix, D, may be a matrix containing only the elastic components of the stress-strain relationship (as it is the case for the existing soil models in PLAXIS), or the full elastoplastic material stiffness matrix (tangent stiffness matrix). Let us consider the very simple example of Hooke's law of isotropic linear elasticity. There are only two model parameters involved: Young's modulus, E, and Poisson's ratio, v. These parameters are stored, respectively, in position 1 and 2 of the model parameters array, Props(1..50). In this case, part 3 of the user subroutine may look like:

```
3  Begin
     { Create effective material stiffness matrix D }
     E     = Props[1]
     v     = Props[2]
     G     = 0.5*E/(1.0+v)
     Fac   = 2*G/(1.0-2*v)     { make sure that v < 0.5 !! }
     Term1 = Fac*(1-v)
     Term2 = Fac*v
     D[1,1] = Term1
     D[1,2] = Term2
     D[1,3] = Term2
     D[2,1] = Term2
     D[2,2] = Term1
     D[2,3] = Term2
     D[3,1] = Term2
     D[3,2] = Term2
     D[3,3] = Term1
     D[4,4] = G
     D[5,5] = G
     D[6,6] = G
   End
```

(By default, D will be initialized to zero, so the remaining terms are still zero; however, it is a good habit to explicitly define zero terms as well.)

If undrained behaviour is considered (IsUndr = 1), then a bulk stiffness for water (Bulk_W) must be specified at the end of part 3. After calling the user subroutine with IDTask = 3 and IsUndr = 1, PLAXIS will automatically add the stiffness of the water to the material `stiffness` matrix D such that: D[i=1..3, j=1..3] = D[i, j]+ Bulk_W. If Bulk_W is not specified, PLAXIS will give it a default value of 100*Avg(D[i=1..3, j=1..3]).

Return the number of state variables (`IDTask = 4`)

This part of the user subroutine returns the parameter nStat, i.e. the number of state variables. In the case of just a single state parameter, the user subroutine should look like:

```
4  Begin
       { Return the number of state variables nStat }
       nStat = 1
   End
```

Return matrix attributes (`IDTask = 5`)

The material stiffness matrix may be stress-dependent (such as in the Hardening Soil model) or time-dependent (such as in the Soft Soil Creep model). When using a tangent stiffness matrix, the matrix may even be non-symmetric, for example in the case of non-associated plasticity. The last part of the user subroutine is used to initialize the matrix attributes in order to update and store the global stiffness matrix properly during the calculation process. For the simple example of Hooke's law, as described earlier, the matrix is symmetric and neither stress- nor time-dependent. In this case the user subroutine may be written as:

```
5  Begin
       { Return matrix attributes NonSym, iStrsDep, }
       {   iTimeDep, iTang                          }
       NonSym   = 0
       iStrsDep = 0
       iTimeDep = 0
       iTang    = 0
   End
```

For NonSym = 0 only half of the global stiffness matrix is stored using a profile structure, whereas for Nonsym = 1 the full matrix profile is stored.

For iStrsDep = 1 the global stiffness matrix is created and decomposed at the beginning of each calculation step based on the actual stress state (modified Newton-Raphson procedure).

For iTimeDep = 1 the global stiffness matrix is created and decomposed every time when the time step changes.

For iTang = 1 the global stiffness matrix is created and decomposed at the beginning of each iteration based on the actual stress state (full Newton-Raphson procedure; to be used in combination with iStrsDep=1).

Create elastic material stiffness matrix (`IDTask = 6`)

The elastic material stiffness matrix, D^e, is the elastic part of the effective material stiffness matrix as described earlier.

In the case that the effective material stiffness matrix was taken to be the elastic stiffness matrix, this matrix may just be adopted here. However in the case that an elastoplastic or tangent matrix was used for the effective stiffness matrix, then the matrix to be created here should only contain the elastic components.

The reason that an elastic material stiffness matrix is required is because PLAXIS calculates the current relative global stiffness of the finite element model as a whole (CSP = Current Stiffness Parameter). The CSP parameter is defined as:

$$CSP = \frac{Total\ elastic\ work}{Total\ work}$$

The elastic material stiffness matrix is required to calculate the total elastic work in the definition of the CSP. The CSP equals unity if all the material is elastic whereas it gradually reduces to zero when failure is approached.

The CSP parameter is used in the calculation of the global error. The global error is defined as:

$$Global\ error = \frac{|unbalance\ force|}{|currently\ activated\ load| + CSP \cdot |previously\ activated\ load|}$$

The unbalance force is the difference between the external forces and the internal reactions. The currently activated load is the load that is being activated in the current calculation phase, whereas the previously activated load is the load that has been activated in previous calculation phases and that is still active in the current phase.

Using the above definition for the global error in combination with a fixed tolerated error results in an improved equilibrium situation when plasticity increases or failure is approached. The idea is that a small out-of-balance is not a problem when a situation is mostly elastic, but in order to accurately calculate failure state, safety factor or bearing capacity, a stricter equilibrium condition must be adopted.

Part 6 of the user subroutine looks very similar to part 3, except that only elastic components are considered here. It should be noted that the same variable D is used to

store the elastic material stiffness matrix, whereas in Part 3 this variable is used to store the effective material stiffness matrix.

```
6  Begin
      { Create elastic material stiffness matrix D }
      D[1,1] =
      D[1,2] =
      D[1,3] =
      .....
      D[6,6] =
   End
```

Using predefined subroutines from libraries

In order to simplify the creation of user subroutines, a number of FORTRAN subroutines and functions for vector and matrix operations are available in PLAXIS in specific compiler libraries (LFUsrLib.lib or DFUsrLib.lib) and in the source code (to be included in the file with the user subroutine). The available subroutines may be called in by User_Mod subroutine to shorten the code. An overview of the available subroutines is given in Appendix B.

Compiling user subroutine

The user subroutine User_Mod has to be compiled into a DLL file using appropriate compiler. Note that the compiler must have the option for compiling DLL files. Below are examples given for two different FORTRAN compilers. It is supposed that the user subroutine User_Mod is contained in the file USRMOD.FOR.

After creating the user subroutine User_Mod, a command must be included to export data to the DLL.

The following statement has to be inserted in the subroutine just after the declaration of variables:

- Using Lahey Fortran (LF90, LF95, ...): DLL_Export User_Mod

- Using Digital Visual Fortran: !DEC$ ATTRIBUTES DLLExport :: User_Mod

In order to compile the USRMOD.FOR into a DLL file, the following command must be executed:

- Using Lahey Fortran 90: LF90 -win -dll USRMOD.FOR -lib LFUsrLib

- Using Lahey Fortran 95: LF95 -win -dll USRMOD.FOR -lib LFUsrLib -ml LF90

- Using Digital Visual Fortran: DF /winapp USRMOD.FOR DFUsrLib.lib /dll

In all cases USRMOD.DLL file will be created. This file should be placed in the PLAXIS program directory, thereafter it can be used together with the existing PLAXIS

calculations program (PLASW.EXE). Once the UD model is used, PLAXIS will execute the commands as listed in the USRMOD.DLL file.

Debugging possibilities

When making computer programs, usually some time is spent to 'debug' earlier written source code. In order to be able to effectively debug the user subroutine, there should be a possibility for the user to write any kind of data to a file. Such a 'debug-file' is not automatically available and has to be created in the user subroutine. In Appendix C a suggestion on how this can be done is given. After the debug-file is created, data can be written to this file from within the user subroutine. This can be done by using, for example, the availably written subroutines (see Appendix B).

9.3   INPUT OF UD MODEL PARAMETERS VIA USER-INTERFACE

Input of the model parameters for user-defined soil models can be done using PLAXIS material data base. In fact, the procedure is very similar to the input of parameters for the existing PLAXIS models.

When creating a new material data set for soil and interfaces in the material data base, a window appears with three tab sheets: *General*, *Parameters*, *Interface*, Figure 9.1. A user-defined model can be selected from the *Material model* combo box in the *General* tab sheet.
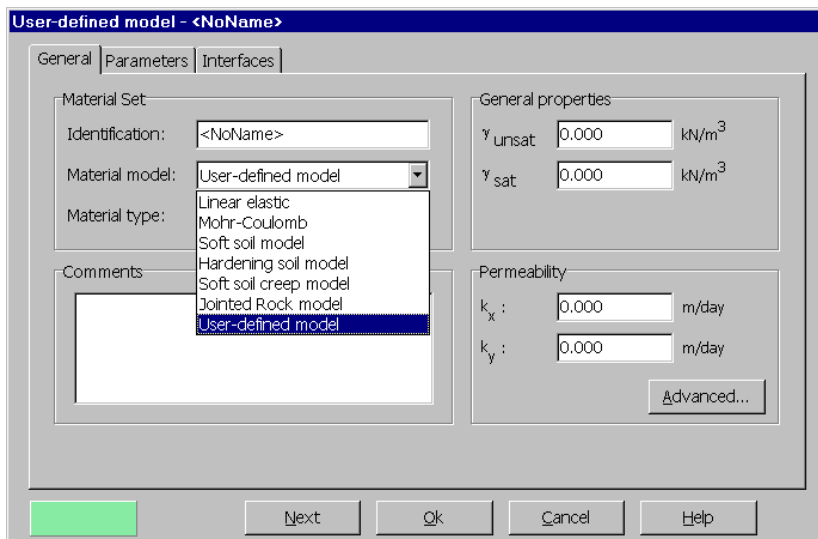
(a)
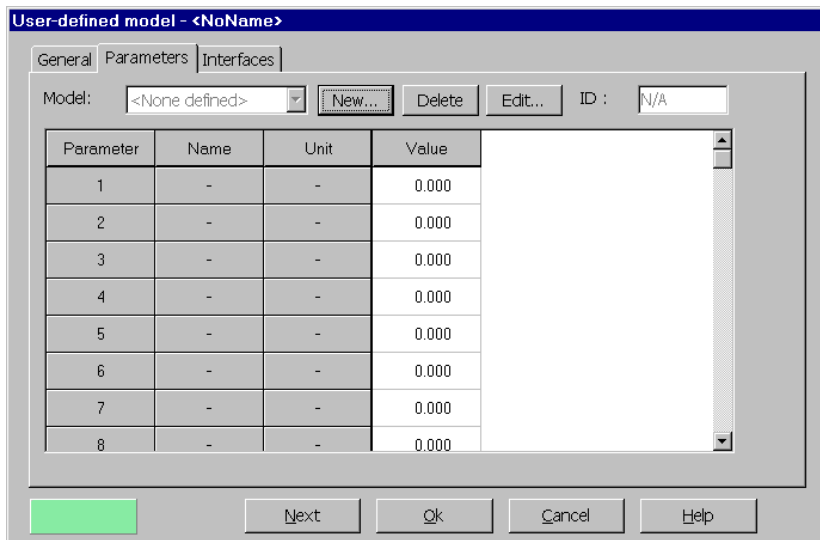
(b)

Figure 9.1. Selection of user-defined soil models (a) and input of parameters (b)

After inputting general properties, the specific model parameters can be entered in the *Parameters* tab sheet. Each UD model has its own set of model parameters, defined by the *Model* parameter. If the parameter set for a particular model has already been defined, it is available in the combo box. In that case the next section can be skipped.

Defining a new set of UD model parameters

When UD model has to be used in a project, the corresponding set of the model parameters has to be defined. This can be done by pressing the <New> button, after which the name of the model should be specified in the Model field. Then the UD model number must be selected correctly from the ID combo box, Figure 9.2. The ID parameter corresponds to the iMod parameter in the User_Mod subroutine.Subsequently, all parameters as required for a particular UD model and their corresponding input unit must be specified in the table. In this way, a maximum of 50 parameters can be entered. The numbering of parameters corresponds to the Props array in the User_Mod subroutine. Figure 9.2 shows the parameters and units for the Hooke's law example described above.

Units may be entered as common abbreviations, but in order to guarantee consistency with the basic units as defined in the General Settings, it is strongly advised to define the parameter units in these basic units (f = unit of force, l = unit of length, t = unit of time). Powers of units can be indicated after using the hat (^) sign. The set of model parameters can be completed by pressing <OK> button.
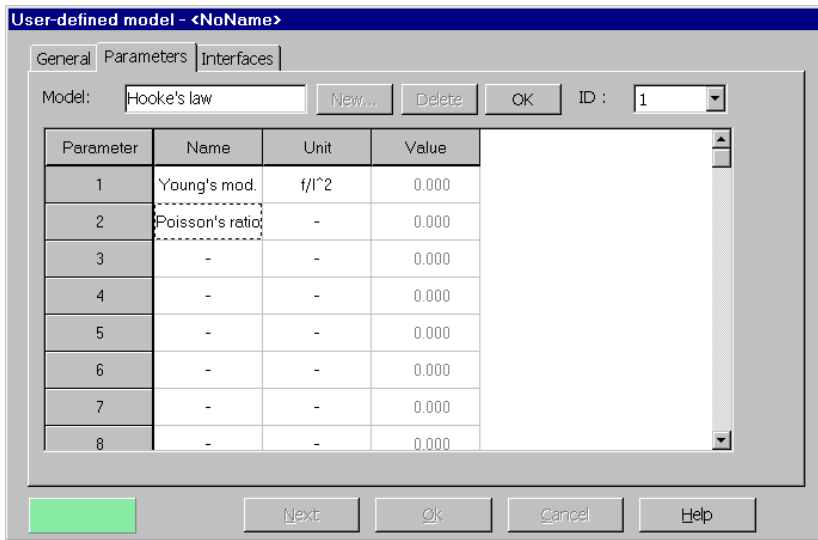
Figure 9.2 Inputting of the UD model parameters

After completing the set of model parameters it appears by its name in the *Model* combo box, Figure 9.3.
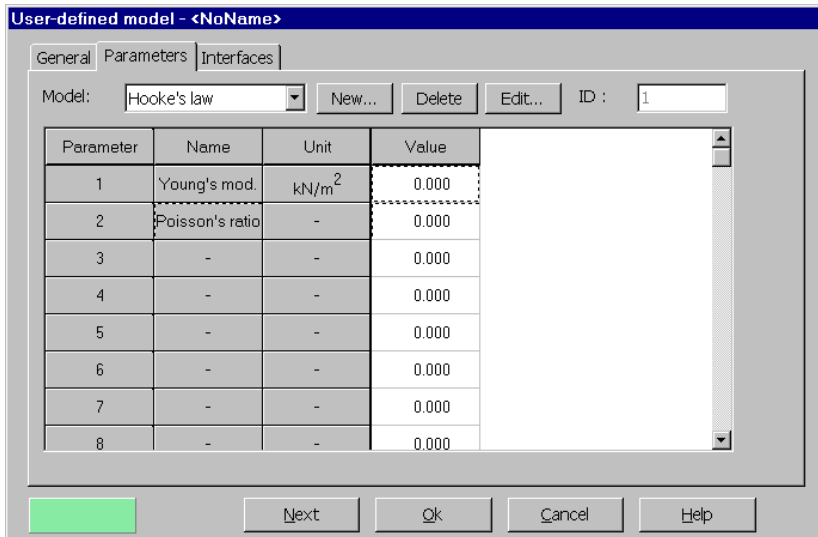
Figure 9.3 Inputting model parameter values

Existing sets may be deleted using the <Delete> button or modified using the <Edit> button. Be careful with deleting or modifying existing parameter sets, since other projects may still use these parameter sets.

Interfaces

The *Interfaces* tab sheet, Figure 9.4, contains the material data for interfaces. Normally, this tab sheet contains the R_{inter} parameter and the selection of the type of interface regarding permeability. For user-defined soil models the interface tab sheet is slightly different and contains the interface oedometer modulus, E_{oed}^{ref}, and the interface strength parameters c_{inter}, φ_{inter} and ψ_{inter}. Hence, the interface shear strength is directly given in strength parameters instead of using a factor relating the interface shear strength to the soil shear strength, as it is the case in PLAXIS models.

Figure 9.4 Interface tab sheet

After having entered values for all parameters, the data sets can be assigned to the corresponding soil clusters, in a similar way as for the existing material models in PLAXIS. The user-defined parameters are transmitted to the calculation program and appear for the appropriate stress points as Props(1..50) in the User_Mod subroutine.

10   REFERENCES

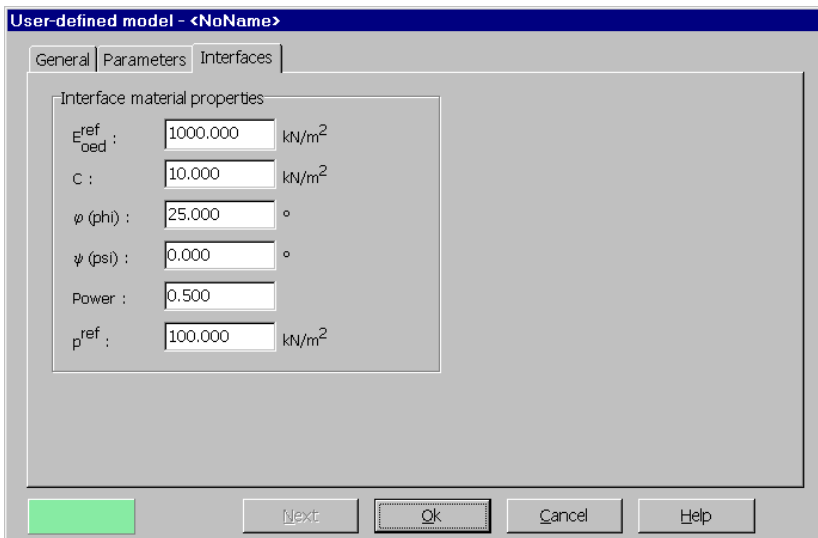[1]   Adachi, T., Oka, F., (1982). Constitutive equation for normally consolidated clays based on elasto-viscoplasticity. Soils and Foundations 22: 57-70.

[2]   Atkinson, J.H., Bransby, P.L., (1978). The Mechanics of Soils. McGraw-Hill, London.

[3]   Belytschko, T., Lasry, D., (1989). Localization limiters and numerical strategies for strain-softening materials. Proc. France-US Workshop on Strain localization and size effect due to cracking and Damage (eds. Mazars & Bazant). pp 349-362.

[4]   Bjerrum, L., (1967). Engineering geology of Norwegian normally-consolidated marine clays as related to settlements of buildings. Seventh Rankine Lecture. Geotechnique 17: 81-118.

[5]   Bolton, M.D., (1986). The Strength and Dilatancy of Sands. Géotechnique, Vol. 36, No. 1, pp. 65-78.

[6]   Borja, R.I., Kavaznjian, E, (1985). A constitutive model for the σ-ε-t behaviour of wet clays. Geotechnique 35: 283-298.

[7]   Borja, R.I., Lee, S.R., (1990). Cam-clay plasticity, part 1: implicit itegration of elasto-plastic constitutive relations. Computer Methods in Applied Mechanics and Engineering 78: 48-72.

[8]   Brinkgreve, R.B.J., Vermeer, P.A., (1992). On the use of Cam-Clay models. Proc. IV Int. Symposium on Numerical Models in Geomechanics (eds. G.N. Pande, S. Pietruszczak). Balkema, Rotterdam, Vol. 2, pp. 557-565.

[9]   Brinkgreve, R.B.J., (1994). Geomaterial Models and Numerical Analysis of Softening. Dissertation. Delft University of Technology.

[10]   Buisman, K., (1936). Results of long duration settlement tests. Proceedings 1st International Conference on Soil Mechanics and Foundation Engineering, Cambridge, Mass. Vol. 1: 103-107.

[11]   Burland, J.B., (1965). The Yielding and Dilation of Clay. (Correspondence). Géotechnique, Vol. 15, pp. 211-214.

[12]   Burland, J.B., (1967). Deformation of Soft Clay. Dissertation. Cambridge University.

[13]   Butterfield, R., (1979). A natural compression law for soils (an advance on e-log p'). Geotechnique 29:469-480.

[14]   Chen, W.F., (1975). Limit Analysis and Soil Plasticity. Elsevier, Amsterdam.

[15]   Drucker, D.C., Prager, W., (1952). Soil Mechanics and Plastic Analysis or Limit Design. Quart. Appl. Math. Vol. 10, No. 2, pp. 157-165.

[16]   Duncan, J.M., Chang, C.-Y., (1970). Nonlinear Analysis of Stress and Strain in Soil. ASCE J. of the Soil Mech. and Found. Div. Vol. 96, pp. 1629-1653.

[17]   Fung, Y.C., (1965). Foundations of Solid Mechanics, Prentice-Hall, New Jersey, USA.

[18]   Garlanger, J.E., (1972). The consolidation of soils exhibiting creep under constant effective stress. Geotechnique 22: 71-78.

[19]   den Haan, E.J., (1994). Vertical Compression of Soils. Thesis, Delft University.

[20]   Hill, R., (1950). The Mathematical Theory of Plasticity, Oxford University Press, London, U.K.

[21]   Janbu, N., (1969). The resistance concept applied to soils. Proceedings of the 7[h] ICSMFE, Mexico City 1:191-196.

[22]   Janbu, J., (1963). Soil Compressibility as Determined by Oedometer and Triaxial Tests. Proc. ECSMFE Wiesbaden, Vol. 1, pp. 19-25.

[23]   Koiter, W.T., (1960). General Theorems for Elastic-Plastic Solids. In: Progress in Solid Mechanics (eds. I.N. Sneddon, R. Hill), Vol. 1., North-Holland, Amsterdam, pp. 165-221.

[24]   Kondner, R.L., (1963). A Hyperbolic Stress Strain Formulation for Sands. 2. Pan. Am. ICOSFE Brazil, Vol. 1, pp. 289-324.

[25]   Kulhawy, F. H., Mayne, P.W., (1990). Manual on Estimating Soil Prperties for Foundation Design. Cornell University, Ithaca, New York.

[26]   van Langen, H., Vermeer, P.A., (1990). Automatic Step Size Correction for Non-Associated Plasticity Problems. Int. J. Num. Meth. Engng., Vol. 29, pp. 579-598.

[27]   Leroueil, S., (1977). Quelques considérations sur le comportement des argiles sensibles. Ph.D. thesis, Laval University, Québec.

[28]   Muir Wood, D., (1990). Soil Behaviour and Critical State Soil Mechanics. Cambridge University Press.

[29]   Neher, H., Vermeer, P.A. (1998). Formulation and application of a soil model that accounts for creep. Int. J. Numer. Anal. Meth. Geomech.

[30]   Prevost, J.-H., (1976). Undrained Stress-Strain-Time Behaviour of Clays. Journal of the Geotechnical Engineering Division GT12: 1245-1259.

[31]   Rowe, P.W., (1962). The Stress-Dilatancy Relation for Static Equilibrium of an Assembly of Particles in Contact. Proc. Roy. Soc. A., No. 269, pp. 500-527.

[32]   Schanz, T., (1998). Zur Modellierung des Mechanischen Verhaltens von Reibungsmaterialen, Habilitation, Stuttgart Universität.

[33]   Schanz, T., Vermeer, P.A., (1996). Angles of Friction and Dilatancy of Sand. Géotechnique 46, pp. 145-151.

[34]   Schanz, T., Vermeer, P.A., (1998). Special issue on Pre-failure deformation behaviour of geomaterials. Géotechnique 48, pp. 383-387.

[35]   Schanz, T., Vermeer, P.A., Bonnier, P.G., (1999). Formulation and verification of the Hardening-Soil Model. In: R.B.J. Brinkgreve, Beyond 2000 in Computational Geotechnics. Balkema, Rotterdam: 281-290.

[36]   Sekiguchi, H., (1977). Rheological characteristics of clays. Proceedings of the 9th ICSMFE, Tokyo 1:289-292.

[37]   Smith, I.M., Griffith, D.V., (1982). Programming the Finite Element Method, Second Edition. John Wiley & Sons, Chisester, U.K.

[38]   von Soos, P., (1990). Properties of Soil and Rock (in German). In: Grundbautaschenbuch Part 4, Edition 4, Ernst & Sohn, Berlin.

[39]   Stolle, D.F.E., (1991). An interpretation of initial stress and strain methods, and numerical stability. International Journal for Numerical and Analytical Methods in Geomechanics 15: 399-416.

[40]   Stolle, D.F.E., Bonnier, P.G., Vermeer, P.A., (1997). A soft soil model and experiences with two integration schemes. Numerical Models in Geomechanics. Numog 1997: 123-128.

[41]   Vaid, Y., Campanella, R.G. (1977). Time-dependent behaviour of undisturbed clay. ASCE Journal of the Geotechnical Engineering Division, 103(GT7), pp. 693-709.

[42]   Vermeer, P.A., de Borst, R., (1984). Non-Associated Plasticity for Soils, Concrete and Rock. Heron, Vol 29, No. 3.

[43]   Vermeer, P.A., van Langen, H., (1989). Soil collapse computations with finite elements. Ingenieur-Archiv 59: 221-236.

[44]   Vermeer, P.A., Stolle, D.F.E., Bonnier, P.G. (1998). From the classical theory of secondary compression to modern creep analysis. Proc. 9th Int. Conf. Comp. Meth. and Adv. Geomech.. Wuhan, China, Vol. 4, pp 2469-2478.

APPENDIX A   SYMBOLS

c	:	Cohesion
csp	:	Current stiffness parameter
C_u , S_u	:	Undrained shear-strength
$\underline{D}^e$	:	Elastic material matrix representing Hooke's law
e	:	Void ratio
E	:	Young's modulus
E_{oed}	:	Oedometer modulus
f	:	Yield function
g	:	Plastic potential function
G	:	Shear modulus
K	:	Bulk modulus
K_0	:	Coefficient of lateral earth pressure
m	:	Power in stress-dependent stiffness relation
M	:	Slope of critical state line in p'-q space
n	:	Porosity
OCR	:	Overconsolidation ratio
p	:	Isotropic stress or mean stress, positive for pressure; negative for tension
p_p	:	Isotropic preconsolidation stress, positive for pressure
POP	:	Pre overburden pressure
q	:	Equivalent shear stress or deviatoric stress
R_f	:	Failure ratio
t	:	Time
$\underline{u}$	:	Vector with displacement components
γ	:	Volumetric weight
α_1	:	Dip angle
α_2	:	Dip direction
Δ	:	Increment
$\underline{\varepsilon}$	:	Vector with Cartesian strain components, normal components positive for extension; negative for compression
ε_v	:	Volumetric strain, negative for compression; positive for extension
κ	:	Cam-Clay swelling index
κ^*	:	Modified swelling index
λ	:	Plastic multiplier
λ	:	Cam-Clay compression index
λ^*	:	Modified compression index
μ^*	:	Modified creep index
ν	:	Poisson's ratio
$\underline{\sigma}$	:	Vector with Cartesian stress components, normal components positive for tension; negative for pressure
σ_p	:	Vertical preconsolidation stress, negative for pressure

φ :   Friction angle
ψ :   Dilatancy angle

APPENDIX B   FORTRAN   SUBROUTINES   FOR   USER-DEFINED   SOIL MODELS

In this appendix, a listing is given of the subroutines and functions which are provided by PLAXIS in libraries and source cod in the user-defined soil models directory. These can be called by the User_Mod subroutine:

Subroutines

MZeroR(R, K):

>   To initialize *K* terms of double array *R* to zero

MZeroI(I, K):

>   To initialize *K* terms of integer array *I* to zero

SetRVal(R, K, V):

>   To initialize *K* terms of double array *R* to *V*

SetIVal(I, K, IV):

>   To initialize *K* terms of integer array *I* to *IV*

CopyIVec(I1, I2, K):

>   To copy *K* values from integer array *I1* to *I2*

CopyRVec(R1, R2, K):

>   To copy *K* values from double array *R1* to *R2*

MulVec(V, F, n):

>   To multiply a vector *V* by a factor *F*, *n* values

MatVec(xMat, im, Vec, n, VecR):

>   Matrix (xMat)-vector(Vec) operation.

>   First dimension of matrix is *im*; resulting vector is *VecR*

AddVec(Vec1, Vec2, R1, R2, n, VecR):

>   To add n terms of two vectors; result in *VecR*

$$VecR_i = R1 \cdot Vec1_i \; + \; R2 \cdot Vec2_i$$

MatMat(xMat1, id1, xMat2, id2, nR1, nC2,
>   nC1, xMatR, idR):

>   Matrix multiplication $\quad xMatR_{ij} = xMat\,1_{ik} \; \cdot \; xMat\,2_{kj}$

>   *id1*, *id2*, *idR* : first dimension of matrices

>   *nR1* number of rows in *xMat1* and resulting *xMatR*

>   *nC2* number of column in *xMat2* and resulting *xMatR*

>   *nC1* number of columns in *xMat2* =rows in *xMat2*

MatMatSq(n, xMat1, xMat2, xMatR):

Matrix multiplication $xMatR_{ij} = xMat\,1_{ik} \cdot xMat\,2_{kj}$

Fully filled square matrices with dimensions n

```
MatInvPiv( AOrig, B, n ):
```

Matrix inversion of square matrices *AOrig* and *B* with dimensions *n*.

AOrig is NOT destroyed, *B* contains inverse matrix of *AOrig*.

Row-pivotting is used.

```
WriVal( io, C, V ):
```

To write a double value *V* to file unit *io* (when *io* > 0)

The value is preceeded by the character string *C*.

```
WriIVl( io, C, I ):
```

As *WriVal* but for integer value *I*

```
WriVec( io, C, V, n ):
```

As *WriVal* but for *n* values of double array *V*

```
WriIVc( io, C, iV, n ):
```

As *WriVal* but for *n* values of integer array *iV*

```
WriMat( io, C, V, nd, nr, nc ):
```

As *WriVal* but for double matrix *V*.

nd is first dimension of *V*, *nr* and *nc* are the number of rows and columns to print respectively.

```
PrnSig( iOpt, S, xN1, xN2, xN3, S1, S2, S3, P, Q ):
```

To determine principal stresses and (for *iOpt*=1) principal directions.

iOpt = 0 to obtain principal stresses without directions

iOpt = 1 to obtain principal stresses and directions

S array containing 6 stress components (XX, YY, ZZ, XY, YZ, ZX)

xN1, *xN2*, *xN3* array containing 3 values of principal normalized directions only when *iOpt*=1.

S1, *S2*, *S3* sorted principal stresses ($S \leq S2 \leq S3$)

P isotropic stress (negative for compression)

Q deviatoric stress

```
CarSig( S1, S2, S3, xN1, xN2, xN3, SNew ):
```

To calculate Cartesian stresses from principal stresses and principal directions.

S1, *S2*, *S3* principal stresses

xN1, *xN2*, *xN3* arrays containing principal directions (from `PrnSig`)

SNew contains 6 stress components (XX, YY, ZZ, XY, YZ, ZX)

```
CrossProd( xN1, xN2, xN3 ):
```

Cross product of vectors *xN1* and *xN2*

```
SetVecLen( xN, n, xL ):
```

To multiply the *n* components of vector *xN* such that the length of *xN* becomes *xL* (for example to normalize vector *xN* to unit length).

Functions

```
Logical Function LEqual( A, B, Eps ):
```

Returns *TRUE* when two values *A* and *B* are almost equal, *FALSE* otherwise.

$LEqual = |A\text{-}B| < Eps * (|A| + |B| + Eps) / 2$

```
Logical Function Is0Arr( A, n ):
```

Returns *TRUE* when all *n* values of real (double) array *A* are zero, *FALSE* otherwise

```
Logical Function Is0IArr( IArr, n ):
```

Returns *TRUE* when all *n* values of integer array *IArr* are zero, *FALSE* otherwise

```
Double Precision Function DInProd( A, B, n ):
```

Returns   the   inproduct   of   two   vectors   with   length   *n*

APPENDIX C   CREATING A DEBUG-FILE FOR USER-DEFINED SOIL MODELS

A debug file is not automatically created and opened in PLAXIS. The user should do this by including the corresponding source code in the user subroutine. The debug file needs only be created and opened once. Since the user subroutine is used many times, it must be checked whether the file, i.e. the corresponding IO unit number, is already open.

When writing a FORTRAN user subroutine and compiling it as a DLL, files are not shared with the main program. This means that any IO unit number can be used without conflicts between the debug file and existing files used by PLAXIS.

Here suggestions are given on how the debug file can be created and opened:

1: Inquire if a unit number is opened. If not, open it.

```
Logical IsOpen
Inquire( unit = 1, Opened = IsOpen)
If (.Not. IsOpen) Then
       Open( Unit = 1, File = ' ... ' )
End If
```

2: Use a DATA statement

```
Logical IsOpen
Data IsOpen /  .FALSE. /
Save IsOpen
If (.Not. IsOpen) Then
       Open( Unit = 1, File = ' ... ' )
       IsOpen = .TRUE.
End If
```

The above suggestions assume that the debug file is located in the currently active directory, which is not necessarily the proper location. It is suggested that the debug file is stored in the DTA-directory of the corresponding PLAXIS project. Therefore it is necessary to include also the pathname in the `File = ' ... '`. The project directory is passed to the user subroutine by means of the parameters *iPrjDir* and *iPrjLen*. The *iPrjDir* array contains the ASCII numbers of the characters of the project directory string and *iPrjLen* is the length of the string (max. 255). This is to avoid character passing conflicts (Fortran - C conflicts). The project directory string will always end with character 92 (\). The user has to rebuild the character string and can directly add the actual name of the debug file.

The example underneath shows how a debug file called 'usrdbg' can be created and opened in the current project directory for debugging purposes:

```
Character fName*255
Dimension iPrjDir(*)
```

```
      Logical IsOpen
      Data IsOpen / .FALSE. /
      Save IsOpen
      If (.Not. IsOpen) Then
           fName = ' '
           Do i=1, iPrjLen
           fName(i:i) = Char( iPrjDir(i) )
           End Do
           fName = fName(:iPrjLen) // 'usrdbg'
           Open( Unit = 1, File = fName )
           IsOpen = .TRUE.
      End If
```

In the user subroutine, values can be written to IO unit 1, using for example the available writing subroutines in Appendix B.

Debugging hints

When developing and debugging a constitutive soil model in the user subroutine, it is very useful to start by testing it with a simple finite element model in which a homogeneous stress state should occur (for example an axisymmetric, 1 x 1 unit model of a one-dimensional compression test or a triaxial test with zero soil weight). The finite element model will still contain many stress points, but the stress state in each point should be the same.

In any case, it is useful to write output for a limited number of stress points only (or for certain step numbers or iteration numbers), in order to avoid large debug files. Examples of writing useful but limited debug information are given below:

```
      io = 0
      If ( iEl .Eq. 1 .And. Int.Eq.1 .And. iStep.Gt.10 )
       io = 1
      ...
      Call WriIVl( io, 'Step', iStep )
      Call WriIVl( io, 'Iter', iTer )
      Call WriVec( io, 'Sig0', Sig0, 6 )
      Call WriVec( io, 'dEps', dEps, 6 )
      Call WriMat( io, 'D', D, 6, 6, 6 )
      ...
      Call WriVec( io, 'Sig', Sig, 6 )
```

The available writing routines do not write when *io* is zero or negative.

Alternatively:

```
      If ( io .Eq. 1 ) Then
```

```
            Write( 2, * ) 'StVar:',(StVar(j),j=1,2)
      End If
```

Note that here file 2 is used. This file must be opened before. When the file has not been opened before, Lahey Fortran will give a Run-Time Error (File not open), however, Digital Fortran will open a file with the name FORT.2 in the current directory or checks the environment variable FORT2.